

**The surface energy balance over drying  
semi-arid terrain in West Africa**

**De oppervlakte energiebalans over  
uitdrogende semiaride gebieden in West  
Afrika**

Dirk Schüttemeyer

**Promotor:**

Prof. dr. A.A.M. Holtslag  
Hoogleraar in de Meteorologie en Luchtkwaliteit

**Co-promotoren:**

Dr. A.F. Moene  
Universitair docent bij de leerstoelgroep  
Meteorology en Luchtkwaliteit, Wageningen Universiteit

Dr. H.A.R. de Bruin  
Universitair hoofddocent bij de leerstoelgroep  
Meteorology en Luchtkwaliteit, Wageningen Universiteit

**Samenstelling promotiecommissie:**

Prof. dr. M. Schaepman – Wageningen Universiteit

Prof. dr. ir. B.J.J.M. van den Hurk – Utrecht Universiteit

Prof. dr. ir. N. van de Giesen – Technische Universiteit Delft

Dr. A. Verhoef – University of Reading, United Kingdom

# **The surface energy balance over drying semi-arid terrain in West Africa**

Dirk Schüttemeyer

Proefschrift  
ter verkrijging van de graad van doctor  
op gezag van de rector magnificus  
van Wageningen Universiteit,  
Prof.dr. ir L. Speelman,  
in het openbaar te verdedigen  
op vrijdag 3 juni 2005  
des namiddags te vier uur in de Aula.

ISBN 90-8504-192-9

**Viele kleine Leute  
an vielen kleinen Orten,  
die viele Dinge tun  
werden das Gesicht der Welt verändern.**  
(Afrikanisches Sprichwort)



## **Preface**

I started this work in November 2000 and went to Africa in the beginning of March 2001. One answer to my question how far it was to reach our destination in Africa while driving was “it is far but not too far”. These words spoken by an African driver sounded funny when I heard them for the first time, but somehow I could not forget these words and during my PhD research these words became important for finishing my work.

For reaching my destination I have been fortunate to have had help and inspiration from a lot of people and the most important ones are of course the (co-) promoters.

First of all I would like to thank my co-promotor Arnold Moene. Your commitment to my work and to the project is unmatched, and I appreciate all of the guidance, wisdom, and attention to detail.

Big thanks also go to my promotor Bert Holtslag. Your support and patience made that the distance to reach my destination really became smaller. Furthermore your experience in guiding people helped for finishing my work.

I also would like to thank Henk de Bruin, who initiated the project and signed responsible in the beginning. He also provided the opportunity to visit the University of Arizona for the MATADOR project.

I would like to thank all three for always keeping in touch especially during the times, when I was not in Wageningen.

This work was carried out in the context of the GLOWA-Volta project and was initiated by the Center of Development research (ZEF) in Bonn, Germany. It was mainly funded by the German ministry of research and education (BMBF). I would like to thank both for the opportunity to work on such a challenging project.

I would like to thank all the people from the Meteorology and Air Quality Department. It was always inspiring to work in a department, where diverse research questions are tackled. Special thanks go to Oscar Hartogensis, who taught me a lot about the organization and carrying-out of measurements. Big thanks also go to Jordi Vila, who listened to all the bits and pieces which were not always related to research.

The field work in Ghana would not have been successful without support from numerous people in Africa, the Netherlands and Germany. I would like to thank them all but in particular Marc Andreini, Roos Zuurbier, Joost Hoedjes, Raymond Kasei, Ronald Groen and Gabriel Akotia.

Special thanks also go to Wouter Meijninger and Jörg Schulz, my “paranimfen”. Both motivated me by talking about their and my research and sometimes it was very helpful to have them looking at my research from a different perspective.

The research was assisted by many fruitful conversations with people from different institutions. I would like to thank them all. Special thanks go to Anton Beljaars and Michael Ek for providing the ECMWF and NOAH land surface models and for taking the time to answer the numerous questions I had.

I would like to thank my family and friends who have supported me in many ways during the last four years. Fortunately, my daughter, Lisann, was born after the bulk of the work was done and enjoys a fairly present and pleasant father.

Lastly, I want to thank my wife Anke, without your support and love, I would be all but lost.



## **Abstract**

One of the fundamental aspects of current research in earth system science is the proper understanding of land-atmosphere interactions. The role of the land surface is crucial in the climate system, since a large fraction of incoming solar radiation passes through the atmosphere and is converted at the surface into turbulent fluxes. For numerous regions, including the semi-arid regions, only little knowledge is available about the diurnal and seasonal cycle of land surface interactions. The semi-arid areas pose a big challenge due to the large contrasts of dry and wet situations within a seasonal cycle. This is especially valid for the semi-arid region in West Africa, since it is one of the most climatically sensitive and ecologically unstable regions in the world. The variability of weather and climate in the region is strongly influenced by complicated interactions and feedbacks between the land and the atmosphere. To analyze and to predict these interactions and feedbacks it is inevitable to measure and model the involved components. Since standard methods for this purpose are not always applicable to the heterogeneous surface in West Africa, new measurement and modeling techniques have to be applied.

The overall objective of this thesis is to analyze and to model the land surface interactions in the Volta basin, West Africa, by using meteorological data obtained in the framework of the GLOWA-Volta project. A focus is put on diurnal and seasonal time scales. For measuring turbulent fluxes the key instrument is the large aperture scintillometer. This robust method yields area-averaged fluxes over complex terrain, which are required when analyzing meteorological data from heterogeneous surfaces. It is found that it is a suitable technique for the kind of environment also in comparison to different measuring techniques.

Based on the analysis of the measurements, two different land surface schemes are evaluated. Both schemes are not able to reproduce the measured seasonal cycle in surface fluxes. Several changes are proposed to obtain enhanced model performance.

Based on the earlier findings a model is constructed, combining the best parts of each of the two land surface schemes. It is shown that the performance of the new formulation is more realistic. Using a factorial design as the sensitivity analysis method it is assessed, which parameters are the most important. Furthermore it is found that those important parameters and their interactions change significantly during one season.

As a final step the gained knowledge is utilized to construct a simple satellite based algorithm to obtain surface water flux as the important flux on a regional basis. For evaluating this first order approach the large aperture scintillometer is utilized to evaluate fluxes on satellite pixel scale.



# Contents

<b>1</b>	<b>Introduction</b>	<b>1</b>
1.1	General Introduction.....	2
1.2	Climate in West Africa.....	3
1.3	The hydrological cycle.....	5
1.4	Land-atmosphere interface.....	7
1.5	Land-atmosphere parameterizations.....	9
1.6	The GLOWA-Volta project.....	10
1.7	Research question and organization of the thesis.....	13
<b>2</b>	<b>Surface fluxes and characteristics of drying semi-arid terrain in West Africa</b>	<b>15</b>
2.1	Introduction.....	17
2.2	Experimental Setup and Observations.....	20
2.2.1	Meteorological measurements.....	22
2.2.2	Flux measurements with Scintillometry.....	23
2.2.3	Intensive observation period 2002.....	25
2.2.4	Site description.....	25
2.2.5	Methods.....	26
2.3	Comparison of LAS and EC derived sensible and latent heat flux.....	26
2.3.1	Sensible heat flux.....	27
2.3.2	Latent heat flux.....	31
2.4	Evaluation of the energy balance closure.....	32
2.4.1	Surfaces fluxes on a seasonal basis.....	33
2.4.2	Tamale.....	35
2.4.3	Ejura.....	36
2.5	Evaluation of surface conductance.....	37
2.6	Conclusions.....	42

<b>3</b>	<b>Evaluation of two Land-Surface Models over drying terrain in West Africa</b>	<b>45</b>
3.1	Introduction .....	47
3.2	Material and Methods.....	49
3.2.1	Model descriptions.....	49
3.2.2	GLOWA-Volta data set.....	51
3.2.3	Forcing data.....	52
3.2.4	Validation data .....	53
3.2.5	Model Parameters.....	54
3.2.6	Model evaluation.....	55
3.3	Results.....	56
3.3.1	The different components of the energy balance .....	56
3.3.2	Influence of initial soil moisture .....	63
3.3.3	The role of canopy conductance.....	63
3.3.4	Simple Adjustments for both test sites.....	66
3.4	Discussion .....	69
3.5	Conclusions.....	70
	Appendix .....	72
<b>4</b>	<b>Assessing the Sensitivity of Water and Energy Exchanges during a seasonal cycle in West Africa</b>	<b>75</b>
4.1	Introduction .....	77
4.2	Material and Methods.....	79
4.2.1	Original model description.....	79
4.2.2	Current model description.....	82
4.2.3	GLOWA-Volta data set .....	82
4.2.4	Forcing and validation data .....	83
4.3	Model validation.....	85
4.3.1	Parameter estimation .....	85
4.3.2	Method of model evaluation .....	86
4.3.3	Model results.....	87
4.4	Response from factorial design .....	91
4.4.1	Theory of factorial design .....	91
4.4.2	Results from two-level factorial design .....	92
4.5	Discussion .....	99
4.5.1	Net radiation.....	99
4.5.2	Sensible Heat Flux .....	100
4.5.3	Latent Heat Flux.....	100
4.5.4	Implications for land surface modeling.....	101
4.6	Conclusions .....	102

<b>5</b>	<b>Satellite based actual evapotranspiration over drying semi-arid terrain in West Africa</b>	<b>105</b>
5.1	Introduction .....	107
5.2	Satellite Data .....	110
5.2.1	Determination of incoming solar radiation from Meteosat .....	110
5.2.2	Determination of near surface temperature from Meteosat .....	112
5.2.3	Green vegetation fraction from MODIS .....	112
5.3	Experimental Setup and Observations.....	113
5.3.1	Site description and experimental setup.....	113
5.3.2	Flux measurements with Scintillometry.....	116
5.3.3	Algorithm evaluation .....	117
5.4	Results and Discussion .....	118
5.4.1	Validation of satellite derived incoming solar radiation.....	118
5.4.2	Validation of satellite derived reference temperature.....	121
5.4.3	Validation of actual evapotranspiration.....	123
5.5	Summary and Conclusions.....	127
<b>6</b>	<b>Summary and Perspectives</b>	<b>129</b>
6.1	Summary.....	130
6.2	Perspectives .....	132
	<b>Bibliography</b>	<b>135</b>
	<b>Samenvatting</b>	<b>149</b>
	<b>Curriculum vitae</b>	<b>153</b>



# **Chapter 1**

## **Introduction**

## 1.1 General Introduction

Human activity in business and society has an impact on local and regional scales within the earth system and it increasingly involves the earth as a whole. This impact represents a challenge requiring new research strategies involving the different scales. Especially the climate system, as part of the earth system, has undergone changes due to human activity (Intergovernmental Panel on Climate Change (IPCC) 1999). Water resources are inextricably linked with climate, so the prospect of global climate change has serious implications for water resources and regional development (Riebsame et al. 1995). Furthermore water resources heavily influence the characteristics of many terrestrial ecosystems, which means that water is fundamental to life.

The natural, technical, and social sciences can provide essential information and evidence needed for decisions on how humanity can deal with changes in the climate system related to water resources and the hydrological cycle. The basis for those decisions depends on the scales involved and therewith varies for the involved regions, depending both on the local nature and consequences of eventual impacts, and also on the adaptive capacity available to cope with changes (IPCC 2001). Studies of projections of climate change use a hierarchy of coupled ocean/atmosphere/sea-ice/land-surface models to provide indicators of global response as well as possible regional patterns of climate change (IPCC 2001). Since land surface modeling is considered as one of the major sources of uncertainty for current climate change prediction (Crossley et al. 2000; IPCC 1996), it is essential to analyze the impact of climate change on hydrology and water resources in detail. In this context the following steps should be addressed (Klemes 1985; Gleick 1989):

- A quantitative estimate of changes in the long term indices of the major climatic variables, such as temperature, precipitation and evapotranspiration, by using quantitative climatic scenarios;
- A simulation of the hydrological cycle for a basin of interest, using the scenarios developed in the previous step, as well as estimation of the climatically induced variations in various hydrological variables of interest;
- An assessment of the implications of the previously identified hydrologic variations for the performance and the reliability of water resource systems, such as aqueducts, dams, reservoirs, groundwater aquifers, etc.



To tackle those challenging tasks, the GLOWA (Global change in the hydrological cycle) project aims to create a basis for the development of innovative technologies and cost-effective services for the sustainable, far-sighted management of water resources (<http://www.glowa.org>). In total GLOWA consists of five subprojects operating in different basins or watersheds. Since assessments (Hulme 1996; IPCC 1998) concluded that the African continent is particularly vulnerable to the impacts of climate change and the consequences of climate change for the water resources, two of the projects deal with sustainable water management in Africa. The important factors for the vulnerabilities are widespread poverty, recurrent droughts, inequitable land distribution, and overdependence on rainfed agriculture. The basin of the Volta River in West Africa is one example for those kinds of circumstances. It is one of the poorest areas in Africa. For the majority of the population, rainfed and some irrigated agriculture is the backbone in the largely rural societies and the principal source of income.

Efforts to provide adequate water resources for such a region will confront several challenges, including population pressure, problems associated with land use, such as erosion/siltation; and possible ecological consequences of land-use change on the hydrological cycle (IPCC 2001).

One crucial point is the natural climate variability in this region. It is one of the most climatically sensitive and ecologically unstable regions in the world (Zeng and Neelin 2000). The very existence of the savanna ecosystem is closely related to environmental variability in a non-equilibrium fashion (Ellis and Swift 1988). Therefore it is really important to understand the current relationship between climate and hydrological response, and investigate the interrelationships of all basin components, before attempting to assess possible changes due to human activity. Furthermore possible impacts of climate change on water resource management should be directed to the needs of the user (Mimikou 1995).

## **1.2 Climate in West Africa**

The general circulation in West Africa is to a large extent controlled by the meridional movement of the intertropical convergence zone (ITCZ) during the year. The ITCZ is defined as the thermal equator, where the surface meridional wind is discontinuous and the vertical motion is upward (Asnani 1993). The movement of the ITCZ tends to coincide with the solar maximum although it lags behind the sun's position by four to six weeks. The movement is amplified by a strong meridional pressure gradient in the lower troposphere, resulting from the existence of a strong thermal depression above the Sahara (Janicot 1992). The ITCZ

remains north of the equator over West Africa throughout the year because of the oceanic influence, i.e. the cold sea surface temperature (SST) over the Gulf of Guinea.

Two jet systems influence the general circulation: The African Easterly Jet (AEJ) and the Tropical Easterly Jet (TEJ). The AEJ provides energy for weather disturbances, whereas the link to weather disturbances of the TEJ is more speculative (Nicholson 1986). Additionally pressure disturbances, which traverse from east to west across Africa (Burpee 1972), influence the general circulation. They all act under the influence of the Hadley and Walker cell circulation, which influence patterns of aridity and precipitation, by exporting angular momentum, moisture, and potential energy poleward (Oort and Peixoto 1983).

The northwards movement of the ITCZ is related to the convergence of moist air advected from the Gulf of Guinea. The moisture convergence is modulated by the AEJ. For West Africa those processes are associated with the West African monsoon season. When the ITCZ is moving south dry continental air masses from the northwest are advected and is associated with the dry season. The change in wind direction in between those two seasons (time of transition) depends critically on the timing of the movement and therewith on the actual latitude of the ITCZ in West Africa. The actual position of the ITCZ and thereby atmospheric humidity and wind direction has a large impact on the length of the monsoon season and the distribution of the yearly average amount of rain. From the coast up north the contrast between dry and moist air during the time of transition is probably more pronounced in time and space than anywhere else (Hólm et al. 2002). For the period from September to December 2002 this is shown in figure 1.1.

Nicholson (1986) examined the spatial patterns of annual rainfall amounts in Africa during the years 1901-1973 in the context of the monsoon season. For West Africa four patterns of large rainfall departures were described. Two of those were related to abnormal latitudinal location of the ITCZ, whereas the other two might be related to the intensity of the Hadley circulation and the TEJ.

For a large fraction of the monsoon season the precipitation is influenced by high values of evapotranspiration from the land surface, which shows a strong feedback mechanism: high precipitation leads to more soil moisture, which enhances evapotranspiration feeding back into high precipitation (Beljaars et al. 1996). This local feedback mechanism contributes approximately 27% of precipitation in West Africa (Eltahir and Gong 1996). This shows that the interaction between the surface and the atmosphere is a potentially important determinant for the regional climate. Outside the monsoon season the soil moisture availability is not the sole determining factor for actual evapotranspiration. Other factors are a reduction in available energy, canopy conductance and a varying rooting depth.

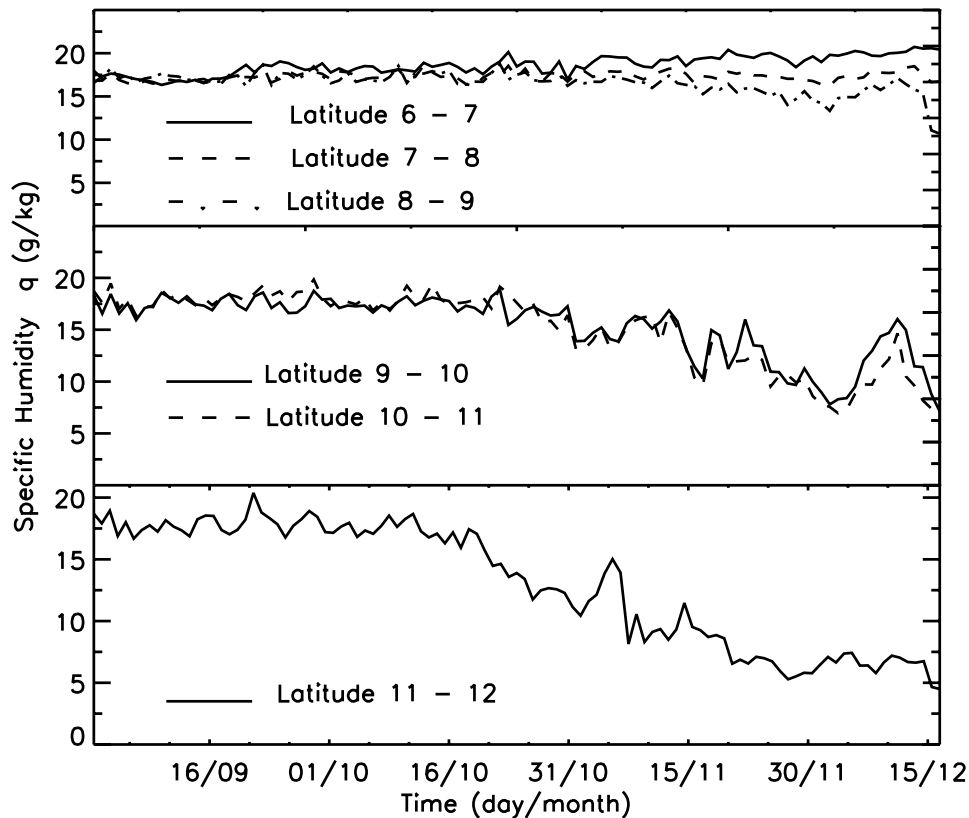


**Fig. 1.1: Averaged specific humidity ( $q$ ) from all available synoptic stations between  $-5$  and  $5$  degree longitude for six latitude bands from  $6$  to  $12$  degree north for September to December 2002. Anton Beljaars, ECMWF, kindly provided the data.**

The appearance of the monsoon connected to the local feedback mechanisms makes the region a challenging test bed for measurements and models. Furthermore it shows that local surface hydrology is an important factor for climate or weather related models operating in that region.

### 1.3 The hydrological cycle

The hydrological cycle is driven by incoming solar radiation, supplying the energy for evapotranspiration from land surfaces and the ocean and for the atmospheric transport of water to be precipitated over land areas and the oceans. It has only a few major components. The hydrological cycle is often represented by pictures of rain, clouds, slopes, trees and water. Those pictures of the hydrological cycle are idealized and make it difficult to develop a conceptual model for the processes involved. Horton (1931) represented the hydrological cycle as a balanced closed cycle (figure 1.2).

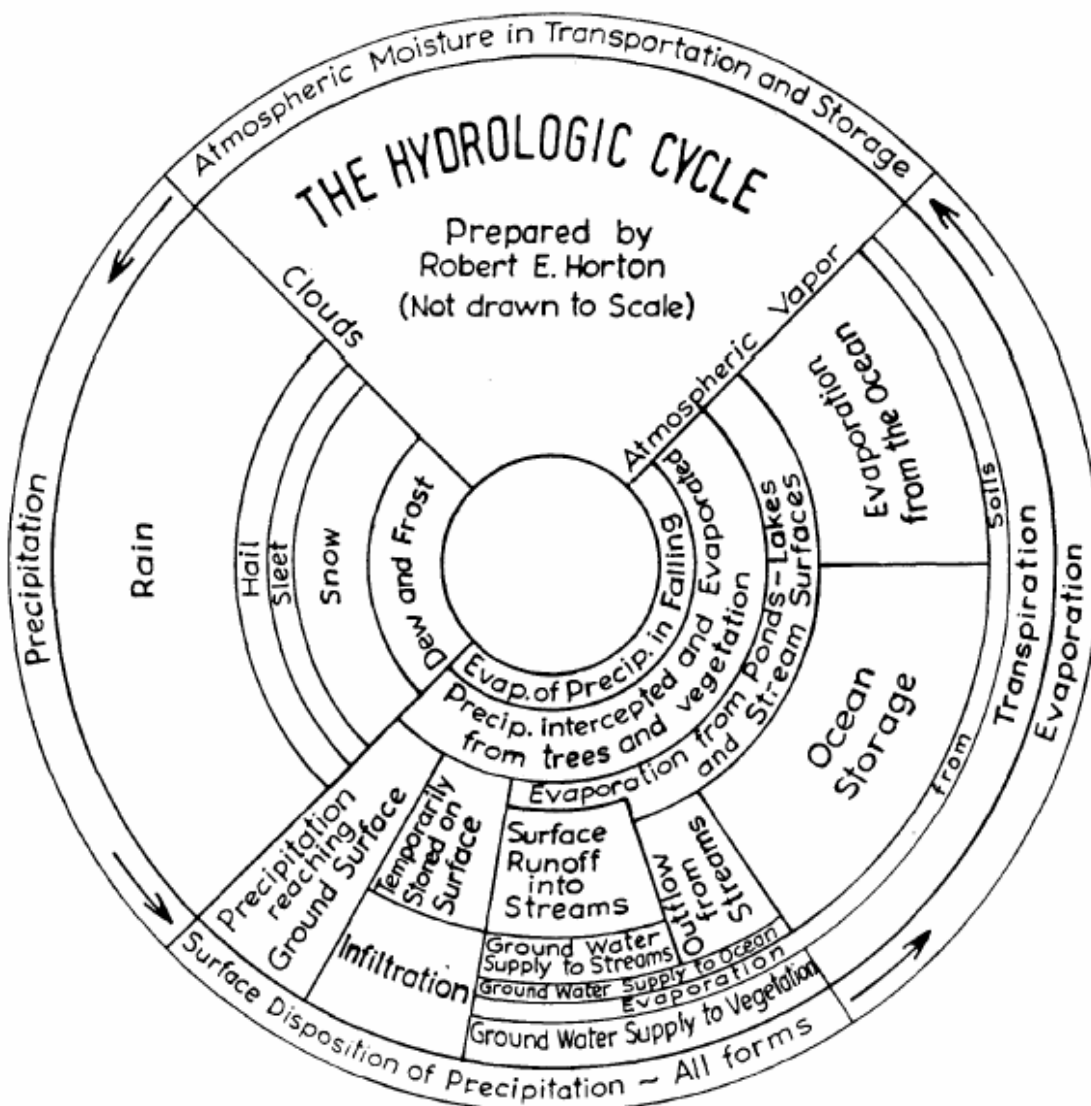


**Figure 1.2: Horton's hydrological cycle.**

In this cycle the starting point is during the transportation and storage of moisture in the atmosphere. After condensation, the water reaches the surface in different forms, is deposited and evaporates again. By dividing the cycle into those four parts, such an approach makes it possible to construct a detailed model for the processes involved, which contains all relevant parameters for the actual application by still being sufficiently realistic and reasonably simple. This should always be the aim, if the problem is imbedded in such an integrated model as utilized in the current project (compare section 1.6). Additionally it helps describing the problem and addressing the crucial questions to scientists of other disciplines.

The stay of the water in different forms of the hydrological cycle is very variable. The mean time that water stays in the atmosphere is about one week, for streams or rivers it is several

days, in the oceans about thirty centuries and from centuries to the millenaries in the big aquifers.

At watershed level the hydrological cycle can be described in a mathematical form by the water balance equation. The main source is precipitation (P), the sinks are evapotranspiration (E), run off (Q), infiltration (I) and storage ( $\Delta S$ ). Depending on the time scale the storage term can be neglected for the West African context.

$$P - E - Q - I = \Delta S \quad (1.1)$$

The individual terms of this equation can be divided again into different sub processes depending on the actual application (compare figure 1.2). The terms of the water balance equation are affected by different geographical and climatic parameters. For example the relief is partly conditioning the precipitation and vegetation cover together with soil moisture influences evapotranspiration.

#### **1.4 Land-atmosphere interface**

In a similar way as the water budget, an energy budget can be established for a certain area based on the fundamental law of energy conservation. It is usually expressed as surface energy balance (SEB) equation (e.g. Meyers and Hollinger 2004; Stull 1988), which can be formulated as follows:

$$H + LE + G + S_p + S_g + S_c - R_n = 0 \quad (1.2)$$

where net radiation ( $R_n$ ) is balanced by the sum of sensible heat flux (H), latent heat flux (LE), and soil heat flux (G), in addition to the energy fluxes for photosynthesis ( $S_p$ ), canopy heat storage in biomass and water content ( $S_c$ ), and soil heat storage above the soil heat flux plate ( $S_g$ ). The surface energy balance equation describes the interaction of many processes occurring at the land atmosphere interface. As long as equation 1.2 contains all relevant terms the conservation of energy requires instantaneous closure. For many situations it is assumed that storage terms can be neglected, which leads to a more simple form of the SEB. It states that the net radiation over the area equals the sum of latent heat flux (energy for evapotranspiration), sensible heat flux (energy for direct heating of the air from the warmer ground) and heat storage in the ground. The partition of energy between sensible and latent

heat flux depends to a large degree on the availability of energy and water. Due to the fact that each component is partly determined by the others, this simple-looking equation is quite complicated.

For all relevant scales in time and space the water balance equation, describing the hydrological cycle, and the surface energy balance, building the interface to the atmosphere, are closely connected through actual evapotranspiration or latent heat flux (compare equation 1.1 and 1.2). The division in time and space depend on the analyzed process or event. The time scale starts at seconds or minutes and ends at months or years, where the diurnal time scale and the seasonal time scale are the most important. For the division in space one possibility in meteorology is the division in microscale, mesoscale, synoptic scale and climatological scale. The connection between the scales of hydrological processes for the atmospheric and the hydrological domains in time and space are shown in figure 1.3. The question how to parameterize the involved processes between the hydrological and the atmospheric domain is discussed in the next section.

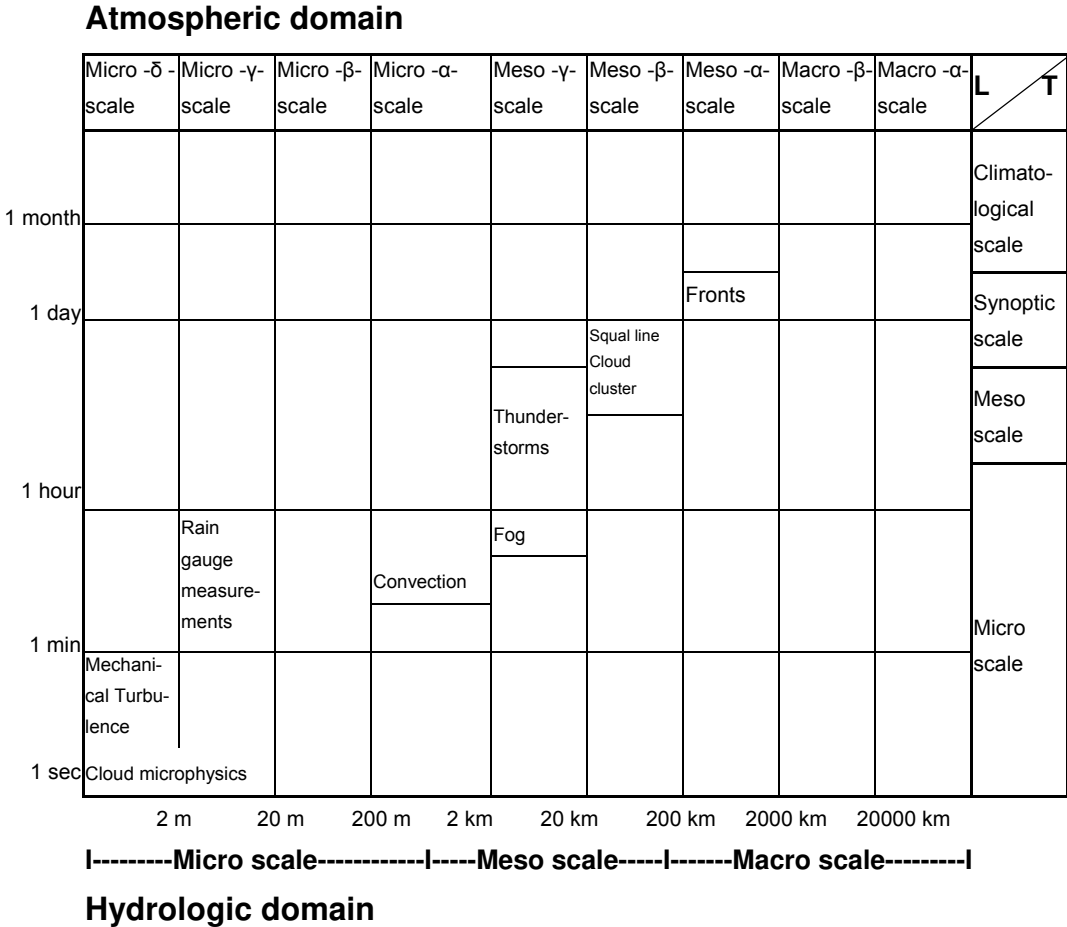


**Figure 1.3: Time and space scales between the atmospheric and hydrologic domain. (Courtesy by Mölders, 1999).**

## 1.5 Land-atmosphere parameterizations

Figure 1.4 illustrates the interaction between the soil and the overlying atmosphere. A complete cycle of a wet period followed by a dry period is shown. Here again the interactions are described following the idea of Horton, based on the work of Dooge (1992) and Viterbo (2002).

Starting with a long period of rainfall at point A the soil is wet and its drying is controlled by the ongoing evapotranspiration. As long as there is enough water in the soil, the ongoing evapotranspiration is determined by the atmospheric moisture content at the near surface and the amount of energy available for the evapotranspiration. As soon as soil moisture drops under a certain value (point B) the evaporation is limited by plant or soil physiological mechanisms. At that point the actual evapotranspiration drops below the optimal evapotranspiration. If there is rain again (point C) infiltration will equal precipitation. From a certain point onwards (depending on the actual soil type) the soil is saturated and some rain goes into runoff. Every land surface scheme should be able to model those processes correctly.

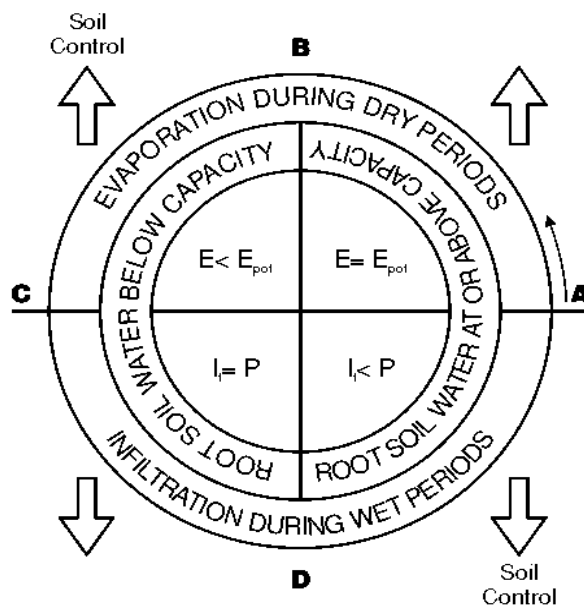


**Figure 1.4: Illustration of the interaction between the land surface and the atmosphere (Dooge 1992, courtesy by Viterbo, 2002).**

During the last decades large efforts have been taken to parameterize the described processes at the land surface. The bucket model (Manabe 1969) was the first attempt. The available

water at the surface was described by precipitation minus interception with a single reservoir of water (bucket). The available water was split into runoff and evapotranspiration. The actual evapotranspiration was described as the product of evaporative fraction  $\beta$  times the potential evaporation, where  $\beta$  was calculated by the actual amount of water in the reservoir and its maximum capacity. As soon as the maximum capacity was reached, runoff was generated.

The next generation took the transpiration of vegetation into account by introducing a stomatal conductance (Monteith 1965), which was scaled up from a single leaf to one canopy conductance (big leaf approach).

Jarvis (1976) related the canopy conductance to empirically derived relations of hydrological and atmospheric variables like incoming solar radiation, air temperature, humidity and a measure of water in the soil.

In situations where the structure of the vegetation becomes more complex with high and low vegetation and a bare soil fraction, like the West African Savanna, the big leaf approach is no longer suitable to describe land surface processes. Deardorff (1978) developed a parameterization, which split the energy balance into a vegetation component and a bare soil component. It was the first Soil-Vegetation-Atmosphere-Transfer (SVAT) model used in large-scale meteorological models (Van den Hurk 1995). Various models, developed later, used this approach as a basis for more detailed description of the processes involved in the hydrological cycle.

Another major step for more realism in complex vegetation structures was the use of multiple soil layers to deal with soil moisture as a major source for evapotranspiration. The available water at the surface infiltrates into the different layers, where only deeper roots can make use of it. This leads to a distinction into low and high vegetation covers in numerous models (e.g. Viterbo and Beljaars 1995).

Nowadays new ideas exist concerning the parameterization of transpiration, which are related to plant physiology (Jacobs 1994; Ronda et al. 2001). Those approaches take the physical processes inside the plant into account and could be more suitable for climate impact studies, as compared to the statistical-empirical functions (Ronda et al. 2002).

## **1.6 The GLOWA-Volta project**

To deal with regional water resource management with the background of climate change and its impacts on the hydrological cycle in the Volta basin, West Africa one of the five GLOWA projects (GLOWA-Volta) was established. The GLOWA-Volta Project, ‘Sustainable Use of Water Resources: Intensified Land Use, Rainfall Variability, and Water Demands in the Volta



Basin', has the stated goal of creating a scientifically sound decision-support system (DSS) for the assessment, development and sustainable use of water resources by means of an integrated model of the basin (Van de Giesen et al. 2001). The decision support system depends on the input from many different scientific disciplines and can provide a formal means of communication between scientists and stakeholders at a regional scale. The project was designed to be interdisciplinary and to focus on a continuing process of regional assessment and not on a snapshot of current conditions. With the exception of the interfaces, the different models used for the DSS should be independent enough to be developed, calibrated, verified and tested individually. The DSS should aid the authorities in the Volta basin to optimize water allocation within the basin. The art of water allocation is to account properly and equitably for the various economic development interests of the region while insuring that the ecosystems that depend on this resource are not threatened (GLOWA-Volta ANNUAL REPORT 2001). This should be done with the recognition that water availability may change under changing global climate conditions (<http://www.glowa.org>). One of the main scientific ambitions is to let the boundaries of the models used within the DSS coincide with physical boundaries of the Volta watershed and not to depend on ad hoc assumptions about population growth, land use change, rainfall variability or hydropower demand (GLOWA-Volta ANNUAL REPORT 2001).

The integration of climatic, ecological and socio-economic factors and correlations with respect to the hydrological cycle is the main scientific challenge within the GLOWA-Volta project. For the natural science precipitation, turbulent energy fluxes and land use act as key components of that integrated model. The integration within the project concerns the interaction between the land surface and the atmosphere. In figure 1.5, the large number of intersecting arrows represents these atmosphere/surface interactions (GLOWA-Volta ANNUAL REPORT 2001).

The proposed Decision Support System (DSS) for the Volta Basin will, *inter alia*, consist of a coupled operational meteorological and hydrological hindcasting system that includes assimilated satellite data and operationalized ground measurements. Those features allow basin wide estimation of water and energy balance (GLOWA-Volta Project proposal 2002). For the hindcasting system a proper parameterization of the involved processes is required. To explore those processes and parameterizations both empirical and numerical simulations are made within the project.

For the purpose of calibration and evaluation of the individual parameterizations in natural science, by accounting for the large variability of the West African climate during the year, three test-sites (Ejura, Tamale and Navrongo, see also figure 2.1) along the climatic gradient running north-south were established in 2001. Ejura belongs to latitude band 7 - 8 degree

north, Tamale belongs to latitude band 9 - 10 degree north and Navrongo is on the edge of 10 - 11 degree north (compare figure 1.1). The stations are at a mutual distance of about 100 - 200 km. Tamale is the central station. Each of these sites was considered representative for larger areas and was chosen taking the different geographical and climatological parameters influencing the hydrological cycle into account. For a more detailed description of the individual sites and measurements taken, we refer to section 2. 2.

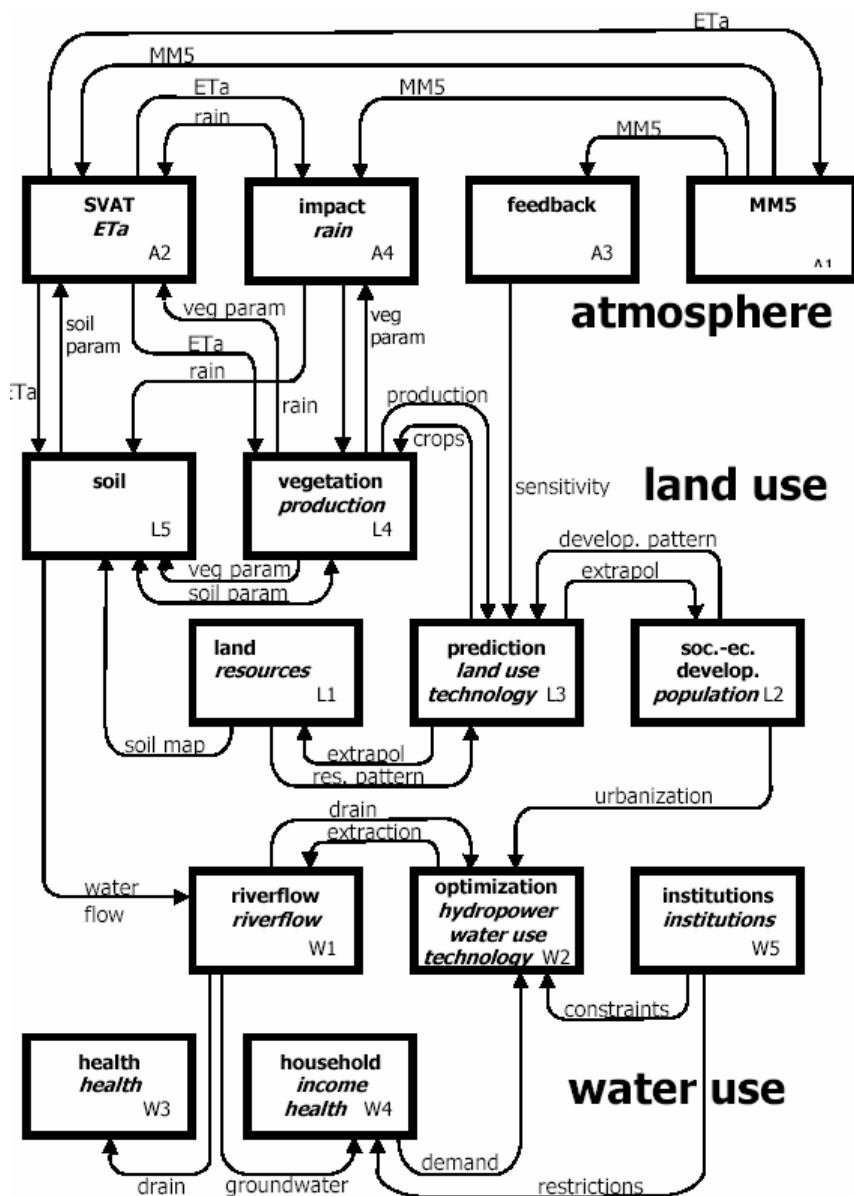


**Figure 1.5: Overview of the GLOWA-Volta project structure with sub-projects.  $E_{ta}$  and  $T_a$  represent the actual evapotranspiration and actual temperature. MM5 represents the PSU/NCAR mesoscale model.**

## 1.7 Research question and organization of the thesis

At the present time, there is only little knowledge about the diurnal and the seasonal development of land surface interactions in the concerned region. Furthermore point observations suitable for homogenous surfaces are not always applicable when measuring over mixed formations of grass, woody plants and bare soil. Therefore the calibration and evaluation of individual models within the DSS require new research strategies for the heterogeneous surfaces in West Africa.

Large aperture scintillometers (LAS) were installed in each of the three experimental watersheds to measure directly the sensible heat flux ( $H$ ) over distances of more than two kilometers. The advantage of the LAS technique is that areally-averaged sensible heat flux can be obtained (up to scales of 5000 m), and its robustness, which makes it suitable for long-term measurements in that kind of environment. By measuring soil heat flux and net radiation, latent heat flux can be calculated as the remaining term in the energy balance (compare equation 1.1 and 1.2).

The key instrument (LAS) together with the other measurements for the components of the energy balance is then utilized to validate the land surface parameterization being part of the operational meteorological and hydrological hindcasting system within the DSS. Effective parameters for the soil and vegetation parameters of the local land use types at the three test sites have to be determined also taking the seasonal changes of those parameters into account. In this context the question has to be answered if the effective parameters are robust enough to be applied for the whole basin. Furthermore it is important to consider the subgrid scale heterogeneity resulting in a better reproduction of the observed circumstances. Besides the evaluation and calibration on a local level, new ideas are required for a basin wide evaluation of important components of the surface energy within the hindcasting system. The central objectives of this thesis are:

- To analyze measurements by exploring the strengths and the weaknesses of the used approach also in comparison to different measurements techniques;
- To test the response of current parameterizations for the surface conductance during the time of transition for diurnal and seasonal time scales;
- To find the optimal land surface parameterization by evaluating two different approaches;
- To optimize a parameterization by using a factorial design, which takes care of main and interaction effects;

- To apply a factorial design at two contrasting sites to test the robustness of important parameters;
- To utilize the gained knowledge from the previous objectives and to develop a simple and robust satellite algorithm to obtain areal averaged evaporation for larger areas.

The thesis is composed of 6 chapters. The named objectives will be investigated in chapter 2 to 5. In chapter 6 the overall results are summarized and perspectives for required work in the future are pointed out.

In chapter 2 the measurements obtained during an intensive observation period (IOP) are analyzed. The IOP took place from the beginning of October until the end of December 2002. The LAS measurements are compared to Eddy-covariance measurements and first ideas of suitable parameterizations are discussed with a focus on the diurnal and seasonal cycle.

Chapter 3 makes use of the measurements during a seasonal cycle from 2002 to 2003 to find the most suitable land surface scheme for the region by taking subgrid variability into account.

In chapter 4 the results of chapter 3 are utilized to apply changes to a land surface scheme and explore the sensitivity of parameter used during a seasonal cycle. Here the seasonal dependence of parameters needed for the different test sites is discussed. Additionally it is investigated if the parameters are robust enough to be applied for the whole Volta basin. Furthermore possible alternatives for the land surface scheme used are discussed.

Based on the results of the previous chapters, chapter 5 introduces first ideas how to obtain basin wide evapotranspiration as a key component of the DSS and the connecting variable of the water and energy balance. A simple satellite based algorithm for estimating actual evaporation based on Makkink's equation is utilized and it is shown that it is possible to monitor evaporation with small errors for the three test sites on a seasonal basis.

In chapter 6 the overall results are discussed and suggestions for future work are given.

## **Chapter 2**

### **Surface fluxes and characteristics of drying semi-arid terrain in West Africa**

---

Material in this chapter is conditionally accepted for Boundary Layer meteorology with A.F. Moene, A.A.M. Holtslag, H.A.R. De Bruin and N. van de Giesen as co-authors.

## **Abstract**

This study examines the seasonal cycle of the components of the surface energy balance in the Volta basin in West Africa as part of the GLOWA-Volta project. The regional climate is characterized by a strong north-south gradient of mean annual rainfall and the occurrence of pronounced dry and wet seasons within one annual cycle, causing a strong seasonal variation in the natural vegetation cover. The observations are conducted with a combined system, consisting of a Large Aperture Scintillometer (LAS) for areally averaged sensible heat flux, radiometers and sensors for soil heat flux. For comparisons the eddy-covariance (EC) method providing the fluxes of momentum, sensible and latent heat fluxes is utilized as well. The measurements of a seasonal cycle in 2002/2003 were gathered including the rapid wet-to-dry transition after the wet season at two locations in Ghana, one in the humid tropical southern region and one in the northern region. A direct comparison and the energy balance closure of the two methods are investigated for day- and nighttime separately. An attempt is made to understand and explain the differences between the two methods and the closure of energy budget found for these. It is found that the two systems correspond well during daytime. During nighttime the LAS seems to perform more realistically than the EC system. Considering the fact that a LAS-system is much easier to use in the climate conditions of the Volta basin, it is concluded that the LAS approach is very suitable in this type of climate conditions. Surface conductances are estimated by rearranging the Penman-Monteith equation and compared to a Jarvis-type model optimized for savannah conditions. It is found that temperature dependence should be included in the conductance formulation in contrast to earlier findings. Based on the findings the gathered data set can be used for further model studies of the climate and environment of West Africa.

## 2.1 Introduction

It is widely recognized that the parameterization of land surface processes, in particular the way energy is partitioned at the earth's surface, highly determines the performance of regional weather and climate models. Since the parameterization schemes in those models are - essentially - semi-empiric, there is a strong need to validate and to calibrate these schemes with experimental data. During the last decade large efforts have been made to establish accurate micrometeorological measurements of energy balance flux components at longer time scales to tackle that need, see for example EFEDA (Bolle et al. 1993) or FLUXNET (Baldocchi et al. 2001). However, there still is a lack of data for numerous ecosystems like the semi-arid regions in West Africa. This is important, because nearly one fifth of the world's population lives in semi-arid regions covered with savannah type vegetation (Solbrig et al. 1996) and those regions, especially in West Africa, have been and will be subjected to pressure resulting from human activities. Furthermore recent research has revealed that the current parameterizations schemes applied to the landscapes in West Africa require improvements. See for instance the African Monsoon Multidisciplinary Analyses (AMMA) project (<http://medias.obs-mip.fr/amma>).

The main vegetational characteristics in the West African landscape are humid tropical regions like the equatorial forests in the South, an intermediate zone with semi-humid areas as the Guinea savannah and a northern region with mainly fallow savannah.

In the past, several projects have been performed yielding information on energy balance flux components in the more northern Sahel region like SEBEX (Wallace et al. 1992) with a focus on the annual cycle. Another example is HAPEX-SAHEL, which took place in 1992 for three months (Goutorbe et al. 1994). Verhoef et al. (1996a) discussed various influences like water vapor pressure deficit (VPD) and soil water content on the surface fluxes in this context.

For the more southern region including the Volta basin there is still a lack of data. The Volta basin is located in the intermediate zone and the southern part of West Africa. It comprises an area of about 400.000 km<sup>2</sup> and is considered as one of the benchmark watersheds for Africa (<http://www.cgiar.org/iwmi/challenge-program>). The present study describes measurements, which are part of long-term observations of the water- and energy balance in Ghana in the Volta Basin. This is done in the context of the GLOWA-Volta project (Global Change in the Hydrological cycle). The GLOWA-Volta Project, 'Sustainable Use of Water Resources: Intensified Land Use, Rainfall Variability, and Water Demands in the Volta Basin', has the goal of creating a scientifically sound decision-support system (DSS) for the assessment, development and sustainable use of water resources by means of an integrated model of the basin (Van de Giesen et al. 2001).

We regard turbulent energy fluxes (sensible and latent heat flux) as key components of that integrated model and since usually a model is only as accurate as the measurements used for its validation, one of the first steps is to analyze the measurements made. Certain techniques exist to measure turbulent energy fluxes as the two main components of the energy balance at the land surface. For the above-mentioned studies in the more northern region only standard methods suitable for homogenous surface (point observations) were used. Unfortunately, the climatic and environmental conditions in West Africa are not favorable to apply standard methods of observation. For instance, the savannah surface type is spatially inhomogeneous and its structure changes seasonally due to the pronounced existence of dry and wet periods. For that reason, there is a need for non-standard methods of observation which yield spatially averaged measurement of the energy balance term and which are suitable for long-term operational application in the West African landscape and climate.

It is worthwhile to test scintillometry for example proposed by De Bruin et al. (1995) for sparse vegetation in Spain.

Therefore it is the objective of this study to investigate the applicability of a large aperture scintillometer to determine the spatially averaged flux of sensible heat and, indirectly, the spatially averaged evaporation. The advantage of the LAS technique is that areally-averaged sensible heat flux can be obtained (up to 5000 m), and its robustness, which makes it suitable for long-term measurements in that kind of environment. For this purpose three test sites have been equipped with LAS along the climatic gradient running north-south. The first focus in this study is on the applicability of the LAS in comparison with the EC method. The agreement between both sensors should also increase the confidence in the gathered data for further applications.

With this background the second focus is on analyzing the conservation of energy. The conservation of energy is usually expressed as energy balance closure, which can be formulated as follows:

$$R_n = H + LE + G \quad (2.1)$$

$R_n$  is net radiation,  $H$  is sensible heat flux,  $L$  the latent heat of vaporization,  $E$  the moisture flux and  $G$  is the soil heat flux. Theoretically the conservation of energy requires instantaneous closure for day and nighttime. In practice energy balance closure can be biased up to 30% during daytime, during nighttime even higher (Wilson et al. 2002), which normally goes along with a negative bias. In a lot of situations the closure is enhanced over homogenous terrain and short vegetation (Mahrt 1998; Twine et al. 2000). The reasons for the



nonclosure are manifold and not always known. General hypotheses state sampling errors, systematic bias in instrumentation, neglected energy sinks, loss of low and/or high frequency contributions to the turbulent flux and neglected advection of scalars (Wilson et al. 2002) as potential sources of errors. In many situations two terms of the energy balance (net radiation and soil heat flux) are point measurements, which give different source areas for all components of the energy balance. Especially soil heat flux is often treated improperly, neglecting or underestimating heat storage between the soil heat flux plate and the surface. If it is not properly measured or adjusted it can cause errors up to  $100 \text{ W m}^{-2}$  (Heusinkveld et al. 2004). Due to the mentioned reasons the energy balance closure is also a common tool to test the quality of turbulent energy flux data (Lamaud et al. 2001; Foken and Wichura 1996).

Furthermore there is a need for a better understanding of the processes, which control evapotranspiration due to seasonal dynamics (Viterbo and Beljaars 1995). Therefore the third focus is on obtaining a better knowledge of the changes in surface conductance during the chosen time period. The surface conductance is estimated from Penman-Monteith equation (Monteith 1981) and compared to a Jarvis-type model (Jarvis 1976) based on the findings of Dolman (1993) and Huntingford et al. (1995), who optimized the model for Savannah conditions. The concept of obtaining surface conductance from Penman-Monteith equation has the potential to model water vapor exchange (Harris et al. 2003) and evaluate evaporation rates correctly (Baldocchi et al. 2004), when conservation of energy is achieved. The relationship between the surface conductance and the driving variables (radiation, vapor pressure deficit, temperature and soil moisture) throughout the time of transition might help in evaluating and validating surface fluxes obtained by regional weather and climate models.

In summary the objectives of this study are:

- To analyze the available data in order to set up a reference data set, suitable for atmospheric and hydrological modeling studies;
- To evaluate the differences of turbulent energy fluxes between LAS and EC based measurements under different meteorological conditions and surface types within the context of the closure of the energy balance.;
- To evaluate the concept of aerodynamic and surface conductances with different surface types and changing meteorological situations.

The experimental setup, including a site description as well as a description of the LAS and EC technique, is given in section 2.2. Section 2.3 describes the comparison of LAS and EC derived turbulent fluxes. In section 2.4 the evaluation of the energy balance closure is

presented. Section 2.5 provides the evaluation of the surface conductance. Each of the different sections includes a discussion of the outcome at the test sites. Finally the major conclusions are reviewed in section 2.6.

## 2.2 Experimental Setup and Observations

The climate system in West Africa is to a large extent controlled by the meridional movement of the intertropical convergence zone (ITCZ) during the year, the African Easterly Jet (AEJ) and pressure disturbances, which traverse from east to west across Africa (Burpee 1972). They all act under the influence of the Hadley and Walker cell circulation. Those mechanisms lead to a pronounced wet and dry season during the year, of which the length depends on the actual latitude. During the time of the year when the wet period ends and the dry period starts (time of transition) the contrast between dry and moist air is probably more pronounced in time and space than anywhere else (Hólm et al. 2002). To account for the large variability during the year three test-sites (Ejura ( $7^{\circ} 20' N$ ;  $1^{\circ} 16' W$ ), Tamale ( $9^{\circ} 29' N$ ,  $0^{\circ} 55' W$ ) and Navrongo ( $10^{\circ} 55' N$ ;  $1^{\circ} 02' W$ ), figure 1) were established in 2001 and are operational since then. The distance between the stations is about 100 - 200 km. Tamale is the central station. In the present study only data from Ejura and Tamale are analyzed.

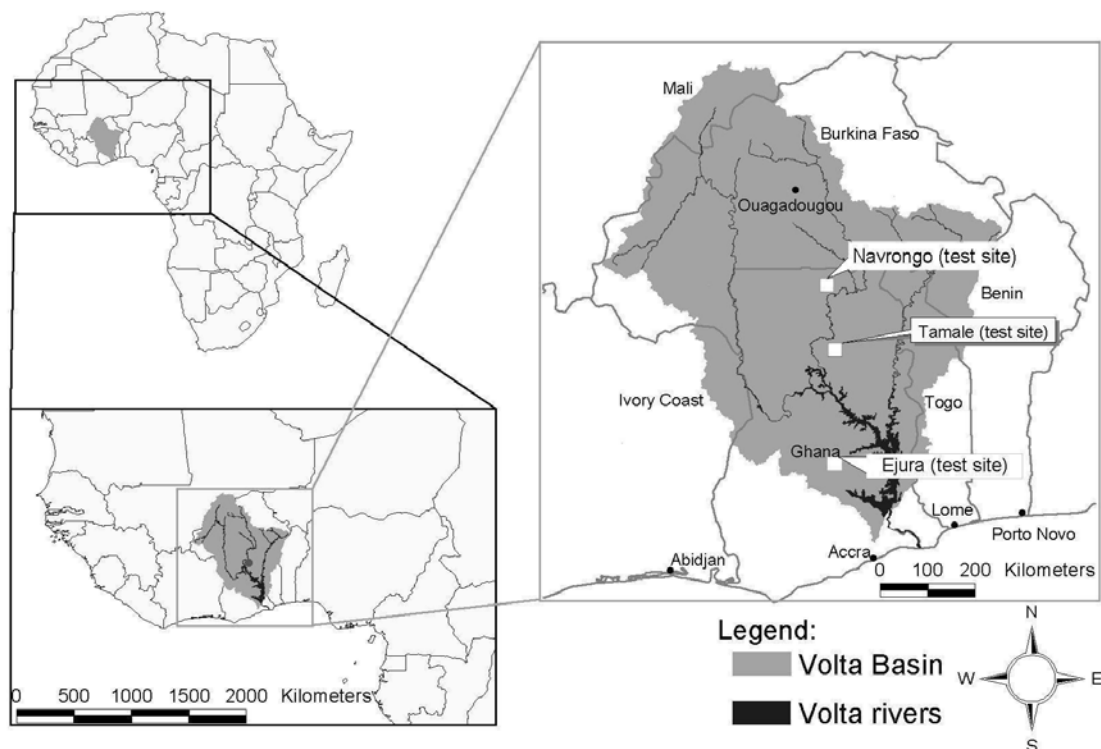


**Fig. 2.1: Location of experimental sites in Ghana within the GLOWA-Volta project (Courtesy by Friesen 2002).**

The annual mean temperature for the three sites varies from the most southern site Ejura (26.6 °C) over Tamale (27.8 °C) to Navrongo (28.2 °C). The annual mean precipitation, which is one of the driving forces for surface fluxes during the rainy period, varies from 900 – 1500 mm, where more than 95% of the rain occurs during the rainy season. The mean annual rainfall at the sites is 1432 mm in Ejura, 1082 in Tamale, and 1043 mm in Navrongo (FAO 1984, including data from 1930 to 1980). For 2002 there is a large difference in precipitation between the research sites. In figure 2.2 daily sums of precipitation are shown for the test sites. For Ejura the yearly sum is 1420 mm. For Tamale it is 1065 mm and for Navrongo the total precipitation in 2002 is 890 mm. The rain events show a relatively regular pattern for all test sites.

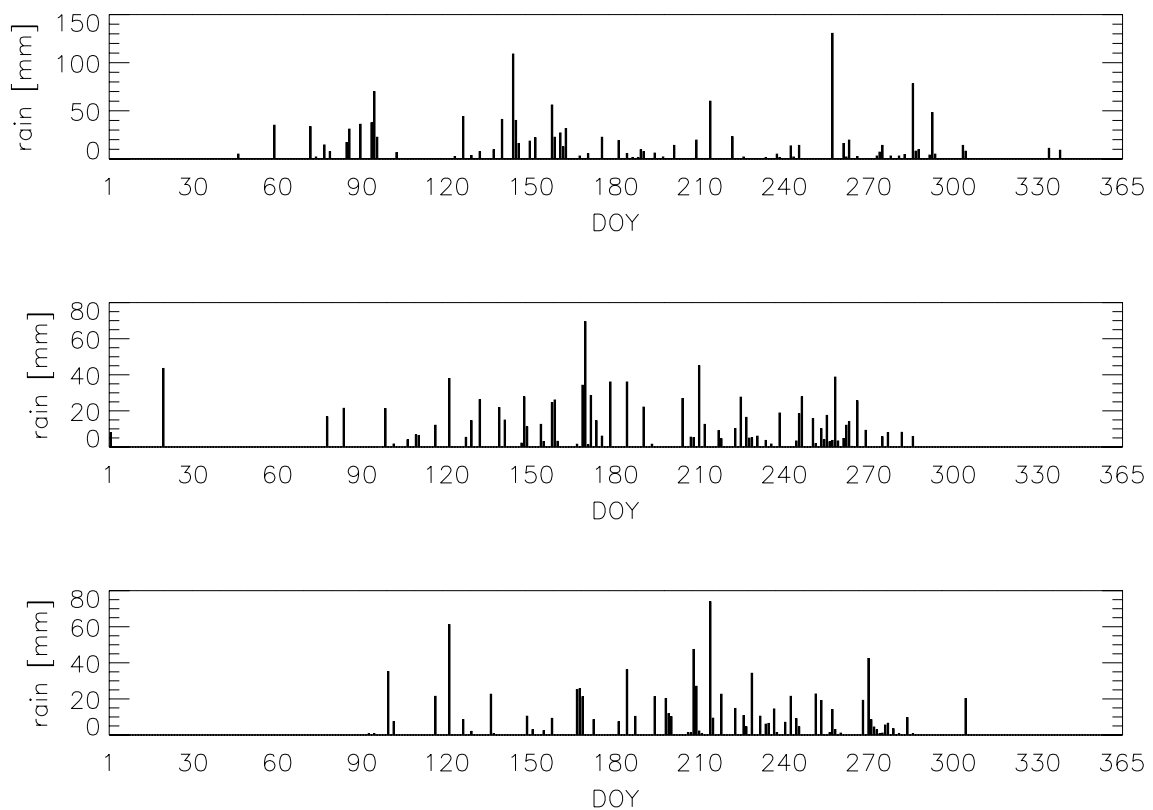


**Fig. 2.2: Daily sums of precipitation for the three test sites in Ejura (top), Tamale and Navrongo (bottom) in 2002.**

The onset of the rainy period for 2002 is estimated to day of year (DOY) 74 for Ejura and DOY 118 for Tamale and Navrongo. The offset is estimated to DOY 343 in Ejura and 290 for Tamale and Navrongo. This is done using the method of Kasei (1988). Malda (personal communication, 2002) analyzed 40 years of precipitation for different stations in the Volta basin and found that the average onset for Ejura was DOY 78 with a standard deviation (SD) of 30 days. For Tamale it is DOY 115 (SD = 20) and Navrongo it is DOY 131 (SD = 19).

Furthermore no long-term trend could be found in his analyses. For the year 2002 the precipitation measurements and the analysis for the length of the season show that the total amount of rain and the length of the season are normal.

### 2.2.1 Meteorological measurements

All sites are equipped with automatic weather stations (AWS), which measure temperature, humidity and incoming solar radiation at a reference level,  $z = 2$  m. Wind speed and direction are measured at eight-meter height. Net radiation is measured directly and calibrations are wind speed corrected, due to the design of the NR-Lite (Kipp and Zonen). Additionally, surface observation for soil heat flux at 0.035 m depth, precipitation, soil moisture at different depth, surface runoff using runoff plots and runoff at the outlet of each watershed using a flume or a weir are collected. Type and brand of the instruments used are described in table 2.1.

**Table 2.1: Instrument used for this study at the two test sites.**

Variable	Location	Instrument
Air Temperature	2 m	50Y Temperature and RH probe (Vaisala)
Relative Humidity	2 m	50Y Temperature and RH probe (Vaisala)
Atmospheric pressure	Inbox	PTB101B Barometric Pressure Sensor (Vaisala)
Wind Speed	8 m	A100R Anemometer (Vector Instruments)
Wind Direction	8 m	Wind vane (Ecotech)
Net Radiation	8 m	NR-LITE (Kipp & Zonen)
Downward solar radiation	2 m	SP-LITE (Kipp & Zonen)
Precipitation	2 m	Tipping bucket (Stelzner)
Sensible heat Flux	10.0 m Site dependent	CSAT3 Sonic anemometer (Tamale), Windmaster Pro (Gill) (Ejura), Large Aperture Scintillometer (LAS) (Manufactured by Wageningen Uni.)
Latent Heat Flux	10.0 m	CS7500 infrared hygrometer (Li-Cor) (Tamale), KH2O Krypton hygrometer (Campbell) (Ejura) Residual of the energy balance
Soil Heat Flux	0.035 m	HFP01 Heat Flux Plate (Hukseflux)
Soil Temperature	Different depth	PT <sub>100</sub> resistance thermometer (Manufactured by Wageningen Uni.)
Soil moisture	Different depth	TDR (Campbell) (Tamale), TDR (Delta-T) (Ejura)

All quantities are originally averaged for ten-minute intervals. Data availability exceeds more than 90% for most of the measurements for all three sites during the year 2002.

The soil heat flux is measured by applying the method of Heusinkveld et al. (2004), whereby the conventional sensor is moved to a location just below the surface and compared to the analysis of the temperature wave propagation into the soil. This added 30 to 40% of soil heat flux at 0.035 m depth on average. Since soil temperature measurements are available in Tamale only, the method is applied there and should be of smaller importance in Ejura due to the fully vegetated surface (daytime: 5–15% of  $R_n$ , night time: 50% of  $R_n$ ) (Stull 1988).

Soil heat flux plates should have a thermal conductivity similar to the soil, but the conductivity may vary due to changes in soil water content and temperature (Verhoef et al. 1996b). For Tamale there was no precipitation during the IOP and for Ejura this is valid for most of the time during the IOP, so the impact due to rainfall should be small.

Additionally sap flow, albedo, leaf area index and tree density data are collected. A survey for soil properties was done in Tamale and Ejura (Agyare 2004). The following data on soil diagnostics were collected: horizon, texture, color, structure, and presence of mottle, roots, and concretions from 0 – 0.15 m and 0.30 – 0.45 m depths.

Soil moisture deficit  $\Theta$  (mm) is calculated by subtracting interpolated moisture contents from the maximum field capacity of the upper and lower soil type, which is calculated from the soil diagnostics based on the work of Schaap et al. (1998).

### 2.2.2 Flux measurements with Scintillometry

The LAS consists of a transmitter emitting electromagnetic radiation towards a receiver. The distance between both can be chosen up to 5000 m for a beam diameter of 0.15 m. In our case the distance varies between 1040 – 2420 m for the different sites. It is installed at a certain height above the surface. The emitted radiation is scattered by the turbulent medium in the path. The variance of intensity of received radiation is proportional to the structure parameter of the refractive index of air ( $C_n^2$ ). At the wavelength used (940 nm) the refractive index mainly depends on temperature, so  $C_n^2$  is mostly determined by temperature fluctuations ( $C_T^2$ ),

$$C_T^2 = C_n^2 \frac{T^2}{A_T^2} \left( 1 + \frac{A_q}{q} \frac{T}{A_T} \frac{c_p}{L_v} \beta^{-1} \right)^{-2} \quad (2.2)$$

$$A_T = T \frac{\partial n}{\partial T} \quad \text{and} \quad A_q = q \frac{\partial n}{\partial q}$$

which are both dependent on optical wavelength, pressure, temperature and humidity content.  $T$  is the mean air temperature and  $q$  is the mean specific humidity,  $c_p$  is the specific heat of air at constant pressure and  $L_v$  is the latent heat of vaporation. The last factor at the right-hand-side of equation 2 reflects an estimate of the influence of humidity on the refractive index (Wesely 1976; Moene 2003). Here  $\beta$  is estimated as follows:

$$\beta = \frac{H_{LAS}}{R_n - G - H_{LAS}} \quad (2.3)$$

Sensible heat flux is calculated from  $C_T^2$  (Obukhov 1960) by using the following expression:  $H_{LAS} = \rho c_p u^* \Theta^*$  with  $u^*$  being the fiction velocity and  $\Theta^*$  being the temperature scale from Monin-Obukhov similarity theory (MOST). In this study a standard Businger–Dyer flux-profile relation is utilized for estimating  $u^*$  from wind speed and roughness length and  $H_{LAS}$  is calculated iteratively.

Stability functions proposed by Wyngaard (1973) are used for daytime values. For nighttime values we follow the formulation of De Bruin et al. (1993). Several tests are made for the use of different stability functions for day and nighttime situations. In general the results are steady and differ at most 10%, but especially during nighttime, the formulation of De Bruin gives the most reliable results. For a more detailed description of the LAS theory and its applications see for example De Bruin et al. (1995) and Meijninger et al. (2002).

The LAS at each site is installed on top of two opposite hills using towers with a minimum height of 5 m. The setup with small differences in installation height of transmitter and receiver and changes in terrain height along the path implies that the height of the beam above the terrain varies along the path. The effective height is calculated using the method of Hartogensis et al. (2003) using the fact that the LAS signal is weighted towards the middle of the path. For both sites the orientation of the optical path is perpendicular to the prevailing wind direction (compare figure 2.5).

Latent heat flux is calculated as a residual from the energy balance (equation 2.1) with the help of the LAS measurements:

$$LE_{LAS} = R_n - H_{LAS} - G \quad (2.4)$$

### 2.2.3 Intensive observation period 2002

Two test sites (Ejura, Tamale) were specifically instrumented with EC systems for an intensive observation period (IOP). The period examined in Tamale started at DOY 307 and ended at DOY 349 in 2002. In Ejura it started at DOY 313 and ended at DOY 28 in 2003. In Tamale additional measurements were taken for soil heat flux and soil temperature at different depths, skin temperature and additional radiation measurements.

Both periods include the transition from wet to dry, with an increase in temperature and vapor pressure deficit. Although the instrumentation of the sites in Ejura and Tamale differed (in terms of sonic anemometers, humidity sensor and sampling frequency), the processing of the EC data was identical for both sites (see table 2.1 for an overview of the instrumentation). From the raw data (20 Hz sampling at Tamale, 10 Hz sampling at Ejura) half-hourly fluxes have been computed taking the following corrections into account:

- The raw data have been linearly detrended;
- The mean signal of the Krypton hygrometer has been adjusted using the humidity measurements of a slow-response sensor);
- Axis rotation using the planar fit method, with planar fit angles determined on a daily basis (see Wilczak et al. 2001). The bias in the vertical velocity was set to zero;
- Sonic temperatures were corrected for humidity (see Schotanus et al. 1983);
- The oxygen-sensitivity of the Krypton hygrometer was corrected for using the coefficients found by van Dijk et al. (2003);
- Corrections for frequency response and path averaging according to Moore (1986);
- The Webb-term for the water vapor flux has been taken into account (see Webb et al. 1980).

More details and software can be found at <http://www.met.wau.nl/projects/jep>.

### 2.2.4 Site description

The site in Ejura is characterized by dense vegetation and a short dry period. The landscape is hilly. The transmitter and the weather station are located in a cashew orchard. The receiver is located at the edge of a forest. The length of the path in between is about 2030 m. The weighted effective height of the LAS is 30.1m. It is a heterogeneous terrain. The area between the transmitter and the receiver can roughly be divided into two parts. On the transmitter side the vegetation consists of cashew trees with a maximum height of 4 m and in between maize and grass with a maximum height of 2 m. On the receiver side there are bushes and trees and

small swamps, but nearly no agriculture. The EC system was installed nearly in the middle of the path of the LAS, but still in the orchard.

The research site in Tamale is mainly characterized by grassland with scattered trees (cover about 15%), with a maximum height of five to eight meters and a large dry period. The landscape is slightly hilly. LAS transmitter and receiver are installed on two hills with a distance in between of about 2420 m. The weighted effective height of the LAS was estimated to 19.5 m. The automatic weather station is installed next to the receiver of the LAS. The EC system was installed nearly in the middle of the path.

### **2.2.5 Methods**

In the current study data from the years 2002/2003 are analyzed. The main focus is on the time of the year, when the monsoon period is ending and the time of transition starts. For all further evaluations the surface fluxes are calculated on half hourly basis. All other measurements are also averaged on that basis. The analyses are made with the background of dividing into day- and nighttime values to overcome the problem of overestimating positive fluxes during the day and underestimating negative fluxes at night (Mahrt 1998). Another reason is the use of different stability functions to calculate sensible heat flux from LAS measurements during unstable and stable situations. To divide into day- and nighttime a simple criterion is chosen. When measured net radiation minus soil heat flux is positive the value is taken as a daytime value, when it is negative or equal zero it is considered as a nighttime value. This shows good correspondence with the daily cycle of the  $C_n^2$  signal from the LAS measurements.

### **2.3 Comparison of LAS and EC derived sensible and latent heat flux**

For the comparison of the LAS to the EC derived sensible heat flux a linear regression is done. The linear regression is done using a least absolute deviation technique (Birkes and Dodge 1993). This method is chosen because of its lower sensitivity to outlying data. Regression coefficients for sensible heat flux of LAS-data against EC-data for all half hour values are calculated as  $H_{LAS} = a + b * H_{EC}$ . The results also include a linear regression forced through the origin (zero intercept). Additionally correlation coefficient and bias corrected root mean square error (RMSE) are calculated. For latent heat flux the same procedure is followed. For Ejura data are divided into two periods. During the first period the prevailing wind direction is southwest, in the second period the wind direction changes more to the East. This change has a major impact on energy balance closure (compare section 2.4.1).



In figure 2.3 it is shown that sensible and latent flux from the EC system are very small during nighttime. Furthermore, during nighttime the footprint of the LAS in upwind direction is on average four times larger compared to the EC footprint. Especially for Ejura the results are very poor (highest  $R^2 = 0.1$ ). Therefore the analyses are restricted to daytime values. The bad results for nighttime situations at Ejura test site might be explained by the influence of the complex terrain, resulting in a flux which is not constant with height, and nighttime gravitational flow. Since there were no measurements at different heights, this could not be confirmed.

**2.3.1 Sensible heat flux**

Figure 2.3 shows a time series of ten days for LAS and EC derived sensible heat flux for both sites. During daytime both sensors show comparable results for H. During nighttime sensible heat flux is higher for most of the nights for the LAS based measurements.

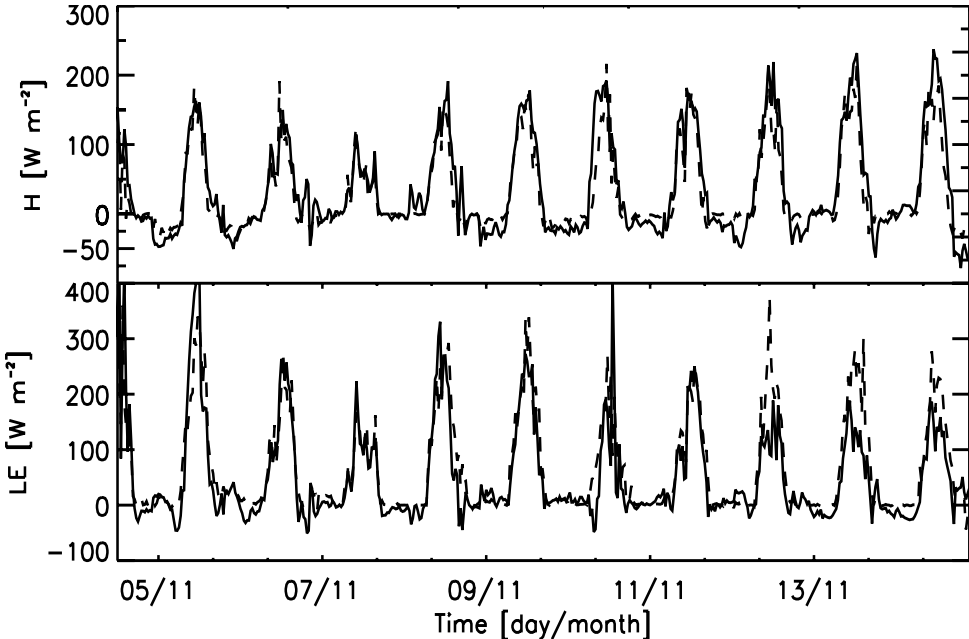


**Fig. 2.3a: Tamale: 10-day series for LAS (continuous line) and EC (dashed line) derived sensible and latent heat flux after the rain had stopped for more than one month.**

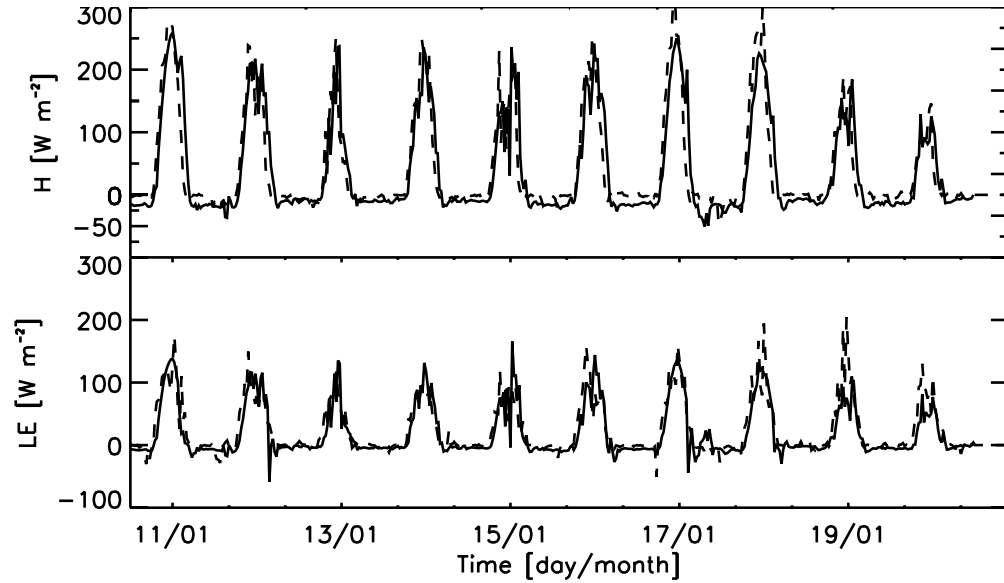


**Fig. 2.3b: Same as figure 2.3a for Ejura. Note the difference in time period.**

Table 2.2 shows the results of the comparison between measured sensible heat flux from EC and LAS measurements for the two sites. The linear regression for sensible heat flux gives reasonable results with a slope of 1.1 and a small intercept for Tamale. This confirms that the diurnal cycle for sensible heat flux is represented well by both systems (compare figure 2.3). For sensible heat flux at Ejura test site the results are not as good as for Tamale. The linear regression gives a lower slope and higher intercept. For both sites figure 2.4 shows scatter plots for  $H_{LAS}$  versus  $H_{EC}$ . For Tamale the amount of scatter increases for higher sensible heat flux. Furthermore there is an overestimation of sensible heat flux obtained from the LAS measurements. For both sites there are a number of measurements in the low end of the measurement range, which do not correspond (compare figure 2.4). This shows that for early morning hours or late afternoon hours the LAS fluxes are higher. The linear regression forced through the origin shows that for higher values of sensible heat flux the slope is closer to one (table 2.2).

**Table 2.2a: Comparison of sensible and latent heat flux for daytime from LAS and EC for the IOP in Tamale (start at DOY 307 and end at DOY 349 in 2002).**

ID Units	Sensible Heat Flux $Wm^{-2}$				Latent Heat Flux $Wm^{-2}$			
	Intercept $Wm^{-2}$	Slope -	$R^2$ -	RMSE $Wm^{-2}$	Intercept $Wm^{-2}$	Slope -	$R^2$ -	RMSE $Wm^{-2}$
normal	5.3	1.10	0.86	34.0	34.0	0.69	0.67	63.8
zero intercept	0.0	1.07	0.87	34.0	0.0	0.93	0.67	63.8

**Table 2.2b: Comparison of sensible and latent heat flux from LAS and EC for the IOP in Ejura divided into two periods, due to the change in wind direction (start at DOY 313 in 2002 and end at DOY 28 in 2003).**

ID Units	Sensible Heat Flux $\text{Wm}^{-2}$				Latent Heat Flux $\text{Wm}^{-2}$			
	Intercept $\text{Wm}^{-2}$	Slope -	$R^2$	RMSE $\text{Wm}^{-2}$	Intercept $\text{Wm}^{-2}$	Slope	$R^2$	RMSE
period until DOY 345	12.2	0.81	0.67	53.4	34.5	0.36	0.60	73.6
zero intercept	0.0	1.08	0.67	53.4	0.0	0.8	0.61	73.6
period from DOY	19.2	0.88	0.70	52.1	30.7	0.40	0.65	60.1
zero intercept	0.0	1.01	0.71	52.1	0.0	0.86	0.68	60.1

The large amount of scatter for Ejura confirms the low correlation and high RMSE for Ejura. The lower correlation compared to Tamale is due to higher random errors, which is also demonstrated by a higher RMSE. The higher random errors might be due to the fact that the terrain at the test site in Ejura is more heterogeneous than in Tamale.

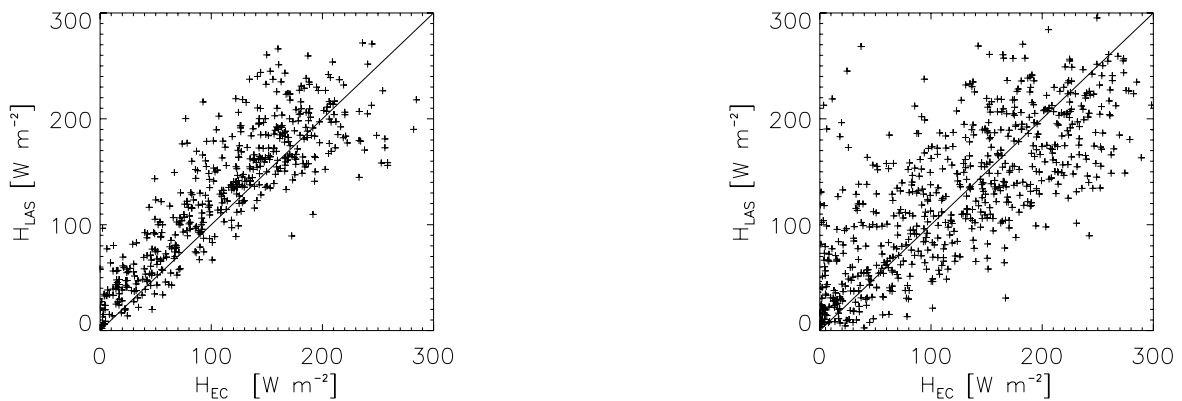


**Fig. 2.4: Tamale and Ejura: EC derived sensible heat flux vs. LAS derived sensible heat flux. Scatterplot for the analysed period during the IOP with daytime values only.**

The assumption behind the comparison of the two methods is that the EC system has been installed to “see” a subsample of the LAS footprint, because it is installed in the center of the path and in a lower height. Both sensors should “see” comparable surfaces, large enough to average out the small-scale inhomogeneities. They should give comparable results as long as the size of the EC footprint is larger than the size of the inhomogeneities. In situations where the size of the EC footprint is marginal compared to the size of the inhomogeneities scatter is introduced. In the present study an approximate analytical footprint model (Hsieh et al. 2002) is used, based on a combination of Lagrangian stochastic dispersion model results and

dimensional analysis. It is utilized to determine the source distance in upwind direction, where 90% of the flux originates from. For both test sites the model calculated that for both systems 98% of the cases originated within 600 m in upwind direction for unstable cases (figure 5). For stable situations the source area gets very large and the flux originated in only 18% of all cases from the first 10000 m in upwind direction, with higher values for the LAS based measurements. The percentage of observations that originate from an area with a length of at most the median of the distance between the trees equals 5% for Tamale and 11% for Ejura. This percentage of the data could scatter due to incomparable footprints. From the footprint analysis and figure 2.4 it is concluded that in Tamale the surface properties in the footprint of both systems are comparable more often than in Ejura. From figure 2.5 it is also concluded that the EC system sees a rather small subsample of the LAS path, since the diameter of the plotting-circle is not even the path length of the LAS. For Ejura there are also differences in surface properties on a larger scale. This might explain even more scatter.

As a first approximation the source area of the LAS can be calculated by multiplying the footprint in upwind direction with the part of the LAS path that covers 90% of the contribution to  $C_n^2$ , based on the weighing function of the LAS. For both sites the size of the source area of a LAS is larger, when the wind direction is not parallel to the path (compare also Meijninger et al. 2002).

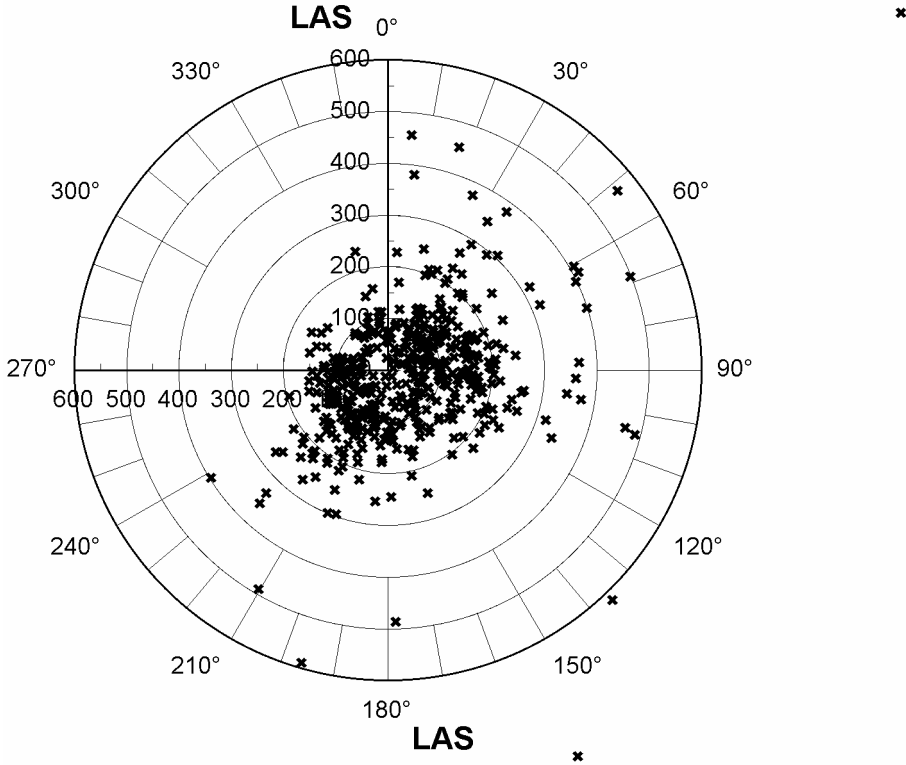


**Fig. 2.5a: Source distance in m of sensible heat flux depending on wind direction during unstable situations. Polarplot for the analyzed period during the IOP in Tamale.**

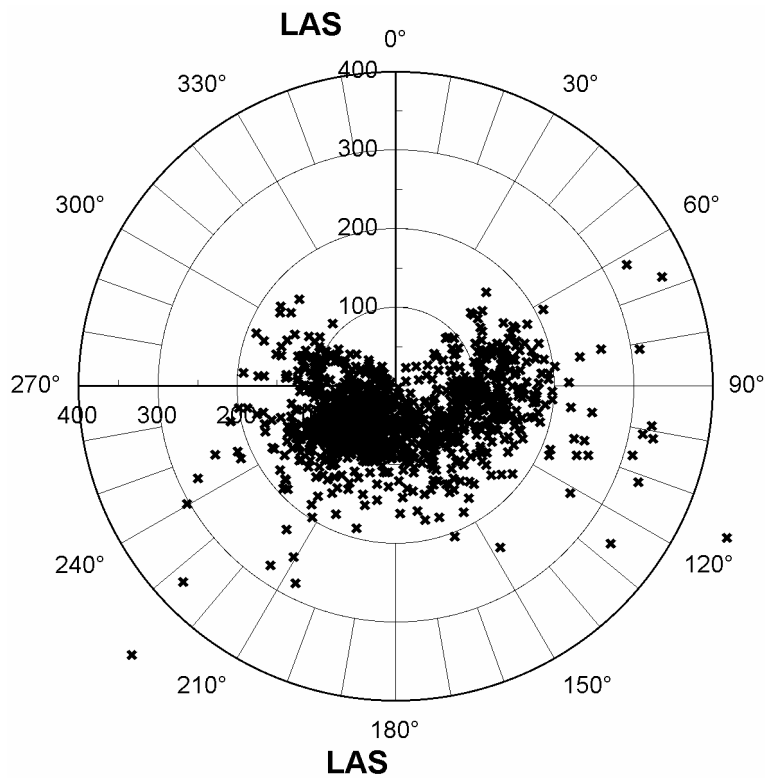


**Fig. 2.5b: Same as figure 5a for Ejura.**

### 2.3.2 Latent heat flux

Figure 2.3 shows that for most of the days the  $LE_{LAS}$  and  $LE_{EC}$  correspond well during the diurnal cycle. During the night  $LE$  is close to 0 for both systems. For the comparisons of the LAS derived latent heat flux and EC data in Tamale the correlation is lower compared to sensible heat flux. The linear regression shows an underestimation of the latent heat flux calculated from the residual of the energy balance. For Ejura the results are not as good as for Tamale. Since for Ejura no measurements were available to calculate the right soil heat flux at the soil surface, there is an error in the calculation for latent heat flux from LAS data. However due to the more dense vegetation cover, this effect should be smaller than in Tamale. The linear regression forced through the origin gives better results, which shows that the main deviations in latent heat flux occur during early morning and late afternoon hours. The correlation coefficient is not as good as for sensible heat flux and the RMSE is large for both sites given a maximum flux of about  $250 \text{ W m}^{-2}$ .

## 2.4 Evaluation of the energy balance closure

For the energy balance closure it is important to remember the reasons for nonclosure mentioned in the introduction. Sampling errors are closely related to the different footprints of the components of the energy balance. Net radiation and soil heat flux will never have the same footprint as sensible and latent heat flux. For soil heat flux the footprint is always much smaller than for all other components of the energy balance. For net radiation, which is the largest component of the energy balance, other studies have found little spatial variability over different kinds of terrain (Twine et al. 2000; Stannard et al. 1994) and errors which are up to a maximum of 6% (Moncrieff 1996) are often assumed. One crucial point for net radiation is that there exists no widely accepted or standard method for measuring and that errors in factory calibration for different sensors can be larger than the accuracy (Halldin and Lindroth 1992). Cobos and Baker (2003) tested the netradiometer, which is used in this study (NR Lite, Kipp & Zonen) and found good agreement with the summation of the four independently measured components of net radiation under most field conditions. However precipitation and condensation affect the performance, but the influence is negligible for Tamale and small for Ejura. The variability in net radiation and soil heat flux also shows that independent measured fluxes are needed (at least for IOPs) when latent heat flux is calculated as a residual from the energy balance.

For the evaluation of the energy balance closure different methods are used. The first method is to calculate the cumulative sum of the available energy ( $R_n - G$ ) and the dependent fluxes ( $LE + H$ ) over the analyzed periods and calculate the Energy Balance Ratio (EBR) (Gu et al. 1999).

$$EBR = \frac{\sum (LE + H)}{\sum (R_n - G)} \quad (2.5)$$

This is a first means to illustrate an overall evaluation for the IOP. The advantage of this method is that it neglects possible random errors in flux estimation. The second method is the derivation of linear regression coefficients for available energy ( $R_n - G$ ) and the dependent fluxes ( $LE + H$ ). The linear regression is done again using the least absolute deviation technique. This is even more important here since random errors for measured net radiation and soil heat flux cannot be specified properly. Regression coefficients are calculated for ( $LE + H$ ) against ( $R_n - G$ ) using the following relationship ( $LE + H$ ) =  $a + b * (R_n - G)$ . Energy balance closure is evaluated with sensible heat flux from the LAS and from EC data, also to gain more confidence in the gathered data. This is especially important for further applications during periods, where there is no EC data available. For both cases LE is

obtained from the EC data.

Since the magnitude of the imbalance of the energy balance closure often shows a close relationship to the diurnal cycle the residual in the relative energy imbalance (REI) is calculated as well to get more insights about the instantaneous errors. It is defined as follows:

$$REI = \frac{R_n - G - LE - H}{R_n - G} \quad (2.6)$$

After calculating REI the data is grouped into three classes. The first class only contains data where deviations in REI ( $\delta REI$ ) with  $|\delta REI| \leq 0.10$ , which means an acceptable closure of the energy balance. The second group contains only data where  $\delta REI > 0.10$  (positive bias) and the third group contains data where deviations in  $\delta REI < -0.1$  (negative bias).

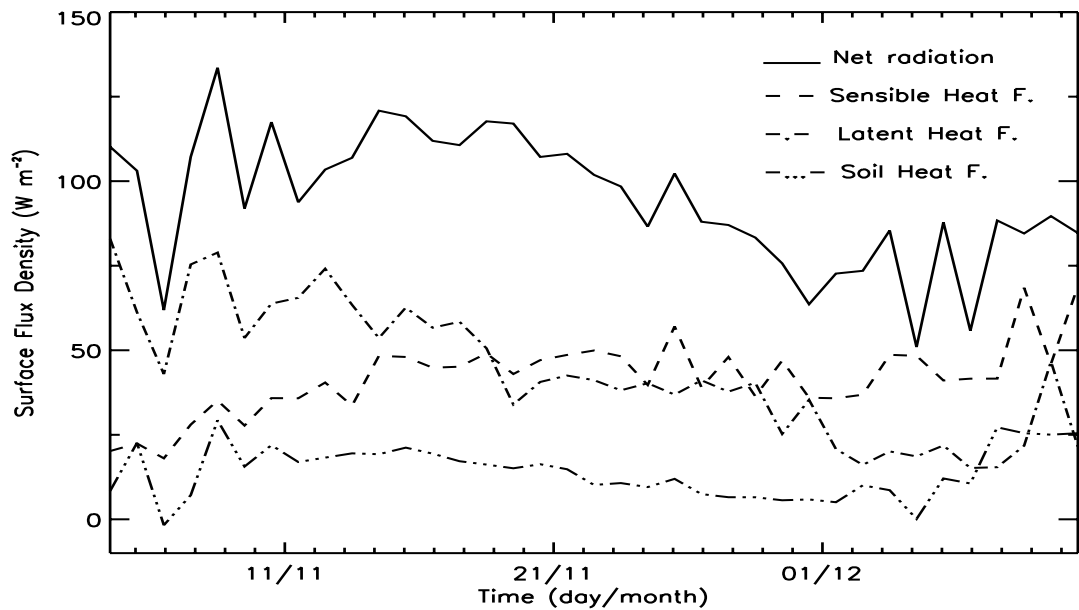
#### 2.4.1 Surfaces fluxes on a seasonal basis

Figure 2.6 shows daily averages of surface fluxes LE and H as well as G and net radiation for the IOP at both sites. Surface flux data are mainly taken from the EC system. During small gaps due to datalogger failure LAS data are used. There is a clear decline in net radiation towards the end of the period mainly due to the decline in incoming solar radiation in combination with changing surface conditions. For soil heat flux there is a small rise from the beginning to the end. For Tamale sensible heat flux shows an increase from the beginning to the end and a clear decline in latent heat flux. For Ejura sensible heat flux remains nearly at one level from the beginning to the end. There is a small decline in latent heat flux during November, but for the rest of the IOP it stays on the same level. It is also evident that latent heat flux is not negligible until the end of the IOPs. The last rain event appeared on DOY 343 in Ejura. In Tamale it was DOY 287. This demonstrates that for large parts of the dry season the plants are able to evaporate. One reason for the ongoing evapotranspiration is the deep rooting system of the trees. The trees are still green and transpiration continues.

For Ejura figure 2.6b shows that there exists a systematic error in the closure of the energy balance until a certain time of the year. Those findings are in contrast to the results of Tamale. The error in the closure of the energy balance corresponds well with a change in wind direction, thus coinciding with a sudden increase in VPD. The error in the beginning of the IOP at Ejura test site shows that there is a clear advective influence on the closure of the energy balance. During the period until DOY 345 the prevailing wind direction is Southwest, resulting in winds from a steep slope ( $>12\%$ ). As soon as the wind direction changes more to the East (sector with mild topography) the energy balance closes better. This effect on the

closure of the energy balance is already observed by Lee and Hu (2002). At the end of the IOP the wind direction changes again more to the Southwest, but this time not resulting in worse closure of the energy balance. A possible reason could be the better turbulent mixing by the end of the IOP.

Since the results for the two sites differ in several aspects, further evaluation is done for the two sites separately.



**Fig. 2.6a: Daily averages of all terms of the energy balance for the IOP in Tamale. Turbulent flux data are mainly taken from the EC measurements.**

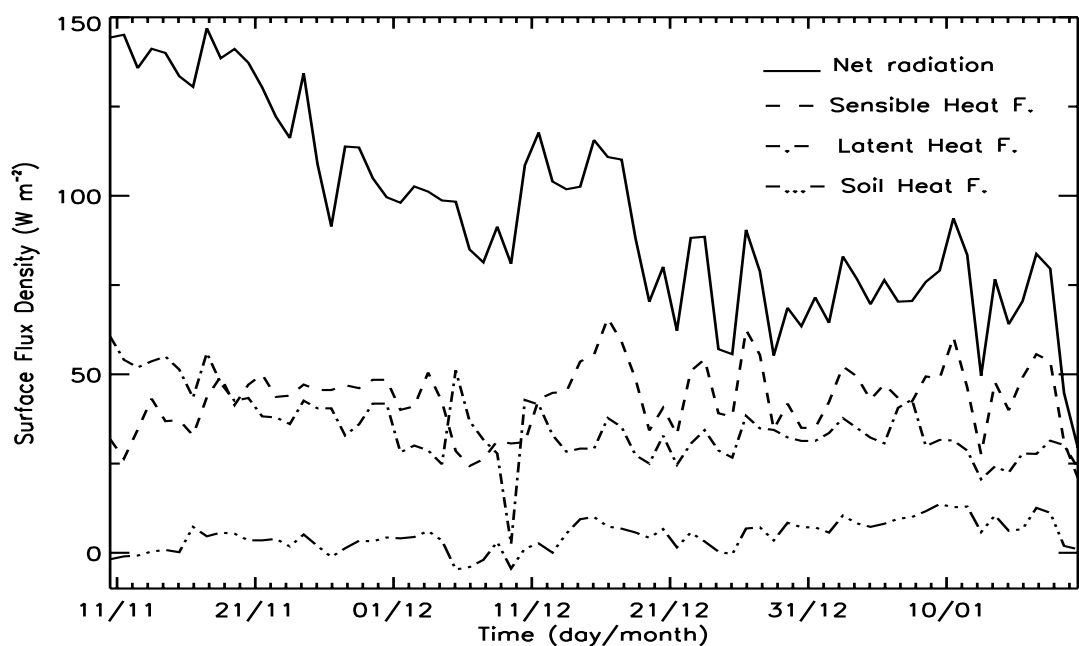


**Fig. 2.6b: Same as figure 2.6a for Ejura.**



## 2.4.2 Tamale

The obtained results nearly show a perfect energy balance closure with both measurements during the day, considering the slope of the linear regression as well as the EBR (table 2.3a), which suggests that the daily cycle is represented realistically and also on the long term there are only small errors.

**Table 2.3a: Tamale: Evaluation of energy balance closure for day and nighttime values with measurements from LAS and EC for the IOP.**

ID Units	Intercept $Wm^{-2}$	Slope -	$R^2$ -	EBR -
With H EC day	6.8	0.98	0.87	0.97
With H LAS day	-4.7	0.99	0.87	1.00
With H EC night	-14.9	0.42	0.32	0.21
With H LAS night	-12.5	0.31	0.38	0.99

For nighttime situations the results show a large difference between the LAS and the EC based measurements. The slope is larger for the EC based measurements. This has to be seen in context of the low  $R^2$ , which is associated to larger random errors. The EBR, which should not be affected by random errors, shows better results for the LAS based measurements.

The relative energy imbalance (REI) was analyzed in this context to get more insights in the instantaneous closure of the energy balance in contrast to the calculated EBR. Therefore the REI is calculated for every daytime and nighttime value. For daytime values the median of REI with sensible heat flux from the EC system is 0.05 and for energy balance closure based on sensible heat flux from LAS it is found to be -0.05. The percentage of acceptable REI with  $|\delta REI| \leq 0.10$  for the energy balance with H from EC is 31.6% and for the LAS based H it is 29.6%. The positively biased class for the EC based system is with 38% higher than the negatively biased class with 29%. For the LAS based system it is the other way around (negative bias = 27.1%; positive bias = 43.2%). To obtain more insights in the instantaneous closure, the daytime values are divided into morning and afternoon hours, by dividing the data into intervals before and after noon. Both systems give the largest deviation in the afternoon, where turbulence normally reaches its highest values. The LAS is overestimating the sum of the turbulent fluxes with 27.2% and the EC systems is underestimating with 23%. This is different compared to other studies (e.g. Wilson et al., 2002), which show larger errors in the morning due to storage terms.

For nighttime values the EC based data show a systematic error since the sum of dependent

fluxes is in 93% of all cases too low. For the LAS based system the percentage of too high and too low REI is nearly equal, which means there is no systematic error. Further analyses show that more than 60% of the measurements show a REI with  $|\delta REI| \leq 0.50$ .

### 2.4.3 Ejura

The energy balance closure is evaluated in the same way as in Tamale. As a first step the energy balance closure is evaluated for the whole period with sensible heat flux from the LAS and from EC data. Regression coefficients are calculated for  $LE + H$  against  $R_n - G$  (table 2.3b).

The EBR during day and nighttime is higher for the LAS measurements. The linear regression gives better results for daytime situations for LAS measurements. This is partly due to the fact that during the first period the LAS gives a higher sensible heat flux compared to the EC system. For nighttime values the results are similar for both systems concerning the linear regression, but are on a low level.

**Table 2.3b: Ejura: Evaluation of energy balance closure for day and nighttime values with measurements from LAS and EC for the whole period.**

ID Units	Intercept $Wm^{-2}$	Slope -	$R^2$ -	EBR -
With H EC day	58.0	0.87	0.82	0.80
With H LAS day	33.7	0.95	0.77	0.85
With H EC night	-16.2	0.14	0.07	0.03
With H LAS night	-15.7	0.16	0.10	1.10

The instantaneous closure expressed with REI during daytime shows an underestimation for both systems. The median of the REI is found with sensible heat flux from the EC system to be 0.20 and for energy balance based on sensible heat flux from LAS it was found to be 0.17. The percentage of acceptable REI with  $|\delta REI| \leq 0.10$  for the energy balance with H from EC is 23.5% and for the LAS based H it is 22.3%. The positively biased class for the LAS and the EC based system is higher (EC=58.5%; LAS=58.8%) than the negatively biased class (EC=18%; LAS = 18.8%). This becomes even clearer, when the dataset is divided again into morning and afternoon classes. Both systems show an underestimation of sensible and latent heat flux during the afternoon hours up to 45%. This might partly be explained by the non-adjusted soil heat flux. It imposes an error in phase, which leads to too high values during the afternoon hours.

For nighttime the same systematic error is observed for the EC based system as in Tamale, whereas the error is nearly equally distributed for the LAS based system. For the LAS based system more than 70% of the measurements show  $|\delta REI| \leq 0.50$ .

In a second step data were divided into the already mentioned two periods (see section 2.3). The EBR is higher for both periods, when sensible heat flux is taken from the LAS (0.71 and 0.95 compared to 0.64 and 0.90 for the EC based system). The same trend is seen in the linear regression.

The third step is to evaluate if the closure of the energy balance can be improved by calculating the Bowen Ratio ( $\beta$ ) from the EC measurements, assuming that the Bowen Ratio is estimated correctly by the EC system (Twine et al. 2000). With the help of the calculated Bowen Ratio a corrected latent heat flux is estimated in the following way:

$$LE_{corr} = \frac{H_{LAS}}{\beta} \quad (2.7)$$

For the first period the EBR now equals 0.76 compared to 0.71 with  $H_{LAS}$  and  $LE_{EC}$  and 0.64 for  $H_{EC}$  and  $LE_{EC}$ . For the whole period the EBR now is 1.0, which is an improvement compared to the LAS based EBR of 0.85. This demonstrates that a simple way of adjusting surface fluxes by using the Bowen Ratio helps in improving the energy balance closure. This might be useful in further model studies.

## 2.5 Evaluation of surface conductance

The surface conductance ( $g_s$ ) is calculated with the rearranged Penman-Monteith equation (e.g., Monteith and Unsworth 1990) following the notation by Harris et al. (2003):

$$g_s = g_a \left[ \frac{\Delta(R_n - G) + \rho c_p VPD g_a}{\gamma LE} - \frac{\Delta}{\gamma} - 1.0 \right]^{-1} \quad (2.8)$$

$\Delta$  to the slope of saturated vapor pressure with temperature ( $\text{pa K}^{-1}$ ),  $\rho$  is air density ( $\text{kg m}^{-3}$ ),  $c_p$  is specific heat of air at constant pressure ( $\text{J kg}^{-1} \text{K}^{-1}$ ),  $\gamma$  equals the psychrometric constant ( $\text{Pa K}^{-1}$ ),  $g_a$  to aerodynamic conductance for water vapor ( $\text{m s}^{-1}$ ). With the measurements of the different components of the energy balance  $g_s$  can be calculated from equation (2.8) and can be considered as the surface conductance for the water vapor transfer between the heterogeneous surface and the atmosphere. For the calculation of the aerodynamic

conductance the method of Verma (1989) with stability corrections by Paulson (1970) is used. The roughness length for momentum was estimated using the approach of Martano (2000) and roughness length for heat was estimated by applying a fixed ratio of roughness length for momentum and heat of 100, which was estimated for Savannah conditions by Huntingford et al. (1995). A more detailed description of the used approach can be found in Harris et al. (2003). Under conditions of low available energy the computation of  $g_s$  can give non-realistic conductances. Therefore the calculation of  $g_s$  is restricted to daytime situations between 9:00am and 5:00pm. The surface conductance is mainly controlled by incoming solar radiation ( $R_g$ ), VPD, temperature and soil moisture. Since evapotranspiration is mainly dominated by transpiration for the two sites and periods, the driving forces should mainly reflect stomatal functions.

There are a number of models utilizing the different factors named above for the calculation of surface conductance. In our study a Jarvis-type model is used given by the following equation:

$$g_s = LAI \cdot g_{\max} \cdot \prod_i f_i(X_i) \quad (2.9)$$

The functions,  $f_i$  can have a range between 0 and 1. Following Dolman (1993) the different  $f_i$  are given by:

$$f_1(D) = e^{-VPD/a_1}, \quad (2.10)$$

$$f_2(T) = \left( \frac{T - T_L}{a_2 - T_L} \right) - \left( \frac{T_U - T}{T_U - a_2} \right)^\tau \quad \text{with} \quad \tau = \frac{T_u - a_2}{a_2 - T_L}, \quad (2.11)$$

$$f_3(R_g) = \frac{R_g}{a_3 + R_g} \left( 1 + \frac{a_3}{R_{g\max}} \right), \quad (2.12)$$

$$f_4(\Theta) = \begin{cases} 1 & \Theta < a_4 \\ \frac{a_5 - \Theta}{a_5 - a_4} & a_4 \leq \Theta < a_5, \\ 0 & \Theta \geq a_4 \end{cases} \quad (2.13)$$

where  $T_U$  (°C) and  $T_L$  (°C) mark the upper and lower temperature limits where transpiration stops.  $T_U$  and  $T_L$  are set to 45 °C and 5 °C and  $R_{g\max}$  equals 1000 W m<sup>-2</sup>.

Huntingford et al. (1995) optimized the different parameters  $a_1, \dots, a_5$  for savannah conditions

during the wet season. We adopt those values and also retain the function  $f_2$  in contrast to Huntingford et al. (1995). We use the findings of Harris et al. (2003) for estimating an expression for  $a_2$ . Table 2.4 shows all values used for both test sites with the error ranges of parameters  $a_1, \dots, a_5$ . From table 2.4 it can already be seen that some of the parameters show a large uncertainty. For  $g_{\max}$  values are used from the USGS NOAA global dataset ([http://edcdaac.usgs.gov/glcc/af\\_int.asp](http://edcdaac.usgs.gov/glcc/af_int.asp)), which is widely used by modelers.

Such an approach is fairly “well-established” and the functions  $f_i$  have been optimized for a lot of regions. In this study our focus is not on optimizing but on testing the response of the surface conductance during the time of transition. It is also very difficult to develop a single solution under the influence of multiple feedback processes that mask the interactions.

**Table 2.4: Parameters from optimizations (Huntingford et al., 1995) of a Jarvis model of surface conductance for Savannah including maximum canopy conductance ( $g_{\max}$ ), Leaf area index (LAI), functional dependence on solar radiation ( $a_1$ ), air temperature ( $a_2$ ), vapor pressure deficit ( $a_3$ ), soil moisture ( $a_4$ ;  $a_5$ ). LAI and  $g_{\max}$  are taken from the regionally dependent USGS database ([http://edcdaac.usgs.gov/glcc/af\\_int.asp](http://edcdaac.usgs.gov/glcc/af_int.asp)).**

ID	LAI	$g_{\max}$	$a_1$	$a_2$	$a_3$	$a_4$	$a_5$
Units	$\text{m}^2 \text{m}^{-2}$	$\text{mm s}^{-1}$	$\text{W m}^{-2}$	$^{\circ}\text{C}$	$\text{g kg}^{-1}$	mm	mm
Tamale	1	10.0	$36.5 \pm 10.0$	$25.0 \pm 4.5$	$36.7 \pm 50.0$	$47.6 \pm 50.0$	$153.0 \pm 20.0$
Ejura	4	4.16	$36.5 \pm 10.0$	$25.0 \pm 4.5$	$36.7 \pm 50.0$	$47.6 \pm 50.0$	$153.0 \pm 20.0$

For both test sites the measured and modeled canopy conductances show a large variability during the examined periods (figure 2.7). For Ejura the surface conductance obtained by the rearranged Penman-Monteith equation shows a large decrease during the first period of the IOP. From the time of the IOP when the energy balance closes better and the VPD rises it remains low. This is important since the closure of the energy balance during the first period was not as good as for the second period, which means that for the further analyses only the second period was considered.

The important factors to model the surface conductance correctly are the different response functions that control the response on different time scales. Soil moisture dependence and VPD dependence are needed to produce reasonable results for the seasonal cycle. Both variables change significantly at both test sites (figure 2.7). Temperature and incoming solar radiation do not change significantly. The surface conductance decreases approximately linear during the day (figure 2.8) (at least from 9:00 am – 5:00 pm) but during the IOP the slope of this decrease gets less steep for Tamale. For Ejura the starting and end point stay nearly

constant during the IOP. The relatively stable surface conductance during the second period in Ejura also shows that the plants are able to transpire during the drying up due to the deep rooting systems.

To analyze the errors in modeled  $g_s$  half hourly values of the dimensionless ratio  $\mu$ :

$$\mu = \frac{g_s}{g_{s\text{ mod}}}, \tag{2.14}$$

were calculated for the IOPs during the hours from 9:00 am to 5:00 pm. Theoretically  $\mu$  should always equal 1. After calculating  $\mu$  the data are grouped into three classes in the same way as for the REI. The first class only contains data where deviations in  $\mu$  with  $|\delta\mu| \leq 0.2$ , which means an acceptable modeled conductance. The second group only contains data where  $\delta\mu > 0.2$  (positive bias) and the third group contains data where deviations in  $\delta\mu < -0.2$  (negative bias). The average  $\mu$  and the percentage of  $|\delta\mu| \leq 0.2$  are shown in table 2.5.

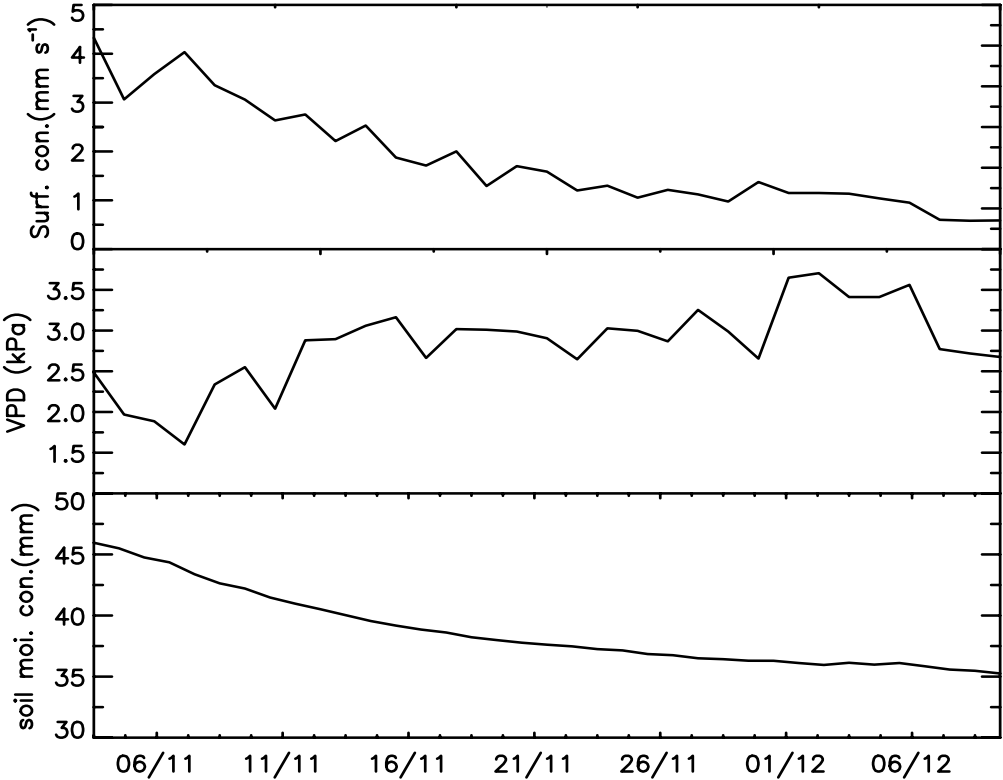


**Fig. 2.7a: Daily Median of surface conductance, daily mean of VPD and daily mean of soil moisture content for the IOP in Tamale.**

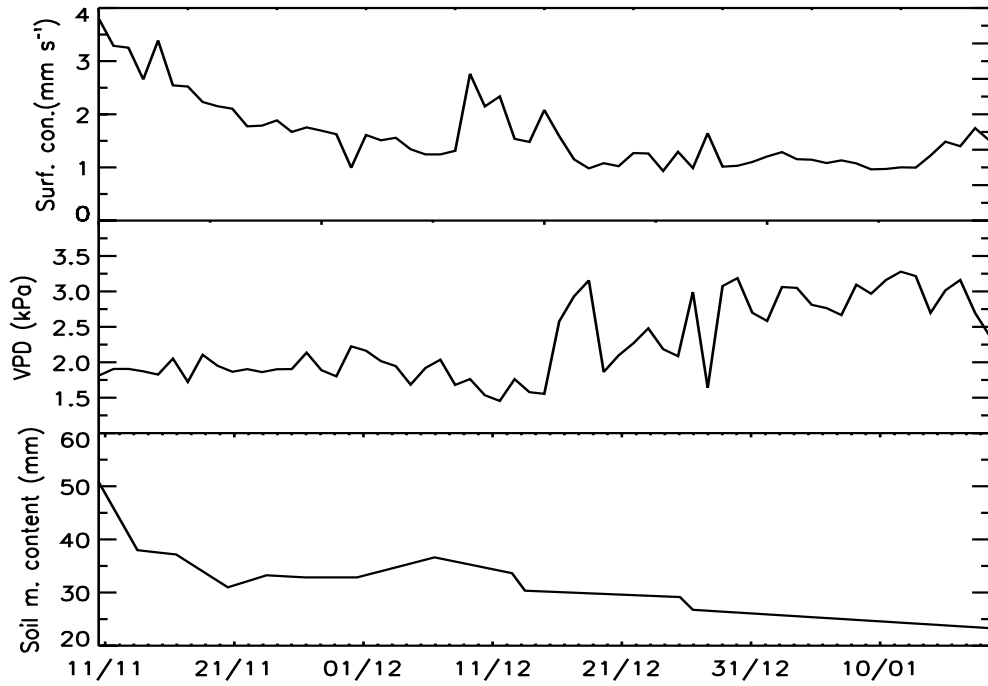


**Fig. 2.7b: Same as figure 2.7a for Ejura.**

**Table 2.5: Average  $\mu$  and the class of  $|\delta\mu| \leq 0.2$  for both test sites taking the four different response functions for the Jarvis-type model into account.**

Jarvis func.	avg. $\mu$ Tamale	avg. $\mu$ Ejura	% with $ \mu  \leq 0.2$ Tamale	% with $ \mu  \leq 0.2$ Ejura
$f_1 f_3$	0.16	0.10	<5%	<5%
$f_1 f_2 f_3$	0.20	0.16	<5%	<5%
$f_1 f_3 f_4$	0.75	0.82	30%	35%
$f_1 f_2 f_3 f_4$	0.93	0.96	40%	41%

When soil moisture ( $f_4$ ) and temperature dependence ( $f_2$ ) are not included, the conductance is highly overestimated during the whole day (compare also figure 2.8). Including only temperature dependence gives a more realistic decrease for  $g_s$  during the day, but the total level is still too high. As soon as soil moisture dependence is included the results are improved and even get better when temperature dependence is included again. The higher percentage of  $|\delta\mu| \leq 0.2$  shows that including temperature dependence helps in modeling surface conductance correctly. The better results when temperature dependence is included could not be achieved by only varying the VPD response function ( $f_1$ ) by varying  $a_1$ , since values for  $a_1$  would be needed, that would have been out of the error ranges to achieve similar results.

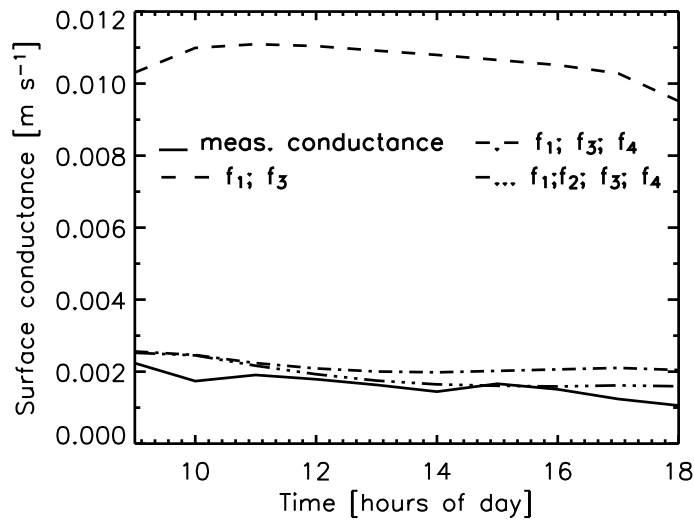


**Fig. 2.8: Illustration of the diurnal course of measured and modeled surface conductance for a 5-day period in Tamale starting at the 14<sup>th</sup> November 2002.**

When those findings are compared to those of Huntingford et al. (1995) it is seen that temperature has a more pronounced diurnal cycle during the time of transition compared to the measurements of Huntingford et al. (1995), which were taken during the wet season.

## 2.6 Conclusions

Three important conclusions can be drawn from this study. First, the GLOWA-Volta project has generated a land surface dataset in a semi-arid region in West Africa. The first obtained results show a good quality and consistency, suitable for further application in the future.

The second conclusion is that the measured energy balance closes well for Tamale test site. The closure for Ejura test site improves during the time of transition for a region. The relative energy imbalance (REI) shows the largest errors in the afternoon, which makes it different from most of the other measurements, which show the largest errors in the morning due to storage terms.

The third conclusion is that a Jarvis-type model works better for the region during the process of drying up when temperature dependence is taken into account. The influence of temperature is also important with the background of simulations of future climate, in which many global climate models predict higher surface temperatures for West Africa.



For modeling evapotranspiration correctly proper soil moisture estimation is crucial, which suggests the need to test more sophisticated land surface models in the future, which take soil physical properties, root distribution and deeper soil moisture content into account.



## **Chapter 3**

### **Evaluation of two land-surface schemes over drying terrain in West Africa**

---

Material in this chapter is submitted to the Journal of Hydrometeorology with A.F. Moene, A.A.M. Holtslag and H.A.R. De Bruin as co-authors.

## **Abstract**

Two land surface schemes currently used in meteorological models at ECMWF and NCEP are evaluated using a new data set including surface fluxes obtained by scintillometry. These two schemes are selected because they differ in the degree of complexity to parameterize land surface processes. Both schemes have been run offline for a seasonal cycle in 2002/2003 using observations as forcings at two test sites in the Volta Basin in Ghana, West Africa. The measurements include the rapid wet-to-dry transition after the wet season. The two locations are in the humid tropical southern region, and one is in the dryer northern region.

The differences in the simulations provide deeper insights into individual model characteristics independent of atmospheric conditions. During the wet part of the season net radiation is described well by both models. During the drying up both models overestimate net radiation. For the sensible heat flux similar results are obtained, whereas for latent heat flux the results are better. Differences between model simulations and measurements can be related to differences in model parameterizations, where the land surface scheme of the ECMWF model appears to simulate surface fluxes physically more realistically.

The simulation of the components of the energy balance can be improved by simple adjustments of model parameters. In particular the ratio of roughness length for momentum and that for heat is found to be an important parameter, but is in need of seasonal adjustments.

### 3.1 Introduction

It is widely established, that the parameterization of land surface processes, in particular the way energy is partitioned at the earth's surface, appears to affect the performance of regional weather and climate models significantly. During the last decades various land-surface-models (LSM) have been developed and improved continuously with the help of long-term field experiments (e.g. FLUXNET (Baldocchi et al. 2001); NOPEX (Halldin 1999)).

The developed models have a different degree of complexity from a simple big leaf concept to multi-layer vegetation models and detailed description of bare soil (Xue et al. 1991). In contrast to those models there is also a growing number of LSMs, which use the "tile" approach to obtain surface fluxes from different surface types within one grid cell independently (Koster and Suarez 1992; Seth et al. 1994).

Inevitably, increasing complexity implies an increasing number of model parameters. To keep the schemes simple while retaining relevant physics there is a need for further model development and evaluation in remote regions. An example is the semi-arid region since recent research has revealed that large differences exist between the feedback mechanisms for land surface processes in midlatitudinal and semi-arid tropical regimes. The midlatitudes show a more soil wetness-related feedback, whereas the semi-arid areas are dominated by vegetative pathways (via stomatal conductance and vegetation cover) (Niyogi et al. 2002). This implies that the current parameterization schemes applied to the landscapes in West Africa require attention, because even minor changes in climate might alter the natural vegetation. The main vegetational characteristics in the West African landscape are humid tropical regions like the equatorial forests in the South, an intermediate zone with semi-humid areas as the Guinea savannah and a northern region with mainly fallow savannah.

A first attempt to gain deeper knowledge about the West African land surface processes in the northern Sahel region was done in the context of SEBEX (Wallace et al. 1992) with a focus on the annual cycle. HAPEX-Sahel (Goutorbe et al. 1994) followed in 1992 with a three-month intensive observation period to obtain information of surface flux estimation at the scale of a typical global climate model (GCM) grid box. Verhoef (1995) studied various land surface schemes in this context and gave first ideas of needed input parameters and their possible temporal variability.

For the more southern region including the Volta basin there is still a lack of data and therewith a lack of model evaluation. The Volta basin is located in the intermediate zone and the southern part of West Africa. The Volta basin comprises an area of about 400.000 km<sup>2</sup>. The climate system in the Volta basin is very much controlled by the meridional movement of the intertropical convergence zone (ITCZ), the African Easterly Jet (AEJ) and pressure

disturbances, which traverse from east to west across Africa (Burpee 1972). They all act under the influence of the Hadley and Walker cell circulation. Those mechanisms lead to a pronounced wet and dry season during the year, of which the length depends on the actual latitude. During the time of the year when the wet period ends and the dry period starts (time of transition) the contrast between dry and moist air is probably more pronounced in time and space than anywhere else (Hólm et al. 2002). There is a strong need to test LSMs on seasonal timescales (Viterbo and Beljaars 1995; Chen et al. 1997)

The objective of this study is to find a suitable LSM for the semi-arid region by using a performance test of two state-of-the-art LSMs for the time of transition in the named region. Similar performance tests have been undertaken in the past for various other regions and surfaces (e.g. Nagai 2002; Gustafsson et al. 2003) however these studies were confined to homogenous surfaces. In this study a large aperture scintillometer (LAS) is utilized (see e.g. De Bruin et al. 1995) because this robust method yields area-averaged fluxes over complex terrain, which are required, when evaluating models with different subgrid surface fractions. Moreover the use of a LAS over semi-arid vegetation types is novel.

The first land surface model employed in this study is the present ECMWF land surface scheme (TESSEL), which is based on the work of Viterbo and Beljaars (1995). This LSM uses the “tile” approach for calculating surface fluxes. It was introduced in the operational scheme at ECMWF in June 2000. The second one is the NOAH model, which is a joint product of National Centers for Environmental Prediction (NCEP), Oregon State University, Air Force and Hydrologic Research Lab. It is based on the former Oregon state University land surface model (OSULSM) (Ek and Mahrt 1991). The NOAH model is one option in PSU/NCAR mesoscale model (MM5) and is employed for studies related the impact of land use on regional climate (Chen and Dudhia 2001). This LSM uses the big leaf approach in combination with a formulation of bare soil evaporation for calculating surface fluxes. The NOAH model can be considered as the simpler scheme. Both models were involved in a number of intercomparisons of land-surface schemes (Betts et al. 1998; Van den Hurk et al. 2000; Schlosser et al. 2000; Boone et al. 2004). These two schemes have never been tested for this climate region before for such a long period.

The first focus of the performance test is on the correct representation of seasonal dynamics of the different components of the energy balance in both models. The second focus is on model parameterization by obtaining a better knowledge of the changes in surface conductance during the chosen time period. Based on the findings the third focus is on simple adjustments for needed parameters in both models to obtain enhanced model performance.

## 3.2 Material and Methods

### 3.2.1 Model descriptions

For both models a brief description is given here with a focus on the main differences of the two models, which are summarized in table 3.1. A full description of TESSEL can be found for example in Viterbo and Beljaars (1995) and Van den Hurk et al. (2000). For NOAH it can be found in e.g. Chen et al. (1997) and Chang et al. (1999).

Both models are run in offline mode to concentrate on the evaluation of the land surface processes for the specific region and on the surface-flux formulation, without dealing with mismatches in the upper boundary condition between a three-dimensional model and observations. It is driven by the prescribed atmospheric forcings described below.

**Table 3.1: Major differences in concept between the two land surface models NOAH and TESSEL.**

CONCEPT	NOAH	TESSEL
subgrid variability over land	no tiles, different treatment for vegetation and bare soil	6 tiles (bare soil, low high vegetation, intercepted water)
	flow characteristics by Zilitinkevich	one common roughness length
surface temperature	1 common surface temperature	1 for each tile
transpiration	Radiation, temperature, VPD, soil moisture	Radiation, vapor pressure deficit*, soil moisture
evapotranspiration	concept of potential evaporation	skin temperature
bare soil evaporation	Based on potential evaporation	surface resistance
vegetative fraction	seasonal dependent	Fixed
*only for high vegetation		

Both models contain a multilayer submodel for the soil. TESSEL utilizes one universal soil type for the different layers, whereas NOAH uses a regionally dependent soil type based on the USGS database ([http://edcdaac.usgs.gov/glcc/af\\_int.asp](http://edcdaac.usgs.gov/glcc/af_int.asp)). The soil is discretized into four layers for both models (0.08, 0.24, 0.72 and 2.16 m in thickness). Bottom boundary conditions are zero heat flux and free drainage. The water and heat budget in the soil is based on the Richards equation coupled to the Fourier law of diffusion. Soil moisture for canopy transpiration is extracted from the soil by means of a weighing function. For TESSEL it includes the root distribution for each layer whereas for NOAH it includes the soil depth for

each layer with a uniform root distribution (see appendix for more details). Both models incorporate a formulation for the preference of the plants to extract water from those layers where the liquid water content exceeds the wilting point.

A skin layer with zero heat capacity is in instantaneous equilibrium with its forcing. The skin layer conductivity provides the thermal connection to the topsoil layer. The coupling of the surface to the atmosphere is based on the skin temperature in both models. It is calculated by solving the energy balance equation:

$$R_n = H + LE + G \quad (3.1)$$

$R_n$  is net radiation,  $H$  is sensible heat flux,  $LE$  is the latent heat flux and  $G$  is the soil heat flux. TESSEL uses a tiled approach for calculating skin temperature, which means one skin temperature for every single tile is calculated and averaged according to the coverage. The averaged skin temperature is coupled to a single soil profile. In total it consists of eight tiles, where four are applied for our study namely bare soil, low vegetation, high vegetation and intercepted water of high and low vegetation. NOAH applies one single skin temperature representing the combined soil/vegetation surface.

For both models an aerodynamic conductance for  $H$  and  $LE$  and a canopy conductance for  $LE$  are utilized. The turbulent exchange is based on an iterative transformation of Richardson's number into Monin-Obukhov stability parameters (Beljaars and Holtslag 1991) for TESSEL. For NOAH the formulation of Paulson (1970) is used to calculate the turbulent exchange coefficient. For the canopy conductance of both models the parameterization of Jarvis (1976) and Stewart (1988) is applied.

In both models evapotranspiration is the sum of bare soil ( $E_{dir}$ ), the interception reservoir ( $E_c$ ) and vegetation ( $E_t$ ), where TESSEL divides into high and low vegetation. The exact formulation of the different evapotranspiration components can be found in appendix A.

Subgrid variability is tackled with the tiled approach for TESSEL and a fixed ratio of roughness length for momentum ( $z_{0m}$ ) and heat ( $z_{0h}$ ) for every tile. The ratio of roughness length for momentum ( $z_{0m}$ ) and heat is expressed commonly in terms of  $kB^{-1}$ , where  $B^{-1}$  is a dimensionless parameter. For NOAH a Reynolds number-dependent formulation for  $kB^{-1}$  proposed by Zilitinkevich (1995) is used.

$$kB^{-1} = \ln\left(\frac{z_{0m}}{z_{0h}}\right), \quad B^{-1} = P_z \sqrt{Re^*}, \quad Re^* = \frac{u^* z_{0m}}{\nu} \quad (3.2)$$



where  $k$  is the von Karman constant ( $k = 0.4$ ),  $\nu$  is the kinematic molecular viscosity,  $Re^*$  is the roughness Reynolds number, and  $u^*$  is the friction velocity.  $P_z$  is an empirical constant and the recommended range for  $P_z$  is 0.2-0.4 (<ftp://ftp.ncep.noaa.gov/pub/gcp/ldas/noahlsn>). It is set to 0.2 in the current study. Both models use a spatial database of vegetation types. Vegetation specific values are chosen for minimum canopy conductance and soil dependent parameters. In case of TESSEL the fractional vegetation cover is fixed in time. For NOAH it varies on a monthly basis, based on the work of Gutman and Ignatov (1998).

### 3.2.2 GLOWA-Volta data set

All measurements are gathered in context of long-term observations concerning the water- and energy balance in the Volta Basin within the GLOWA-Volta project (Global Change in the Hydrological cycle). GLOWA-Volta is a multidisciplinary effort to study the physical and socioeconomic determinants of the hydrological cycle (Van de Giesen et al. 2001).

The data in this study are based on measurements from meteorological stations in Ejura ( $7^\circ 20' N$ ;  $1^\circ 16' W$ ) and Tamale ( $9^\circ 29' N$ ,  $0^\circ 55' W$ ) in year 2002. The two sites show major differences concerning the vegetation, soils, land use, slopes and also climate.

The site in Ejura is the more tropical site. The landscape is hilly. Here the transmitter of the LAS (further description below) and the automatic weather station (AWS) are located in a cashew orchard. The receiver of the LAS is located at the edge of a forest. The length of the path in between is about 2030m. The weighted effective height of the LAS was estimated to 30.1m. It is a heterogeneous terrain. The area between the transmitter and the receiver can roughly be divided into two parts. On the transmitter side the vegetation consists of cashew trees with maize and grass in between. On the receiver side there are bushes and trees and small swamps, but nearly no agriculture.

The research site in Tamale is mainly characterized by natural grassland with scattered trees, with a maximum height of six to eight meters. The landscape is slightly hilly. The LAS transmitter and receiver are installed on two hills with a distance in between of about 2420 m. The weighted effective height of the LAS was estimated to be 19.5m. The automatic weather station was installed next to the receiver of the LAS.

For Ejura (Tamale) the yearly sum of rainfall in 2002 is 1420 mm (1065 mm). The mean annual rainfall at the sites is 1432 mm and 1082 mm (FAO 1984, including data from 1930 to 1980). Precipitation shows a relatively regular pattern for both test sites until the rain stops. From 40 years of data the average onset was estimated to day of year (DOY) 78 for Ejura (DOY 118 for Tamale) with a standard deviation (SD) of 30 days (20 days). The onset of the rainy period for 2002 was estimated to day of year 74 for Ejura and for Tamale it was DOY

115. The offset is estimated to day 343 in Ejura. This was done using the method of Kasei (1988). This shows that the length of the rainy season and the total amount of rain are normal for 2002/2003.

Data availability exceeds more than 90% for most of the measurements for the two sites during the studied season. Due to measurement problems there are no sensible and latent heat fluxes available for the test site in Tamale until DOY 287 and for the last three to four weeks of the studied time for both sites.

### 3.2.3 Forcing data

The forcing data for the two models are obtained from the AWS, which measures temperature, humidity and global radiation at a reference level  $z = 2$  m. Wind speed is measured at eight-meter height. Additionally, surface observations for precipitation are recorded. All quantities are averaged for ten-minute intervals. A list of instruments is given in table 3.2. The current forcing data sets do not always provide longwave radiation. For those situations where longwave radiation measurements were not available it is calculated using air temperature and relative humidity following Idso and Jackson (1969) for clear sky situations. The contribution due to clouds is calculated using the following expression:

$$L_{total}^{\downarrow} = L_{cloudless}^{\downarrow} + L_{cloud}^{\downarrow} \quad \text{with } L_{cloud}^{\downarrow} = 60 \cdot C \quad (3.3)$$

Since no observations for cloudiness were available,  $C$  was estimated by calculating the transmissivity ( $\tau$ ) of the atmosphere from observed global radiation and using that information for obtaining a linear function for  $C$  for cloudy situations:

$$C = f\left(\frac{R_{et}}{R_g}\right) \quad \text{with } \begin{cases} C = 1 & \tau < 0.3 \\ C = 1 - \frac{\tau - 0.3}{0.4} & 0.3 < \tau < 0.7 \\ C = 0 & \tau > 0.7 \end{cases} \quad (3.4)$$

where  $R_{et}$  is the extraterrestrial radiation and  $R_g$  is the global radiation at the surface. This approach was tested for one of the sites of HAPEX-Sahel and for Tamale test site during the period where there was data available. A linear regression against direct measurements gave reasonable results (intercept  $4.7 \text{ W m}^{-2}$ , slope 0.95 for HAPEX-Sahel, similar for Tamale test site).

**Table 3.2: Instrument within the GLOWA-Volta project.**

Variable	Location	Instrument
Air Temperature	2 m	50Y Temperature and RH probe (Vaisala)
Relative Humidity	2 m	50Y Temperature and RH probe (Vaisala)
Atmospheric pressure	Inbox	PTB101B Barometric Pressure Sensor (Vaisala)
Wind Speed	8 m	A100R Anemometer (Vector Instruments)
Wind Direction	8 m	Wind vane (Ecotech)
Net Radiation	8 m	NR-LITE (Kipp & Zonen)
Downward solar radiation	2 m	SP-LITE (Kipp & Zonen)
Precipitation	2 m	Tipping bucket (Stelzner)
Sensible Heat Flux	Site dependent	Large Aperture Scintillometer (LAS) (Manufactured by Wageningen Uni.)
Latent Heat Flux		Residual of the energy balance
Soil Heat Flux	0.035 m	HFP01 Heat Flux Plate (Hukseflux)
Soil Temperature	Different depth	PT <sub>100</sub> resistance thermometer (Manufactured by Wageningen Uni.)
Soil moisture	Different depth	TDR (Campbell) (Tamale), TDR (Delta-T) (Ejura)
Skin temperature	2m	Infrared (IR) temperature probes (Heimann)

### 3.2.4 Validation data

Available energy at the surface is validated with the taken net radiation and soil heat flux measurements. Net radiation is measured directly at 8 m height and soil heat flux is measured at 0.035 m depth. Sensible heat flux is validated with the LAS measurements. The LAS are installed at a certain height above the surface. The emitted radiation is scattered by the turbulent medium in the path. The variance of intensity of received radiation is proportional to the structure parameter of the refractive index of air ( $C_n^2$ ). At the wavelength used (940nm) the refractive index mainly depends on temperature, so  $C_n^2$  is mostly determined by temperature fluctuations ( $C_T^2$ ). The influence of humidity on the refractive index is considered, according to the work of Wesely (1976) and Moene (2003).

Sensible heat flux is calculated from  $C_T^2$  using Monin-Obukhov similarity theory (MOST). Stability functions proposed by Wyngaard (1973) were applied for daytime values. For nighttime values we follow the formulation of De Bruin et al. (1993). For a more detailed description of the LAS theory and its applications see for example De Bruin et al. (1995) or Meijninger et al. (2002).

Latent heat flux is calculated as a residual from the energy balance, which showed good correspondence with eddy covariance data obtained during an intensive observation period

(IOP) during the drying up in 2002. One has to remember that this approach forces the energy balance to close. The energy balance was closed for the IOP in 2002 in Tamale and for large parts of the season in Ejura, with the four terms measured independently (Schüttemeyer et al. 2004, submitted to Boundary-Layer Meteorology).

### 3.2.5 Model Parameters

For NOAH the vegetation type is set to Savannah for Tamale and to Broadleaf-Evergreen Trees (tropical forest) for Ejura. For TESSEL the vegetation types for low and high vegetation are a mixture of grass and interrupted trees in case of Tamale and for Ejura it is only high vegetation (Broadleaf-Evergreen Trees). The chosen values for various parameters for the test sites are given in table 3.3. The soil type is universal for TESSEL. The soil type for NOAH at both test sites is loamy sand. From a detailed survey for soil properties (Agyare 2004) it was found that the soil type for Ejura corresponds better to a sandy clay loam and for Tamale it is a sandy loam in the top soil (0.15 m) and loam for the subsoil (0.3 – 0.45 m). Other model parameters are set to values generally used within the operational 3D version of the ECMWF model corresponding to the values at the closest grid point (in case of geographically dependent parameters) or data from the US Geological Survey's (USGS) is taken. For both models no locally adopted parameters are utilized.

**Table 3.3a: Ejura: Model parameter values for TESSEL and NOAH.**

Parameter Ejura	NOAH	TESSEL	
		High vegetation	Low vegetation
roughness length momentum (m)	0.4	0.4	0.4
roughness length heat (m)	based on Zilitinkevich	0.04	0.04
LAI (m <sup>2</sup> m <sup>-2</sup> )	4	5	1
Minimum canopy resistance (sm <sup>-1</sup> )	150	240	100
Albedo (-)	J F M A M J J A S O N D		
	0.18 0.18 0.18 0.17 0.16 0.14 0.15 0.15 0.15 0.15 0.16 0.17		
vegetation coverage (-)	see table 2c	1	0
Bare soil fraction (-)	see table2c	0.1	0.4
soil porosity (m <sup>3</sup> m <sup>-3</sup> )	0.421	0.472	
Water content at wilting point (m <sup>3</sup> m <sup>-3</sup> )	0.029	0.171	
water content at field capacity (m <sup>3</sup> m <sup>-3</sup> )	0.283	0.323	
b Parameter (-)	4.26	6.0	
root distribution in % over 4 layers (m <sup>3</sup> m <sup>-3</sup> )	uniform	25; 34; 27; 14	27; 37; 27; 9

**Table 3.3b: Model parameter values for TESSEL and NOAH for Tamale.**

PARAMETER TAMALE	NOAH	TESSEL	
		High vegetation	Low vegetation
roughness length momentum (m)	0.2	0.2	0.2
roughness length heat (m)	based on Zilitinkevich	0.02	0.02
LAI (m <sup>2</sup> m <sup>-2</sup> )	3	2.5	1
Minimum canopy resistance (sm <sup>-1</sup> )	120	175	100
Albedo (-)	J F M A M J J A S O N D		
	0.19 0.20 0.20 0.18 0.17 0.16 0.15 0.16 0.15 0.16 0.17 0.18		
vegetation coverage (-)	see table 2c	1	0
Bare soil fraction (-)	see table 2c	0.01	0.4
soil porosity (m <sup>3</sup> m <sup>-3</sup> )	0.434	0.472	
Water content at wilting point (m <sup>3</sup> m <sup>-3</sup> )	0.047	0.171	
water content at field capacity (m <sup>3</sup> m <sup>-3</sup> )	0.312	0.323	
b Parameter (-)	4.74	6.0	
root distribution in % over 4 layers(m <sup>3</sup> m <sup>-3</sup> )	uniform	19; 35; 36; 10	27; 37; 27; 9

**Table 3.3c: Seasonal dependent vegetation fraction for NOAH at both test sites.**

Vegetation Frac.	J	F	M	A	M	J	J	A	S	O	N	S
Ejura	0.17	0.22	0.35	0.49	0.70	0.75	0.65	0.66	0.71	0.66	0.58	0.36
Tamale	0.04	0.02	0.05	0.08	0.24	0.40	0.47	0.56	0.61	0.51	0.30	0.12

Both models were run in offline mode at the two locations. The time step for integration is set to 600 s according to the measured quantities. The model runs for Tamale were done for the period from DOY 238 until DOY 21 and for Ejura it was the period from DOY 269 until DOY 52. Both periods cover the transition time from the wet to the dry season in the studied region. Since there were no measurements for soil temperature profiles available at both sites those initial values were obtained by calculating the daily, weekly, monthly, yearly air temperature and using those values for the four soil layers. In case of initial soil moisture the values for Ejura were estimated from the closest measurements in time. For Tamale the routinely measured values were taken. For initial soil moisture for the lowest level the values from the level above were taken.

### 3.2.6 Model evaluation

Simulated fluxes are compared to measured quantities namely net radiation, soil heat flux, sensible heat flux and latent heat flux.

As a first check for the different components of the energy balance the mean bias error (MBE) and rmse are calculated. To account for the seasonal dynamics the same procedure is done for weekly periods from the beginning to the end at the two sites. One has to keep in mind that the errors in sensible, latent and soil heat flux do not necessarily add up for every week, since some measurements for sensible and latent heat flux were rejected due to insufficient quality. With the help of the measurements the canopy conductance is calculated and compared to the modeled ones.

### 3.3 Results

In this section the comparison of the simulated and measured components of the energy balance are presented for the two sites separately. The role of the canopy conductance is analyzed and simple adjustments to obtain enhanced model performance are discussed. The main interpretation is done in section 3.4.

#### 3.3.1 The different components of the energy balance

##### a) Ejura

There is a clear decline in global radiation ( $R_g$ ) and available energy ( $R_n-G$ ) (Fig. 3.1). It starts at the end of November 2002 until the third week of year 2003. This is the period where the rain decreased, stopped and started again. The decline in net radiation implies a decline in the sum of sensible and latent heat flux during that time. The water vapor pressure deficit (VPD) in Ejura increases from less than 0.5 kPa up to 2 kPa in the first two weeks of December. Before that date it nearly stays constant (Fig. 3.1). The overall results show a good estimation of net radiation for both models (table 3.4a). The seasonal dynamics give a weekly correlation coefficient, which is always 0.99 for both models throughout the studied season. For the MBE there is a clear trend from small negative values in the beginning to larger positive values in the end with a peak around the end of year 2002 (Fig. 3.2). The last rain appeared on DOY 343 (week 49) and started again on DOY 23 (week 4). During that period the MBE in net radiation increases up to  $34 \text{ W m}^{-2}$  and the relative MBE shows a maximum close to 50% for NOAH. This suggests that the process of drying up is influencing the model runs, since the decrease in available energy starts earlier (Fig. 3.1), but the MBE stays on a low level (MBE for soil heat flux discussed below). The higher MBE towards the end might be due to wrong surface temperature and/or albedo. For the first five weeks TESSEL shows slightly higher negative values for the MBE than NOAH. From week 46 TESSEL shows similar or lower values for the MBE. The rmse (not shown) shows a similar trend as the MBE (average around

$30 \text{ W m}^{-2}$ ). It also reaches its maximum ( $38 \text{ W m}^{-2}$  for NOAH) during the beginning of 2003, when the process of drying up is approaching the maximum.

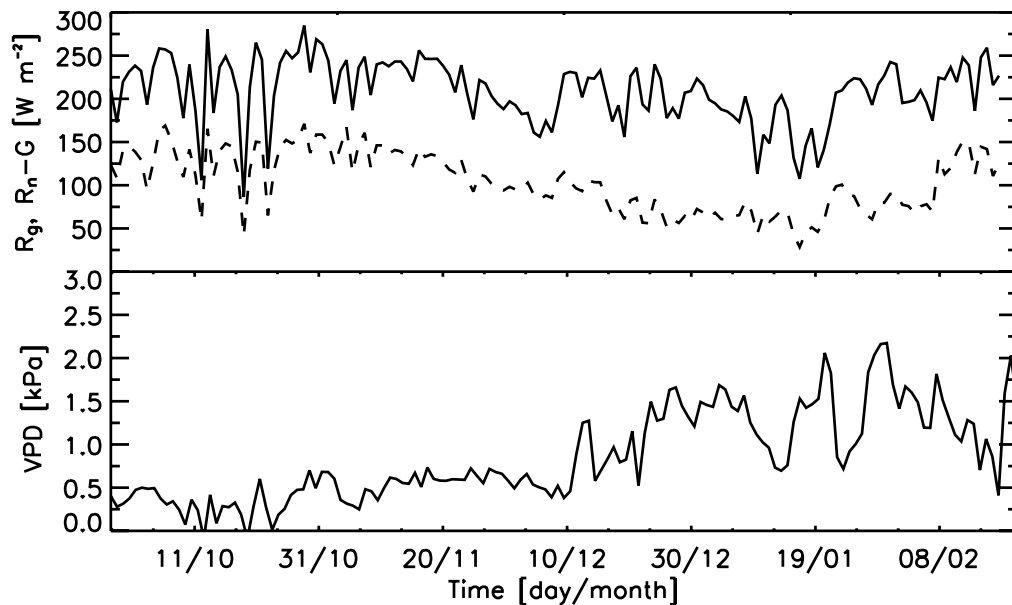


**Fig. 3.1: Ejura: Daily averages for global radiation ( $R_g$ ), available energy ( $R_n-G$ ) and VPD for the period from the end of September 2002 until the end of February 2003.**

For Ejura there were no soil temperature measurements available for correcting soil heat flux measurements. Therefore no direct comparison of the soil heat flux at the surface can be done for this site. Due to the more dense vegetation cover, the effect of heat storage above the sensor at 0.035 m depth should be definitely smaller than in Tamale (there it was on average 30% during daytime of the measured soil heat flux at 0.035 m depth) (compare Hatfield and Prueger 2000). To give a first idea of the differences in measured and modeled soil heat fluxes the measured values at 0.035 m depth are compared to the modeled ones at the surface (table 3.4a). The rmse is on a high level, which should be related to a time shift between the soil heat flux at the surface and at 0.035 m depth. The overall MBE is negative for both models, which suggests that both underestimate soil heat flux. The weekly evaluation shows that there is no trend in MBE or rmse. Both models give values, which are fluctuating around the MBE for the whole season. The overall MBE for sensible heat flux (table 3.4a) is large for both models. The seasonal dynamics in the MBE for sensible heat flux are shown in figure 3.3. Both models show the same trend from negative to positive values throughout the whole period also with an increase towards the end of the season.

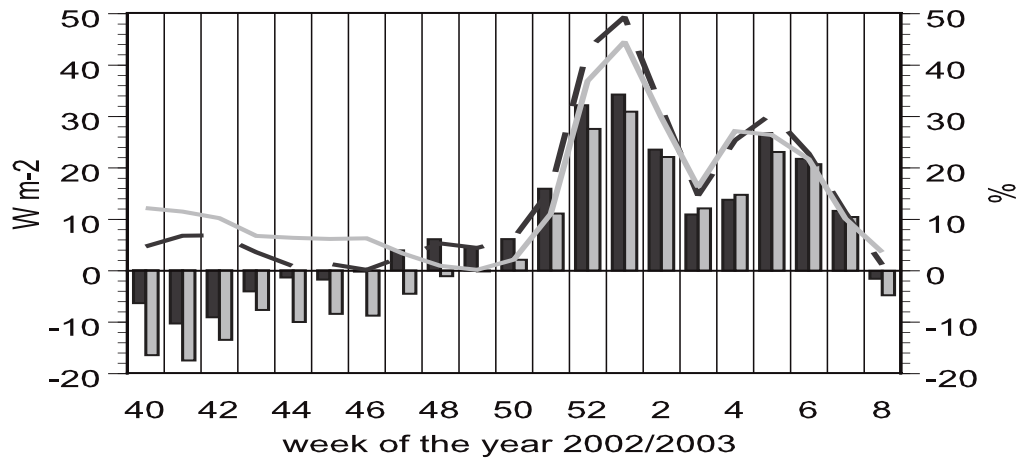


**Fig. 3.2: Ejura: Weekly MBE of net radiation for NOAA (black bars) and TESSEL (gray bars) in  $W m^{-2}$  (bars) and relative MBE as a percentage of total mean flux (lines) for the studied season.**

Due to the lack of LAS data the measurements end earlier than for net radiation and soil heat flux. The highest values ( $30 W m^{-2}$ ) appear during the time when the process of drying up reaches its maximum. The weekly correlation is always higher than 0.7 with a maximum of 0.94 at the end of the period. The rmse shows the same trend as for net radiation on a slightly higher level. TESSEL shows higher values for the MBE for large parts of the studied season. The errors in sensible heat flux during the drying up imply that available energy, turbulent exchange coefficient or the surface temperature is not modeled correctly by both models (see discussion below).

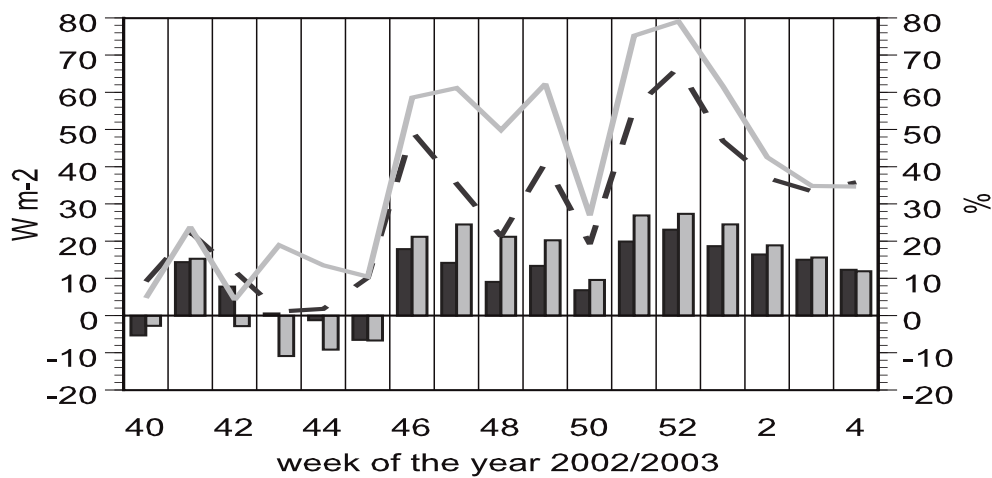


**Fig. 3.3: Ejura: same as figure 3.2 for sensible heat flux.**



The overall results for latent heat flux show a negative MBE for NOAH and a positive MBE for TESSEL (table 3.4a). Compared to sensible heat flux the relative MBE is on a lower level. The rmse is on a slightly higher level than the rmse for sensible heat flux. The seasonal dynamics show different results for the two models (fig. 3.4). For TESSEL the seasonal dynamics show the highest positive values for the MBE in the beginning and the end. For NOAH the MBE is smaller in the beginning and the end compared to TESSEL. For the time in between both models give comparable results. The correlation shows a clear trend from high values (0.97) for the first eight weeks. After that period it slowly decreases to 0.75 for both models. The rmse shows the same trend as for net radiation but on a higher level (min.  $32 \text{ W m}^{-2}$ , max.  $75 \text{ W m}^{-2}$ ).

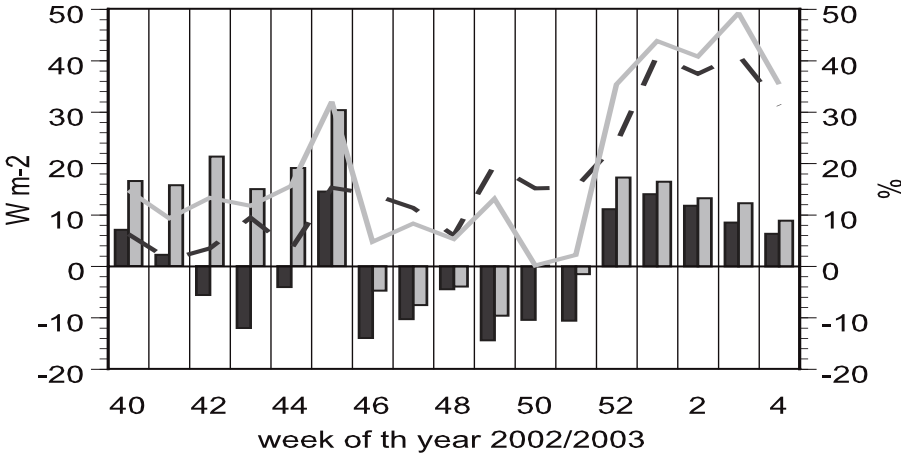


Fig. 3.4: Ejura: same as figure 3.2 for latent heat flux.

Table 3.4a: Overall statistics for the components of the energy balance for Ejura. For soil heat flux no percentage is calculated since the mean flux was small. Errors in the components of the energy balance do not necessarily add up, since different periods were analyzed.

	Correlation		MBE ( $\text{Wm}^{-2}$ )		rmse ( $\text{Wm}^{-2}$ )		Relative MBE (%)	
	NOAH	TESSEL	NOAH	TESSEL	NOAH	TESSEL	NOAH	TESSEL
$R_n$	0.99	0.99	8.3	3.9	30.6	31.2	7.4	3.6
G	0.88	0.82	-3.3	-9.9	36.6	32.0	*	*
H	0.84	0.82	12.6	15.3	39.9	45.2	30.9	37.1
LE	0.92	0.90	-4.0	7.9	49.7	58.3	5.5	11.3

b) Tamale

For Tamale the decline in global radiation and available energy (fig. 3.5) starts by the end of October and continues until the end of the measurements. The VPD starts growing by the end of October and reaches higher values than in Ejura.

The overall evaluation gives reasonable results for both schemes (table 3.4b). The overall MBE and rmse for net radiation are higher compared to Ejura. The weekly correlation coefficient for net radiation is always close to one for both models throughout the whole period. The seasonal dynamics of the MBE for net radiation are given in figure 3.6. There is a clear trend from a small negative MBE in the beginning to a higher positive MBE towards the dry season in both models. In the beginning TESSEL shows slightly lower values for the MBE, towards the end they are higher compared to NOAH. The same trend is seen in the rmse. This shows that the largest errors appear, when the process of drying up proceeds, as seen for Ejura before. This suggests that surface temperature is not modeled correctly and/or there is a problem with albedo estimation.

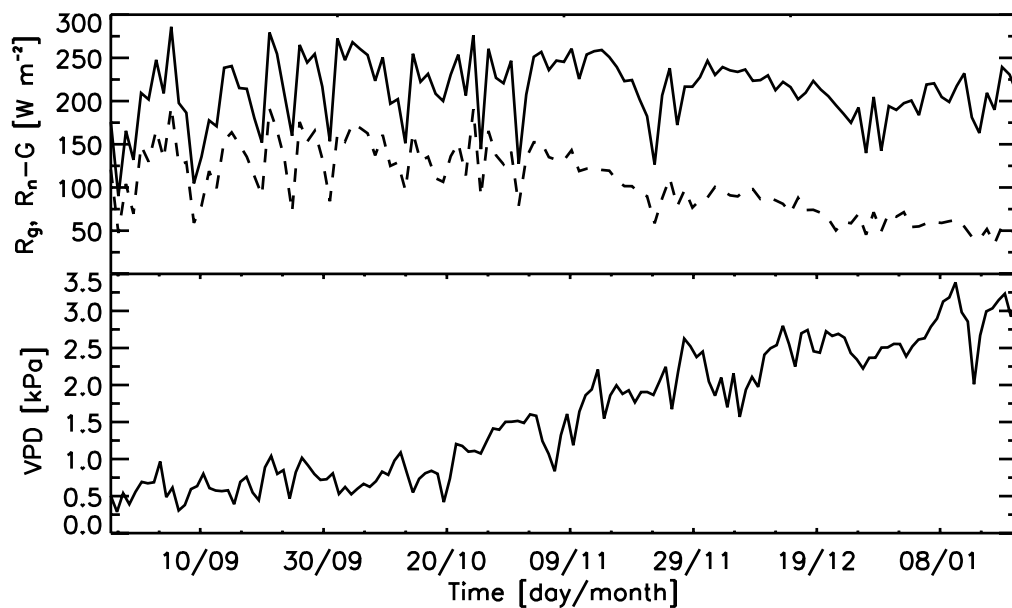


**Fig. 3.5: Tamale: Daily averages for Global radiation ( $R_g$ ), available energy ( $R_n-G$ ) and VPD for the period from the end of August until the end of January 2003.**

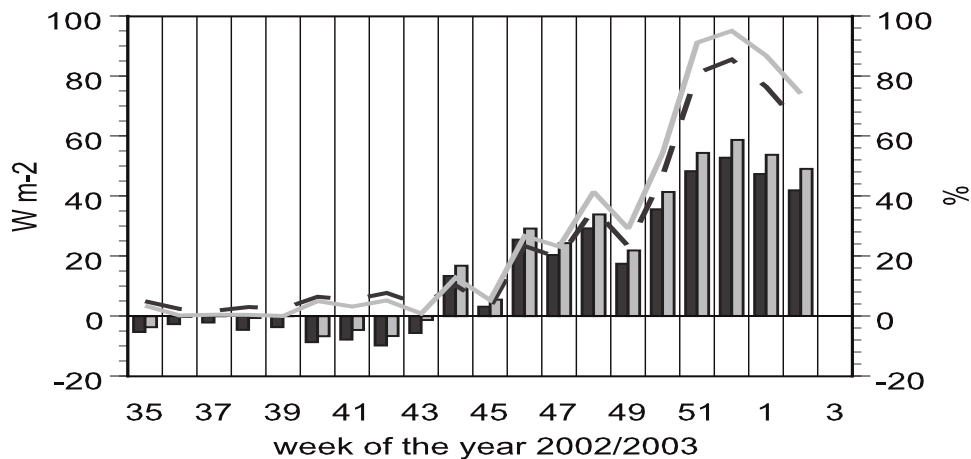


**Fig. 3.6: Tamale: Weekly MBE for NOAH (black bars) and TESSEL (gray bars) of net radiation in  $W m^{-2}$  (bars) and relative MBE as a percentage of total mean flux (lines) for the studied season.**

For this test site soil heat flux is calculated on top of the soil, combining data from the soil heat flux plates and the soil temperature. This is done by applying the method of Heusinkveld et al. (2004). The overall results are shown in table 3.4b. The long-term MBE is small for both models. One has to remember that soil heat flux on top of the soil reaches values up to  $200 W m^{-2}$  during the time of transition. The seasonal dynamics of soil heat flux show small positive MBE throughout the season for NOAH and small negative values for TESSEL. The same survey for soil properties as for Ejura was done here and it was found that the soil type does not correspond to the one from the USGS database, which is loamy sand with a quartz content of 0.82. The real soil is a sandy loam with quartz content of 0.57. It might also explain the higher rmse for NOAH since model runs with the right soil type showed better agreement with the measurements on a long term and weekly basis. The model runs started on DOY 238, but due to measurements problems of the LAS the comparison of surface fluxes starts on DOY 287.

For sensible heat flux the overall results are given in table 3.4b. The relative MBE is on a high level. The weekly correlation is rising for both models from 0.68 in the first week to values close to 1 at the end. The seasonal dynamics in MBE for sensible heat flux (fig. 3.7) show a similar trend for both models with slightly higher values for TESSEL. The rmse for both models decreases in time starting around  $50 W m^{-2}$  and ending around  $30 W m^{-2}$ .

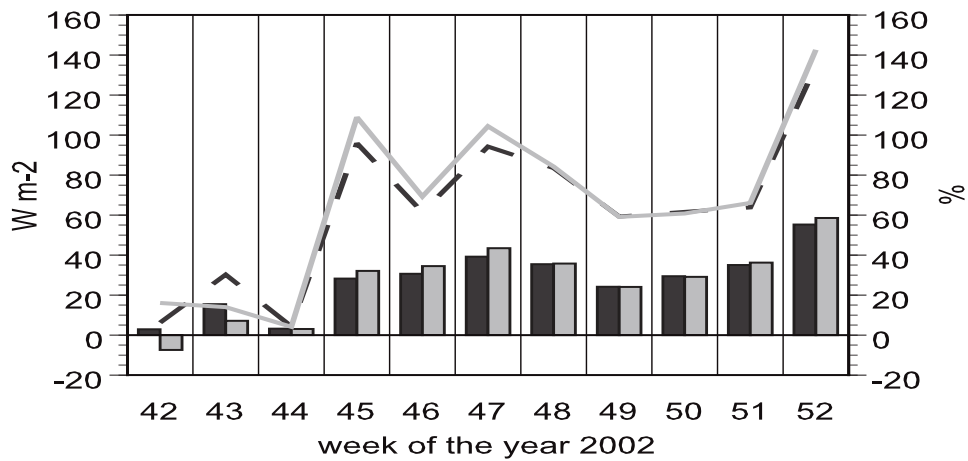


**Fig. 3.7: Tamale: same as figure 3.6 for sensible heat flux.**

The overall results for latent heat flux show the same correlation for both models. The overall MBE shows a much higher value for NOAH. The weekly correlation is decreasing for both models from the beginning to the end from 0.97 to 0.72. The MBE for both models shows small fluctuating values for large parts of the season (fig. 3.8).

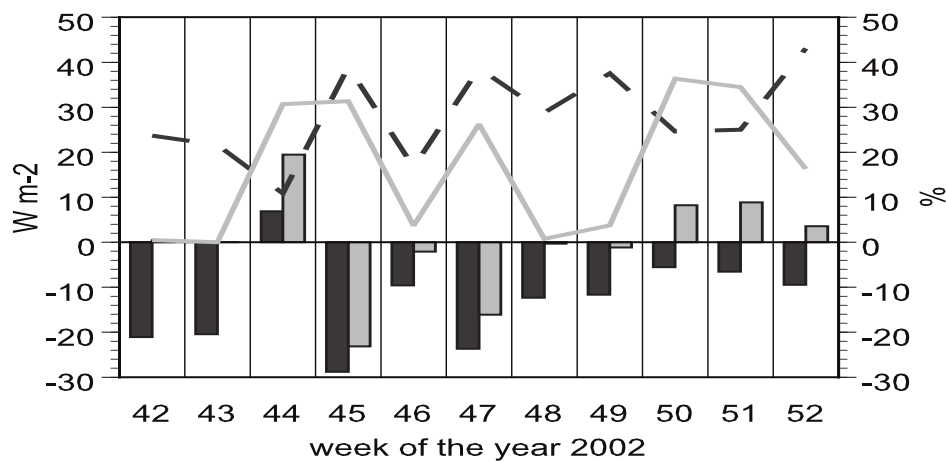


**Fig. 3.8: Tamale: same as figure 3.6 for latent heat flux.**

**Table 3.4b: Same as table 3.3a but for Tamale.**

	Correlation		MBE ( $Wm^{-2}$ )		rmse ( $Wm^{-2}$ )		Relative MBE (%)	
	NOAH	TESSEL	NOAH	TESSEL	NOAH	TESSEL	NOAH	TESSEL
$R_n$	0.98	0.98	16.0	20.1	38.8	41.4	15.4	19.4
G	0.88	0.88	4.0	-4.3	32.4	34.6	*	*
H	0.90	0.90	27.5	27	39.9	40.1	58.8	57.9
LE	0.89	0.89	-12.0	0.69	50.1	44.1	23.1	1.3

### 3.3.2 Influence of initial soil moisture

The influence of the initial model settings is examined by varying the initial soil moisture content for both models and sites. The volumetric soil moisture content in each layer is varied by an increase and decrease of 0.05 and 0.1  $\text{m}^3 \text{m}^{-3}$ . To analyze resulting differences, the weekly average differences in the components of the energy balance are calculated.

The influence for net radiation at both sites for NOAH is 0 for higher soil moisture and negligible ( $<0.5 \text{ W m}^{-2}$ ) for lower soil moisture content. For TESSEL the influence of changing initial soil moisture content is detectable throughout the season for both sites. The average weekly difference in net radiation with lower initial soil moisture of 0.1  $\text{m}^3 \text{m}^{-3}$  is about  $10 \text{ W m}^{-2}$  during the wet part of the season and it increases to  $20 \text{ W m}^{-2}$  towards the end. For higher initial soil moisture the net radiation also changes, but the effect is smaller. For sensible and latent heat flux modeled by NOAH the weekly differences are small (max.  $2 \text{ W m}^{-2}$ ) for the first 4 to 5 weeks and 0 afterwards. For TESSEL the differences in surface fluxes with lower initial soil moisture are about 10 to  $15 \text{ W m}^{-2}$  for the wet part. After that the differences reach values up to  $20 \text{ W m}^{-2}$  for a reduction of soil moisture content of 0.1  $\text{m}^3 \text{m}^{-3}$  in sensible heat flux and lower values of about  $5 \text{ W m}^{-2}$  for latent heat flux. The largest influence in latent heat flux is seen when the rain stops and the drying up process starts.

### 3.3.3 The role of canopy conductance

Since TESSEL has no seasonal variation in the vegetation fraction the vegetation is transpiring throughout the whole period for Ejura, whereas only during and after rain events evaporation from interception occurs. The canopy conductance is responsible for regulation of the evaporation during the drying up. For NOAH, which includes a seasonal variation in the vegetation fraction, it is observed that there is always a certain amount of bare soil evaporation, which is not realistic for the conditions in Ejura during the studied time.

For Tamale the vegetation characteristics show a mixture of mainly vegetation (low in case of TESSEL) and bare soil for both models, with seasonally dependent vegetation fraction for NOAH. The different components of evaporation show a clear trend for the NOAH model. Evaporation is reduced during the drying up, where the total amount of bare soil evaporation is high. For TESSEL the interception, high vegetation evapotranspiration and bare soil evaporation is again modeled more realistically.

The canopy conductance is calculated from the observations using the rearranged Penman-Monteith equation (e.g., Monteith and Unsworth 1990) following Harris et al. 2003. For the calculation of the aerodynamic conductance the method of Verma (1989) with stability

corrections by Paulson (1970) is applied. The roughness length for momentum was estimated using the approach of Martano (2000) and roughness length for heat was estimated by applying a fixed ratio of roughness length for momentum and heat of 100, which was estimated for Savannah conditions by Huntingford et al. (1995). Under conditions of low available energy the computation of  $g_s$  can give non-realistic large conductances. Therefore the calculation of  $g_s$  is restricted to daytime situations between 9:00 am and 5:00 pm.

Concerning the MBE of latent heat flux both models gave different results for Ejura (fig. 3.4). When analyzing the canopy conductance it is found that TESSEL gives more realistic values for both sites, when compared to the conductance calculated by the rearranged Penman-Monteith equation (fig. 3.9).

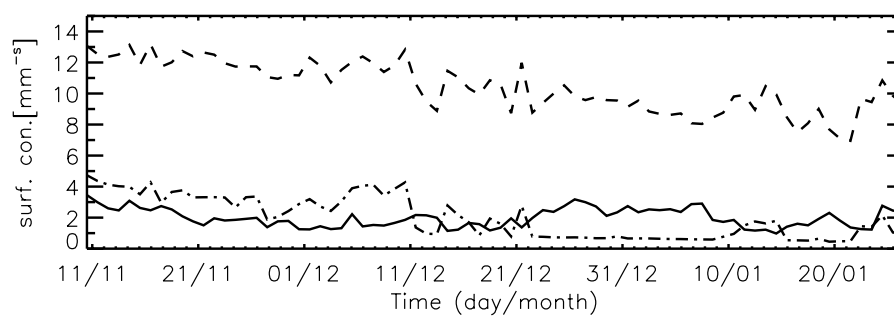


**Fig. 3.9: Ejura: Measured (solid line) and modeled surface conductance (NOAH: dashed line; TESSEL: dashed dotted line) for the main period of drying up during the studied season.**

It is also seen that in the beginning the canopy conductance from TESSEL is too high, which means that too much evaporation is going on. This is confirmed by the positive MBE of latent heat flux (fig. 3.4). For parts of the period where the MBE is negative the canopy conductance is too low compared to the measurement-based calculation. At the end the signal is not as clear as before for TESSEL, which might partly be explained by the fact that the rain started again and canopy conductance is not as important as before. Since the MBE of NOAH is comparable to that of TESSEL and the canopy conductance for NOAH is too high the time-dependent vegetation fraction must be the largest controlling mechanism in determining evapotranspiration. The reason for the differences in model performance is due to the different formulation of canopy conductance (Appendix A). The different functions in the framework of the total canopy conductance are shown in figure 3.10a (3.11a) and 3.10b (3.11b) for Ejura (Tamale). The influence of temperature is only shown for NOAH, since TESSEL does not make use of this dependence. It can be seen that the value of this function is close to 1 throughout the season, which means that there is a small influence on the canopy conductance on a seasonal basis. For the radiation dependent function it is seen that both

models show a similar curve with values closer to 1 for NOAH throughout the season. For the VPD dependent functions both models show the same trend. Both models start with similar values for this response function but the decrease is more pronounced in TESSEL. The soil moisture response function shows saturation in the beginning for both models and drops for TESSEL as soon as the time of transition starts. From that point onwards the largest differences appear in this function. TESSEL shows a large decrease of this value, whereas NOAH gives a much smaller decrease. This means that the largest control mechanism should be indeed the vegetation fraction for NOAH and soil moisture for TESSEL.

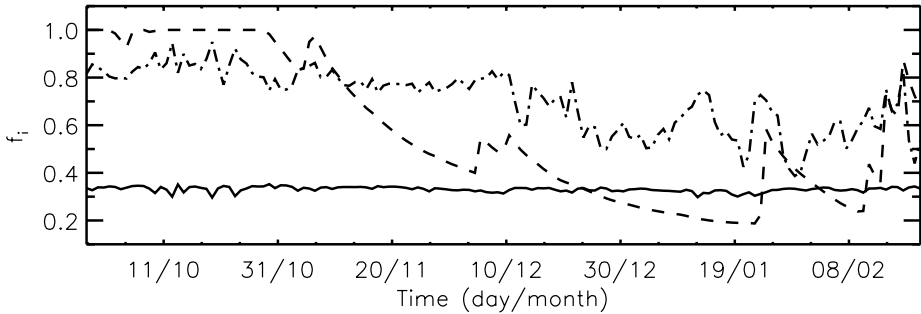


**Fig. 3.10a: Ejura: Daily averages of the different functions  $f_i$  of Jarvis-Stewart formulation for TESSEL in the context of transpiration calculation. Solid line corresponds to radiation response, dashed line to soil moisture response and dashed dotted line to VPD.**

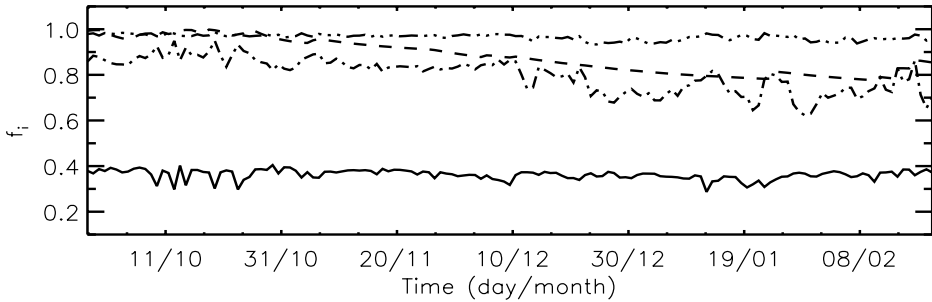


**Fig. 3.10b: Ejura: Daily averages of the different functions  $f_i$  of Jarvis-Stewart formulation for NOAH in the context of transpiration calculation. Solid line corresponds to radiation response, dashed line to soil moisture response, dashed-dotted line to VPD and dashed dot dot line to temperature response.**

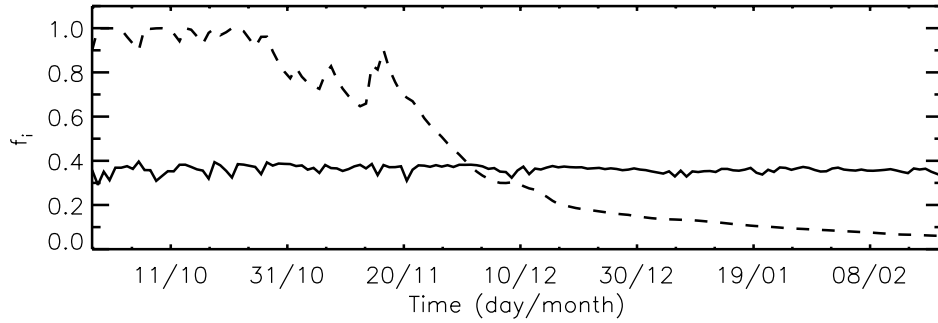


**Fig. 3.11a: Tamale: Daily averages of the different functions  $f_i$  of Jarvis-Stewart formulation for TESSEL in the context of transpiration calculation. Solid line corresponds to radiation response, dashed line to soil moisture response.**

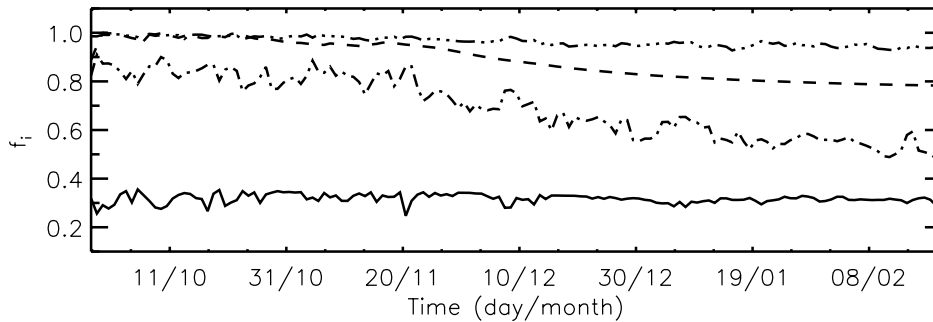


**Fig. 3.11b: Tamale: Daily averages of the different functions  $f_i$  of Jarvis-Stewart formulation for NOAH in the context of transpiration calculation. Solid line corresponds to radiation response, dashed line to soil moisture response, dashed-dotted line to VPD and dashed dot dot line to temperature response.**

### 3.3.4 Simple Adjustments for both test sites

The large MBE in sensible heat flux during the drying up suggests that the surface temperature is not calculated correctly for both models. For Ejura this cannot be proven, since there are no surface temperature measurements available. For Tamale there are measurements available, but only during the IOP, which took place in November and December 2002. From the direct comparison of measured surface temperature and the modeled surface temperature from NOAH (one universal) and TESSEL (separate surface temperatures for bare soil and low vegetation) it is seen that during daytime in the beginning of the IOP (week 44) the differences between measured (sensor placed above a mixture of bare soil and grass) and modeled surface temperatures are small and the differences grow towards the end of the year



(Fig. 3.12). This might partly explain the growing MBE in net radiation (Fig. 3.8) but not the magnitude of the MBE for sensible heat flux in Tamale.

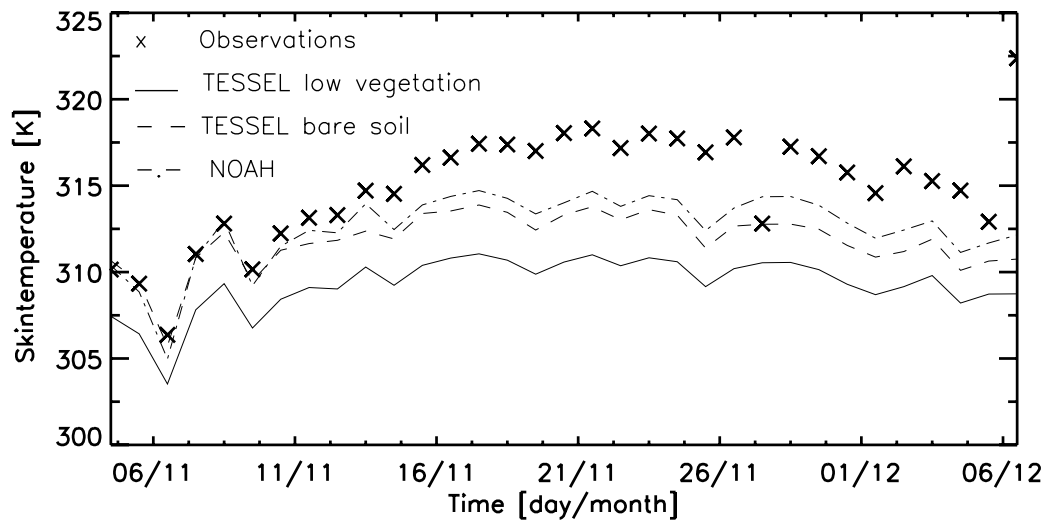


**Fig. 3.12: Comparison of measured and modeled skin temperature (averages between 900 am and 500 pm) for an intensive observation period in November and December 2002 in Tamale.**

Another error source could be the exchange coefficient for heat. Chen et al. (1997) compared different atmospheric surface-layer parameterization schemes and concluded that the differences in the schemes and the resulting surface exchange coefficients did not, in general, lead to significant differences in model simulated surface fluxes and skin temperature.

The models were more sensitive to changes of ratio of roughness length for momentum and heat. Therefore the next step is to vary those ratios for both models (see also Holtslag and Ek 1996). Huntingford et al. (1995) estimated a ratio of 100 for savanna type vegetation in contrast to the ratio of 10 of TESSEL. To test the influence of a changed ratio of roughness length for momentum and heat a ratio of 100 and 1000 is employed. NOAH uses equation 3.2. For further analysis  $P_z$  is set to 0.4 and 0.6 instead of 0.2. For both models the surface temperature is in better agreement with the measurements during the IOP. The MBE for net radiation decreases during the drying up when the above mentioned changes are applied. For the test site in Tamale the weekly changes in MBE for NOAH and TESSEL are shown in Fig. 3.13a and 3.13b. It is seen that the MBE is reduced towards the end of the season, whereas the MBE rises in the beginning. The changed roughness length ratio on soil heat flux is negligible. The changes in latent heat flux are small with values around  $2 \text{ W m}^{-2}$ . For both models the largest impact is seen in sensible heat flux. For NOAH the weekly differences

increase from  $5 \text{ W m}^{-2}$  to  $15 \text{ W m}^{-2}$  towards the end of the studied period. For TESSEL the changes are nearly constant ( $6 \text{ W m}^{-2}$ ) throughout the season. For Ejura the same trends with similar changes are seen during the time of drying up. There is also a similar increase in MBE before the drying up.

For TESSEL the vegetation fraction is fixed. From the measurements of tree density at the two test sites it was seen that the values of the percentage of high and low vegetation differs from the actual one. Further model runs showed that when real percentages were utilized the impact on surface fluxes were small. This could be related to the root distribution, since the observed root distribution differed from the actual. To quantify that impact more thoroughly extended data on root distribution and leaf area index would be needed.

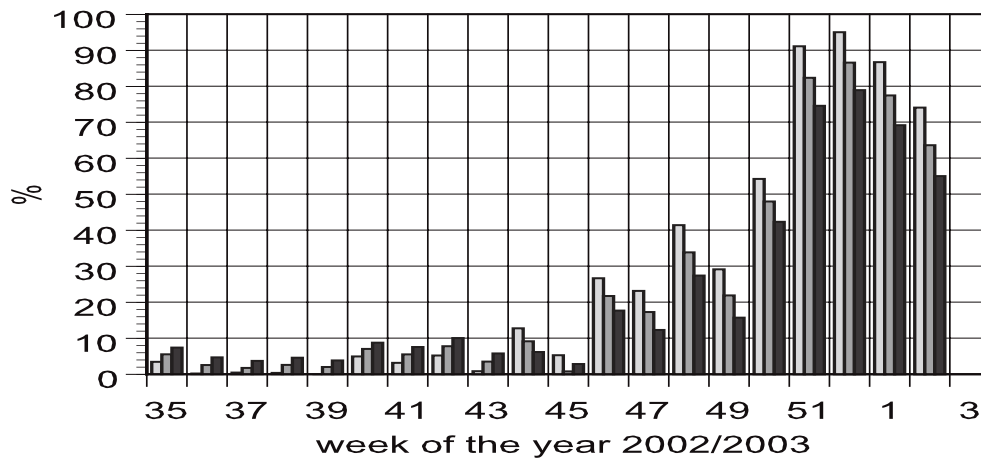


**Fig. 3.13a: Relative MBE for net radiation for TESSEL, when applying roughness length ratios of 10 (gray bar), 100 (dark gray bar) and 1000 (black bar).**

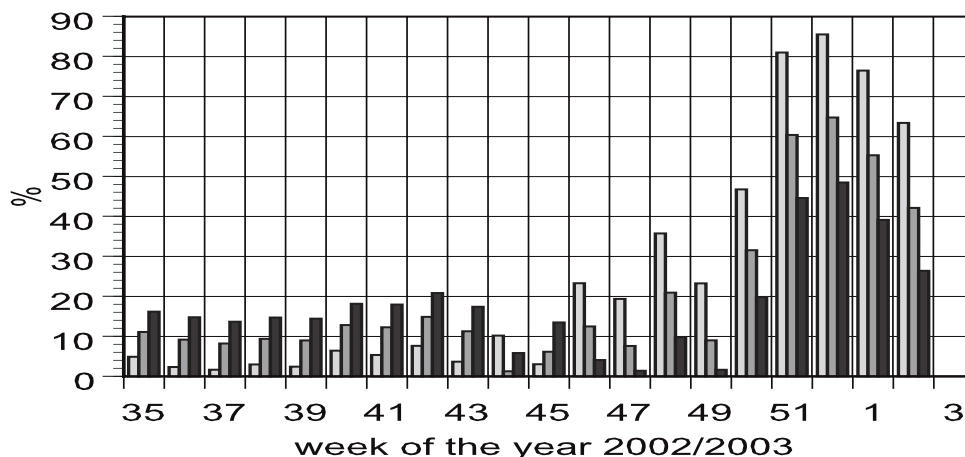


**Fig.3.13b: Relative MBE for net radiation for NOAH, when  $P_z$  of 0.2 (gray bar), 0.4 (dark gray bar) and 0.6 (black bar).**

### 3.4 Discussion

The offline evaluation of two state-of-the-art land surface models with different parameterization for surface fluxes was presented.

The results for both test sites show a very good correlation throughout the studied season for net radiation. For the southern test site in Ejura the MBE and rmse are relatively small but growing during the drying up. This feature is also observed for the test site in Tamale with higher values for the MBE and rmse towards the end of the season. This should be related to an enhanced process of drying up for the northern region in Tamale. Due to this process larger changes in surface cover occur during the studied period compared to Ejura. In the beginning the trees and the grass were green and towards the end the grass was brown and only the trees were green (cover 15%), whereas for Ejura most of the vegetation cover was still green by the end of the period. The two models show small errors during the wet part of the season but may fail to spot the dynamics of surface temperature and of the albedo, due to those processes.

For soil heat flux it is observed that the seasonal errors are relatively small for both sites. There is a trend for larger errors when the surface becomes dryer, which is only observed at Tamale test site. Since the errors in soil heat flux are small the observed errors in net radiation should be compensated by the errors in the calculation of turbulent fluxes.

The comparison of modeled and measured sensible heat fluxes showed for both models and test sites, that when the surface becomes dryer the model results were inferior to those during the wet season. For Tamale test site (Savanna type vegetation) the errors are larger in sensible heat flux for the dryer part of the season. Here the relative MBE reaches values close to 100%. The model results show smaller errors for NOAH. This suggests that the more dynamic formulation of roughness length ratio helps to reduce the errors in contrast to the fixed ratio for TESSEL. For latent heat fluxes the weekly errors are smaller compared to sensible heat flux. There is not such a clear trend as seen for sensible heat fluxes.

It was shown that the canopy conductance parameterization combined with a fixed vegetation fraction in TESSEL reduces the amount of latent heat flux during the time of transition. The daily median of canopy conductance showed better agreement between the Penman-Monteith formulation and TESSEL. Here an adjusted maximum canopy conductance based on more detailed vegetation types could even help to improve model performance. For NOAH the driving force in reducing evapotranspiration during the drying up is the vegetation fraction, since the reduction in canopy conductance did not show a comparable response as seen for TESSEL. The formulation for evapotranspiration in NOAH mostly depends on the accuracy of the estimated vegetation fraction at the actual time and not on the plant specific variables

related to the Jarvis-Stewart formulation, which makes it more difficult to optimize needed parameters in this context.

One point when analyzing the behavior of evapotranspiration might be that deeper soil moisture content could not be evaluated, since there were no measurements available. For this reason it cannot be evaluated if both schemes model deeper soil moisture correctly.

The calculation of canopy conductance for TESSEL is based on soil moisture and radiation in case of low vegetation and water vapor pressure is included only for high vegetation. Since the conductance formulation shows a large response to soil moisture content in the different layers, it is crucial to initialize the model runs with correct soil moisture content. When the initial soil moisture content was varied it could be shown that this had a small but observable effect on the calculation of surface fluxes in TESSEL throughout the studied period. This behavior could not be observed for NOAH due to the different calculation of canopy conductance. Furthermore the changes in soil moisture showed a nonlinear response (lower values lead to larger changes) in the components of the energy balance, which was already observed by Niyogi et al. (2002).

Tuning the Zilitinkevich constant in case of NOAH and applying a different roughness length ratio in case of TESSEL could improve the results for both test sites. The upcoming issue when applying this is that the results got worse during the wet period. This suggests that due to the seasonal changes in vegetation cover the above named variables have a seasonal dependence. The Zilitinkevich constant, which acts as a tuning factor in the NOAH model, needs to be adjusted and it was shown that it is sensitive to the relatively small changes made. The lower MBE for NOAH when applying a different Zilitinkevich constant might be related to the more dynamic formulation for the ratio of roughness lengths, since the daily variability of wind speed increased towards the end of the season. Those dynamics cannot be tackled by a fixed ratio of roughness lengths as applied for TESSEL.

Employing the right soil type for NOAH for both test sites reduced the errors for soil heat flux by up to 10%. The better results for NOAH, when the right soil type was taken, show that if one employs regionally dependent soil type in land surface modeling it is crucial to have the right one. For large parts of West Africa high quality data concerning soil parameters are not available. Therefore the workaround might be using one universal soil type as realized by TESSEL.

### **3.5 Conclusions**

Both land surface models showed similar overall errors for the different components of the energy balance with higher errors for the less dense vegetated test site in the northern region.

The seasonal evaluation on the basis of weekly error estimation showed similar tendencies for both models with larger errors when the surface became dryer. Concerning the evapotranspiration formulation the performance of TESSEL seems to be more realistic due to the fact that the canopy conductance parameterization showed a clear seasonal dependence for both test sites as observed by the measurements. This performance was in contrast to the one in NOAH. This feature of TESSEL offers the possibility to analyze the errors more detailed or do sensitivity analyses, whereas this is more difficult for NOAH. The dependence on vegetation fraction is also important for modeling the regional climate with NOAH, since it cannot be specified properly for future climates.

Simple adjustments helped in reducing the larger errors during the dryer part of the season but at the expense of larger errors during the wetter part. For the future a different formulation of the ratio of roughness length for heat and momentum like the one proposed by Kubota and Sugita (1994) might help in reducing the errors. A seasonal evolution of vegetation related parameters as already mentioned by Van den Hurk et al. (2000) might also be necessary to improve the erroneous surface fluxes by both models.

## Appendix A

### The evapotranspiration parameterization for NOAH and TESSEL

For both models a canopy conductance parameterization is utilized to calculate evapotranspiration. In this study evapotranspiration is the sum of evaporation from bare soil ( $E_{dir}$ ), the interception reservoir ( $E_c$ ) and dry vegetation ( $E_t$ ).

#### A1 Parameterization for NOAH

For NOAH the total evapotranspiration  $E$  is estimated as the sum of the three named components, which is  $E = E_{dir} + E_c + E_t$ . Bare soil evaporation is computed in the following way:

$$E_{dir} = (1 - \sigma_f) \beta E_p \quad (A1.1)$$

$$\text{with } \beta = \frac{(\Theta_1 - \Theta_w)}{(\Theta_{ref} - \Theta_w)} \quad (A1.2)$$

here  $E_p$  is the potential evaporation, which is calculated based on a Penman energy balance approach that includes a stability-dependent aerodynamic conductance (Mahrt and Ek 1984).  $\Theta_{ref}$  and  $\Theta_w$  are the water content at field capacity and wilting point, and  $\sigma_f$  is the parameter for partitioning of total evaporation between bare-soil evaporation and canopy transpiration.

The wet canopy evaporation is determined by

$$E = \sigma_f E_p \left( \frac{W_c}{S} \right)^n \quad (A1.3)$$

with  $W_c$  as the intercepted canopy water content,  $S$  is the maximum canopy capacity (0.5 mm) and  $n = 0.5$ . Similar functions are used by Noilhan and Planton (1989) and Jacquemin and Noilhan (1990).

The transpiration from high and low vegetation is determined by

$$E_t = \sigma_f E_p B_c \left[ 1 - \left( \frac{W_c}{S} \right)^n \right] \quad (A1.4)$$

where  $B_c$  is a function of canopy conductance and is formulated as

$$B_c = \frac{\left( 1 + \frac{\Delta}{R_r} \right)}{\left( 1 + g_c C_h \frac{\Delta}{R_r} \right)} \quad (A1.5)$$

here  $C_h$  is the surface exchange coefficient for heat and moisture,  $\Delta$  is the slope of the saturation specific humidity curve and  $g_c$  is the canopy conductance.  $R_r$  is a function of air temperature, surface pressure and  $C_h$ . The approach of Jacquemin and Noilhan (1990) is based on the work of Jarvis and Stewart (Jarvis 1976; Stewart 1988) and  $g_c$  is obtained in the following way:

$$g_c = g_{c\max} (LAI \cdot F_1 \cdot F_2 \cdot F_3 \cdot F_4) \quad (A1.6)$$

where

$$F_1 = g_{c\max} / g_{c\min} + \frac{f}{(1+f)} \quad (A1.7)$$

$$\text{with } f = 0.55 \frac{R_s}{R_{GL}} \frac{2}{LAI}$$

$$F_2 = \frac{1}{[1 + h_s (q_s(T_a) - q_a)]} \quad (A1.8)$$

$$F_3 = 1 - 0.0016(T_{ref} - T_a)^2 \quad (A1.9)$$

$$F_4 = \sum_{i=1}^4 \left( \frac{((\Theta_i - \Theta_w) d_{zi})}{((\Theta_{ref} - \Theta_w)(d_{z1} + d_{z2}))} \right) \quad (A1.10)$$

$F_1$  to  $F_4$  represent the influence of solar radiation, vapor pressure deficit, air temperature and soil moisture and 0 and 1 act as the lower and upper boundaries. The variable  $g_{c\max}$  is the maximum stomatal conductance, LAI is the leaf area index,  $g_{c\min}$  is the cuticular conductance of the leaves,  $T_{ref}$  is set to 298 K according to Noilhan and Planton (1989),  $R_{GL}$  and  $h_s$  are site dependent. The two values are set to 30 W m<sup>-2</sup> and 41.69 in case of Ejura and for Tamale the values are set to 65 W m<sup>-2</sup> and 54.52.

## A2 Parameterization for TESSEL

For TESSEL evapotranspiration is calculated separately for each tile and after that the weighted average is calculated with the respective grid box fractions. It is calculated for tile  $i$  in the following way:

$$L_v E_i = \frac{L_v \rho_a}{g_c + g_a} (q_a - q_{sat}(T_{sk,i})) \quad (A2.1)$$

$L_v$  is latent heat for vaporization and  $\rho_a$  is the air density, where  $g_c$  is only needed for high and low vegetation and  $g_a = (|U_a| c_{H,i})$ .  $g_c$  is based on the following formulation (Jarvis 1976).

$$g_c = g_{c\max} (LAI \cdot F_1 \cdot F_2 \cdot F_3) \quad (A2.2)$$

$$F_1 = \min \left[ 1, a \frac{(1 + bR_s)}{bR_s + c} \right] \quad (\text{A2.3})$$

where  $a = 0.81$ ,  $b = 0.004(\text{W m}^{-2})^{-1}$  and  $c = 0.05$ .

$$F_2(\varpi)^{-1} = \begin{cases} 0 & \varpi < \Theta_w \\ \frac{\varpi - \Theta_w}{\Theta_{ref} - \Theta_w} & \Theta_w < \varpi < \Theta_{ref} \\ 1 & \varpi > \Theta_{ref} \end{cases} \quad (\text{A2.4})$$

with  $\varpi = \sum_{k=1}^4 R_k \max(f_{liq,k} \omega_k, \Theta_w)$  and  $k$  the number of soil layers.

root density ( $R_k$ ) is calculated according to Zeng et al. (1998).

$$F_3(D_a)^{-1} = \exp(-g_D D_a) \quad (\text{A2.5})$$

where  $g_D$  depends on the vegetation type and exceeds 0 only for high vegetation and  $D_a$  is the atmospheric humidity deficit ( $D_a = e_{sat}(T_a) - e_a$ ).

For bare soil evaporation  $g_a$  is substituted by

$$g_{soil} = g_{soil,min} F_2(F_{liq,1} W_1) \quad (\text{A2.6})$$

with  $g_{soil,min} = 50 \text{ m s}^{-1}$  and  $F_2$  given by equation A2.4.



## **Chapter 4**

### **Assessing the Sensitivity of Water and Energy Exchanges during a seasonal cycle in West Africa**

---

Material in this chapter is submitted to the Journal of Hydrometeorology with A.F. Moene and A.A.M. Holtslag as co-authors.

## **Abstract**

Land surface parameterizations developed for meteorological and hydrological models depend upon the specification of a number of vegetation and soil related parameters. The values for those parameters are still uncertain for remote regions including the semi-arid regions in West Africa. Additionally there is only little knowledge about their possible seasonal dependence due to the large seasonal changes between wet and dry conditions. In this study, an assessment of the surface energy balance is done for two sites in the Volta Basin, West Africa, by running the NOAA land surface model (National Center for Environmental Prediction (NCEP), Oregon State University, Air Force and Hydrologic Research Lab) in off-line mode for a seasonal cycle. A different parameterization for evapotranspiration estimation is employed and the results are compared to the original formulation. Results indicate that the new formulation physically performs more realistic than the one used before.

A factorial design is utilized to investigate the sensitivity of this new formulation to prescribed parameters by including interaction effects. This would not be possible with a simpler one-at-a-time sensitivity analysis. The results suggest that there is a need for seasonal dependent parameters and/or different approaches to deal with the seasonal changes, depending on the actual research question.

## 4.1 Introduction

The exchange estimates of momentum, heat and moisture between the earth's surface and the atmosphere are essential to regional modeling of weather, climate and water resources. The interface between the surface and the atmosphere is usually built by a land surface model (LSM). During the last decades numerous LSMs have been developed and a focus has been put on the accuracy of the parameterizations used in the LSMs (e.g. Schlosser et al. 2000; Boone et al. 2004). During recent years various datasets for different regions have been gathered to study long-term trends in the accuracy of those parameterizations e.g. FLUXNET (Baldochi et al. 2001) or NOPEX (Halldin et al. 1999). A first attempt to gain deeper knowledge about the West African land surface processes in the northern Sahel region was done in the context of SEBEX (Wallace et al. 1992) with a focus on the annual cycle. For the more southern region including the Volta basin there is still no long-term dataset available and therewith model validation and improvement is lacking.

The regional climate of the Volta basin is characterized by a strong north-south gradient of mean annual rainfall and the occurrence of pronounced dry and wet seasons within one annual cycle. This causes a strong seasonal variation in the natural vegetation fraction and therewith a large variability in actual evapotranspiration. Hólm et al. (2002) stated that the contrast between dry and moist air is probably more pronounced in time and space than anywhere else. Those features show that the parameterizations applied to the landscapes in West Africa require attention. Furthermore recent research has revealed that large differences exist between the feedback mechanisms for land surface processes in midlatitudinal and semi-arid tropical regimes. The midlatitudes show a more soil wetness-related feedback, whereas the semi-arid areas are dominated by vegetative pathways (via stomatal resistance and vegetation fraction) (Niyogi et al. 2002).

To obtain deeper knowledge about the mentioned feedback mechanisms, not only by further development and measurement comparison, various studies have been undertaken about the uncertainty and the sensitivity of LSMs (Henderson-Sellers 1993, Betts et al. 1997, Hales et al. 2004). One important issue when undertaking sensitivity analysis is that the response to changes in parameters is related to direct and interaction effects (Niyogi et al. 1999). The interaction effects cannot be resolved with a one-at-time (OAT) mode of analysis. Therefore other tools are required to explore the main and the interaction effects when surface parameters are varied in land surface modeling. One possibility is a factorial experiment, which offers information about interactions between parameters and is thus a more powerful tool compared to OAT analysis (Betts et al. 1997).

In this study we assess the sensitivity of water and energy exchanges within the NOAH land surface model, which is a joint product of the National Center for Environmental Prediction (NCEP), Oregon State University, Air Force and Hydrologic Research Lab. It is based on the former Oregon state University land surface model (OSULSM) (Ek and Mahrt 1991). NOAH uses the big leaf approach in combination with a formulation of bare soil evaporation for calculating surface fluxes. It stands for a broader range of LSMs, utilizing the mentioned approach (compare e.g. Boone et al. 2004). NOAH is one option in PSU/NCAR mesoscale model (MM5) and is used for studies related to the impact of land use change on regional climate (Chen and Dudhia 2001). Recent investigations on various aspects of land-atmosphere interactions for savanna type vegetation showed that the actual formulation of evapotranspiration in NOAH depends more on prescribed changes in vegetation fraction than on the actual physics (Schüttemeyer et al., submitted to Journal of Hydrometeorology).

Therefore the first objective of this study is to test a different formulation for evapotranspiration estimation built in a land surface model together with a fixed vegetation fraction for a seasonal cycle in a semi-arid region in West Africa. The focus is on validating the seasonal dynamics of the different components of the energy balance for the new formulation. The results of the original and the new formulations are compared to the measured components at two different semi-arid locations in the Volta Basin, Ghana, one in the humid tropical southern region and one in the northern region. The observations are conducted with a combined system, consisting of a Large Aperture Scintillometer (LAS) for areally averaged sensible heat flux, radiometers and sensors for soil heat flux. The LAS yields area-averaged fluxes over complex terrain, which are required when measuring over a mixed formation of grass, woody plants and bare soil.

The new formulation within NOAH offers the possibility to analyze errors in more detail and perform sensitivity analyses, whereas this was more difficult for the original version of NOAH, since a big control mechanism for semi-arid regions was the vegetation fraction.

Therefore the second objective is utilizing a two-level factorial design to find main effects and interaction of important parameters. The focus of the factorial design is on the effects, which have to be taken into account when trying to optimize needed parameters and therewith model performance. Furthermore the question is addressed how those effects change during the season also in comparison to the measurements. In addition the effects of two contrasting sites are compared.

## 4.2 Material and Methods

A brief description of NOAH is given here followed by a section about which changes are applied to the model. A full description can be found in e.g. Chen et al. (1997) and Chang et al. (1999). The model is run in offline mode to concentrate on the evaluation of the land surface processes for the specific region and on the surface-flux formulation, without dealing with mismatches in the upper boundary condition between a three-dimensional model and observations. It is driven by the prescribed atmospheric forcings described in section 4.2.4.

### 4.2.1 Original model description

The model contains a multilayer submodel for the soil. A regionally dependent soil type is utilized, based on the USGS database ([http://edcdaac.usgs.gov/glcc/af\\_int.asp](http://edcdaac.usgs.gov/glcc/af_int.asp)). The soil is discretized into four layers (0.08, 0.24, 0.72 and 2.16 m in thickness). Bottom boundary conditions are zero heat flux and free drainage. The water and heat budget in the soil is based on the Richards equation coupled to the Fourier law of diffusion. Soil moisture used for canopy transpiration is extracted from the soil using a weighing function including the root depth together with a uniform root distribution. A skin layer with zero heat capacity is in instantaneous equilibrium with its forcing. The skin layer conductivity provides the thermal connection to the topsoil layer. The coupling of the surface to the atmosphere is based on the skin temperature. It is calculated by solving the energy balance equation:

$$R_n = H + LE + G \quad (4.1)$$

$R_n$  equals net radiation,  $H$  equals sensible heat flux,  $LE$  equals latent heat flux and  $G$  equals soil heat flux. NOAH applies one skin temperature representing the combined soil/vegetation surface.

Subgrid variability is tackled with a Reynolds number-dependent formulation for the ratio of roughness length for momentum ( $z_{0m}$ ) and heat ( $z_{0h}$ ). This ratio is commonly expressed in terms of  $kB^{-1}$ , where  $B^{-1}$  is a dimensionless parameter. For NOAH a Reynolds number-dependent formulation for  $kB^{-1}$  proposed by Zilitinkevich (1995) is used:

$$kB^{-1} = \ln\left(\frac{z_{0m}}{z_{0h}}\right), \quad B^{-1} = C\sqrt{\text{Re}^*}, \quad \text{Re}^* = \frac{u^* z_{0m}}{\nu} \quad (4.2)$$

where  $k$  is the von Kármán constant ( $k = 0.4$ ),  $\nu$  is the kinematic molecular viscosity,  $Re^*$  is the roughness Reynolds number, and  $u^*$  is the friction velocity. For small  $C$  values (e.g.  $C < 0.01$ ),  $z_{0m}/z_{0t}$  tends to be 1 throughout the physical range of  $Re^*$ , while large  $C$  values drastically decrease  $z_{0t}$  (Chen et al. 1997 also for further discussion). The recommended range for  $C$  is 0.2-0.4 (<ftp://ftp.ncep.noaa.gov/pub/gcp/ldas/noahlsm>).

An aerodynamic resistance for  $H$  and  $LE$  and a canopy resistance for  $LE$  are employed. The formulation of Paulson (1970) is utilized to calculate the turbulent exchange coefficient. The canopy resistance is parameterized by the approach of Jarvis (1976) and Stewart (1988).

The total evapotranspiration ( $LE$ ) is estimated as the sum of evaporation from bare soil ( $E_{dir}$ ), the interception reservoir ( $E_c$ ) and dry vegetation ( $E_t$ ). Bare soil evaporation is computed in the following way:

$$E_{dir} = (1 - \sigma_f) \beta E_p \quad (4.3)$$

$$\text{with } \beta = \frac{(\Theta_1 - \Theta_w)}{(\Theta_{ref} - \Theta_w)} \quad (4.4)$$

$E_p$  is the potential evaporation, which is calculated based on a Penman energy balance approach that includes a stability-dependent aerodynamic resistance (Mahrt and Ek, 1984).  $\Theta_{ref}$  and  $\Theta_w$  represent water content at field capacity and wilting point, and  $\sigma_f$  is the vegetation fraction for the partitioning of total evaporation between bare-soil evaporation and canopy transpiration.

The wet canopy evaporation is determined by:

$$E_c = \sigma_f E_p \left( \frac{W_c}{S} \right)^n \quad (4.5)$$

with  $W_c$  as the intercepted canopy water content,  $S$  is the maximum canopy capacity (0.5 mm) and  $n = 0.5$ . Similar functions are used by Noilhan and Planton (1989) and Jacquemin and Noilhan (1990).

The transpiration from vegetation (no distinction between high and low vegetation) is determined by:

$$E_t = \sigma_f E_p B_c \left[ 1 - \left( \frac{W_c}{S} \right)^n \right] \quad (4.6)$$

The vegetation fraction varies on a monthly basis, based on the work of Gutman and Ignatov (1998).  $B_c$  is a function of canopy resistance and is formulated as:

$$B_c = \frac{\left(1 + \frac{\Delta}{R_r}\right)}{\left(1 + r_c C_h \frac{\Delta}{R_r}\right)} \quad (4.7)$$

here  $C_h$  is the surface exchange coefficient for heat and moisture,  $\Delta$  is the slope of the saturation specific humidity curve and  $r_c$  is the canopy resistance.  $R_r$  is a function of air temperature, surface pressure and  $C_h$ . The approach of Jacquemin and Noilhan (1990) is based on the work of Jarvis and Stewart (Jarvis 1976; Stewart 1988) and  $r_c$  is obtained in the following way:

$$r_c = r_{c\min} / (LAI \cdot F_1 \cdot F_2 \cdot F_3 \cdot F_4) \quad (4.8)$$

where

$$F_1 = r_{c\min} / r_{c\max} + \frac{f}{(1+f)} \quad (4.9)$$

$$\text{with } f = 0.55 \frac{R_g}{R_{GL}} \frac{2}{LAI}$$

$$F_2 = \frac{1}{[1 + h_s (q_s(T_a) - q_a)]} \quad (4.10)$$

$$F_3 = 1 - 0.0016(T_{ref} - T_a)^2 \quad (4.11)$$

$$F_4 = \sum_{i=1}^4 \left( \frac{((\Theta_i - \Theta_w) d_{zi})}{((\Theta_{ref} - \Theta_w)(d_{z1} + d_{z2}))} \right) \quad (4.12)$$

$F_1$  to  $F_4$  represent the influence of solar radiation, vapor pressure deficit, air temperature and soil moisture and 0 and 1 act as the lower and upper boundaries. The variable  $r_{c\min}$  is the minimum stomatal resistance, LAI is the leaf area index,  $r_{c\max}$  is the cuticular resistance of the leaves,  $R_g$  is the global radiation at the surface,  $R_{GL}$  and  $h_s$  are site dependent (table 2), and  $d$  is the soil depth.

### 4.2.2 Current model description

For the current version the basic features of the submodel for the soil are kept unchanged. One major change is the use of a different weighing function for extracting water from the soil based on a variable root distribution. The root distribution decreases with depth based on the work of Viterbo and Beljaars (1995) and is vegetation type dependent (Van den Hurk et al. 2000). For a more detailed discussion see Ek and Holtslag (2004). The vegetation fraction is fixed in time and the highest value in the monthly database is taken for both sites. For dry canopy evaporation in the current version the functions  $F_1$  and  $F_3$  are kept identical,  $F_2$  and  $F_4$  are changed in the following way:

$$F_2(D_a)^{-1} = \exp(-g_D D_a) \quad (4.13)$$

for  $g_D$  an optimized parameter for savannah conditions  $36.7 \text{ g kg}^{-1}$  is utilized (Huntingford et al. 1995) and  $D_a$  is the atmospheric humidity deficit ( $D_a = (q_s(T_a) - q_a)$ ).

$$F_4(\varpi)^{-1} = \begin{cases} 0 & \varpi < \Theta_w \\ \frac{\varpi - \Theta_w}{\Theta_{ref} - \Theta_w} & \Theta_w < \varpi < \Theta_{ref} \\ 1 & \varpi > \Theta_{ref} \end{cases} \quad (4.14)$$

with  $\varpi = \sum_{k=1}^4 R_k \max(f_{liq,k} \omega_k, \Theta_w)$  and  $k$  the number of soil layers. The root density ( $R_k$ ) is calculated according to Zeng et al. (1998).

### 4.2.3 GLOWA-Volta data set

All measurements are part of long-term observations of the water- and energy balance in the Volta Basin within the GLOWA-Volta (Global Change in the Hydrological cycle) project (Van de Giesen et al. 2001). The data are based on measurements from meteorological stations in Ejura ( $7^\circ 20' \text{ N}$ ;  $1^\circ 16' \text{ W}$ ) and Tamale ( $9^\circ 29' \text{ N}$ ,  $0^\circ 55' \text{ W}$ ) for year 2002/2003. The two sites show major differences concerning the climate, vegetation, slopes, soils and land use. The site in Ejura is the tropical site. It is a heterogeneous terrain. The landscape is hilly. Here the transmitter of the LAS (description below) and the automatic weather station (AWS) are located in a cashew orchard. The research site in Tamale is characterized by mainly natural grassland with scattered trees, having a maximum height of five to eight meters. The landscape is slightly hilly. The annual mean temperature for the two sites varies



from the southern site Ejura (26.6 °C) to Tamale (27.8 °C). The annual mean precipitation, which is one of the driving forces for surface fluxes during the rainy period, varies from 900 – 1500 mm between the two sites. More than 95% of the precipitation occurs during the rainy season. For 2002 there is a large difference in precipitation between the research sites. For Ejura the yearly sum is 1420 mm. For Tamale it is 1065 mm.

The onset of the rainy period for 2002 was estimated to day of year (DOY) 74 for Ejura and DOY 118 for Tamale. The offset is estimated to DOY 343 in Ejura and DOY 290 for Tamale. This is done using the method of Kasei (1988). Malda (personal communication, 2002) analyzed 40 years of precipitation for different stations in the Volta basin and found that the average onset for Ejura was DOY 78 with a standard deviation (SD) of 30 days. For Tamale it is DOY 115 (SD = 20). For the year 2002 this shows that the length of the season and the total amount of rain are normal.

#### 4.2.4 Forcing and validation data

The forcing data for the model are obtained from the AWS, which measure temperature, humidity and global radiation at a reference level  $z = 2$  m. Wind speed is measured at eight-meter height. Additionally, surface observations for precipitation are recorded. All quantities are averaged for ten-minute intervals. A list of instruments is given in table 4.1.

**Table 4.1: Instrument used for this study.**

Variable	Location	Instrument
Air Temperature	2 m	50Y Temperature and RH probe (Vaisala)
Relative Humidity	2 m	50Y Temperature and RH probe (Vaisala)
Atmospheric pressure	Inbox	PTB101B Barometric Pressure Sensor (Vaisala)
Wind Speed	8 m	A100R Anemometer (Vector Instruments)
Wind Direction	8 m	Wind vane (Ecotech)
Net Radiation	8 m	NR-LITE (Kipp & Zonen)
Downward solar radiation	2 m	SP-LITE (Kipp & Zonen)
Precipitation	2 m	Tipping bucket (Stelzner)
Sensible Heat Flux	Site dependent	Large Aperture Scintillometer (LAS) (Manufactured by Wageningen Uni.)
Latent Heat Flux		Residual of the energy balance
Soil Heat Flux	0.035 m	HFP01 Heat Flux Plate (Hukseflux)
Soil Temperature	Different depth	PT <sub>100</sub> resistance thermometer (Manufactured by Wageningen Uni.)
Soil moisture	Different depth	TDR (Campbell) (Tamale), TDR (Delta-T) (Ejura)
Skin temperature	2m	Infrared (IR) temperature probes (Heimann)

The data set does not always provide longwave radiation. For those situations where longwave radiation measurements were not available it was calculated using air temperature and relative humidity following Idso and Jackson (1969) for clear sky situations. The contribution due to clouds is calculated by the following expression:

$$L_{total}^{\downarrow} = L_{cloudless}^{\downarrow} + L_{cloud}^{\downarrow} \quad \text{with } L_{cloud}^{\downarrow} = 60 \cdot C \quad (4.15)$$

Since no observations for cloudiness were available, C was estimated by calculating the transmissivity ( $\tau$ ) and using that information for obtaining a linear function for C for cloudy situations:

$$C = f\left(\frac{R_{et}}{R_g}\right) \quad \text{with } \begin{cases} C = 1 & \tau < 0.3 \\ C = 1 - \frac{\tau - 0.3}{0.4} & 0.3 < \tau < 0.7 \\ C = 0 & \tau > 0.7 \end{cases} \quad (4.16)$$

where  $R_{et}$  is the extraterrestrial radiation. This approach was tested for one of the sites of HAPEX-Sahel and for Tamale site during the period where there was data available. A linear regression against direct measurements gave reasonable results (intercept  $4.7 \text{ W m}^{-2}$ , slope 0.95 for HAPEX-Sahel, similar for Tamale test site).

Net radiation and soil heat flux are validated with direct measurements. Net radiation is measured directly at 8-meter height and soil heat flux is measured at 0.035 m depth. Sensible heat flux is measured with a LAS. It consists of a transmitter emitting electromagnetic radiation towards a receiver. The distance in between both can be chosen up to 5000 m for a beam diameter of 0.15 m. In our case the distance varies between 2040 m for Ejura and 2420 m for Tamale. It is installed at a certain height above the surface (30.1 m Ejura; 19.5 m Tamale). The emitted radiation is scattered by the turbulent medium in the path. The variance of intensity of received radiation is proportional to the structure parameter of the refractive index of air ( $C_n^2$ ). At the wavelength used (940nm) the refractive index mainly depends on temperature, so  $C_n^2$  is mostly determined by temperature fluctuations ( $C_T^2$ ). The influence of water vapor on the refractive index was taken into account as a small correction (Moene, 2003). Sensible heat flux is calculated from  $C_T^2$  using Monin-Obukhov similarity theory (MOST). Stability functions proposed by Wyngaard (1973) were applied for daytime values. For nighttime values we follow the formulation of De Bruin et al. (1993). For a more detailed description of the LAS theory and its applications see for example De Bruin et al. (1995) or Meijninger et al. (2002). Latent heat flux is calculated as a residual from the energy balance,

which showed good correspondence with eddy covariance data obtained during an intensive observation period (IOP) during the drying up in 2002. One has to remember that this approach forces the energy balance to close. The observed energy balance was closed for the IOP in 2002 in Tamale and for large parts of the season in Ejura, with the four terms measured independently (Schüttemeyer et al., submitted to *Boundary-Layer Meteorology*).

### **4.3 Model validation**

In this section the two different formulations for evapotranspiration within NOAH are evaluated with measurements. The focus is on the seasonal dynamics in net radiation and latent heat flux. The discussion in relationship to the sensitivity analysis is done in section 5.

#### **4.3.1 Parameter estimation**

The model runs for Ejura were done for the period from DOY 269 until DOY 52 and for Tamale it was the period from DOY 238 until DOY 21. Both periods cover the transition time from the wet to the dry season. Since there were no measurements for soil temperature profiles available at both sites the initial values were obtained by calculating the daily, weekly, monthly, yearly mean air temperature and using those as initial values for the four soil layers. In case of initial soil moisture the values for Ejura were estimated from the measurements closest in time. For Tamale the routinely measured values were taken. In case of initial soil moisture for the lowest level the same values as for the level above were utilized.

The vegetation type in the model is set to Savannah for Tamale and to Broadleaf-Evergreen Trees (tropical forest) for Ejura. Both types are set according to the SiB vegetation classes (Dorman and Sellers, 1989). The soil type at both test sites according to the database is loamy sand. From a detailed survey of soil properties (Agyare, 2004) it was found that the soil type for Ejura corresponds better to a sandy clay loam. For Tamale it is a sandy loam. The soil types are changed accordingly. All additional input parameters can be found in table 4.2. The time step for integration is set to 600 s according to the measured quantities.

**Table 4.2a: Model parameter values for NOAH at both test sites.**

Parameter NOAH	Tamale	Ejura	Units
roughness length momentum	0.2	0.4	m
roughness length heat	based on Zilitinkevich		m
LAI	3	3	-
Minimum canopy resistance (RS)	120	150	s m <sup>-1</sup>
Albedo	see table 2b		-
vegetation fraction (VF)	see table 2b		-
soil porosity	0.434	0.421	m <sup>3</sup> m <sup>-3</sup>
water content at wilting point	0.047	0.029	m <sup>3</sup> m <sup>-3</sup>
water content at field capacity	0.312	0.283	m <sup>3</sup> m <sup>-3</sup>
b Parameter	4.74	4.26	-
root distribution over 4 layers(original)	uniform	uniform	%
root distribution over 4 layers(current)	27; 37; 27; 9	25; 34; 27; 14	%
Reference Temperature	298.0	298.0	K
Rgl	30.0	41.69	W m <sup>-2</sup>
Hs	65.0	54.52	-

**Table 4.2b: Seasonal dependent vegetation fraction (VF) and albedo at both test sites.**

Parameter	Location	J	F	M	A	M	J	J	A	S	O	N	D
VF	Ejura	0.17	0.22	0.35	0.49	0.70	0.75	0.65	0.66	0.71	0.66	0.58	0.36
	Tamale	0.04	0.02	0.05	0.08	0.24	0.40	0.47	0.56	0.61	0.51	0.30	0.12
Albedo	Ejura	0.18	0.18	0.18	0.17	0.16	0.14	0.15	0.15	0.15	0.15	0.16	0.17
	Tamale	0.19	0.20	0.20	0.18	0.17	0.16	0.15	0.16	0.15	0.16	0.17	0.18

### 4.3.2 Method of model evaluation

Simulated fluxes are compared to measured values of net radiation, sensible heat flux and latent heat flux. As a first check for the different components of the energy balance the mean bias error (MBE) and rmse are calculated. The term MBE refers to the difference between the modeled value and the measured value. Positive (negative) MBE occurs when the modeled value is higher (lower) than the measured value. Furthermore the relative MBE is calculated by dividing the absolute MBE by the mean flux. To account for the seasonal dynamics this procedure is followed for three-day periods from the beginning to the end at the two sites. One has to keep in mind that the errors in sensible, latent and soil heat flux do not necessarily add up for every period, since some measurements for sensible and latent heat flux are rejected due to insufficient quality.

### 4.3.3 Model results

There is a clear decline in net radiation (figure 4.1) for both sites due to changes in the surface cover. The decline starts as soon as the amount of rainfall decreases. The decline in net radiation implies a decline in the sum of sensible and latent heat flux during that time, since the magnitude of soil heat flux is nearly constant throughout the season.

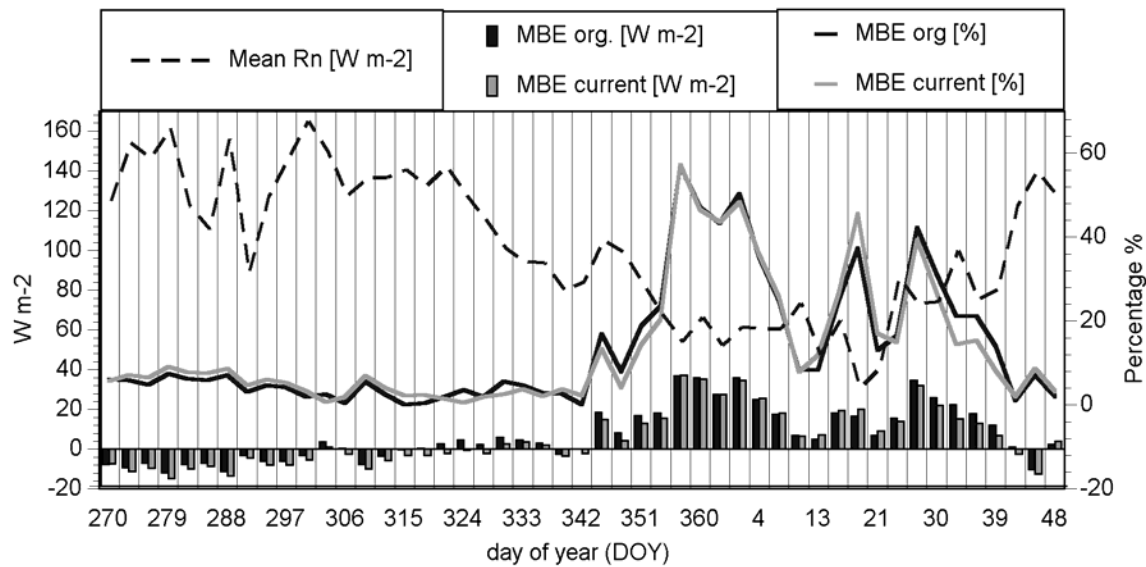


**Fig. 5.1a: Ejura: 3-day intervals of averaged measured net radiation (dashed line), MBE for net radiation in  $W m^{-2}$  (bars) and relative MBE (lines). The black lines and bars refer to the original model, the gray once to the current model.**

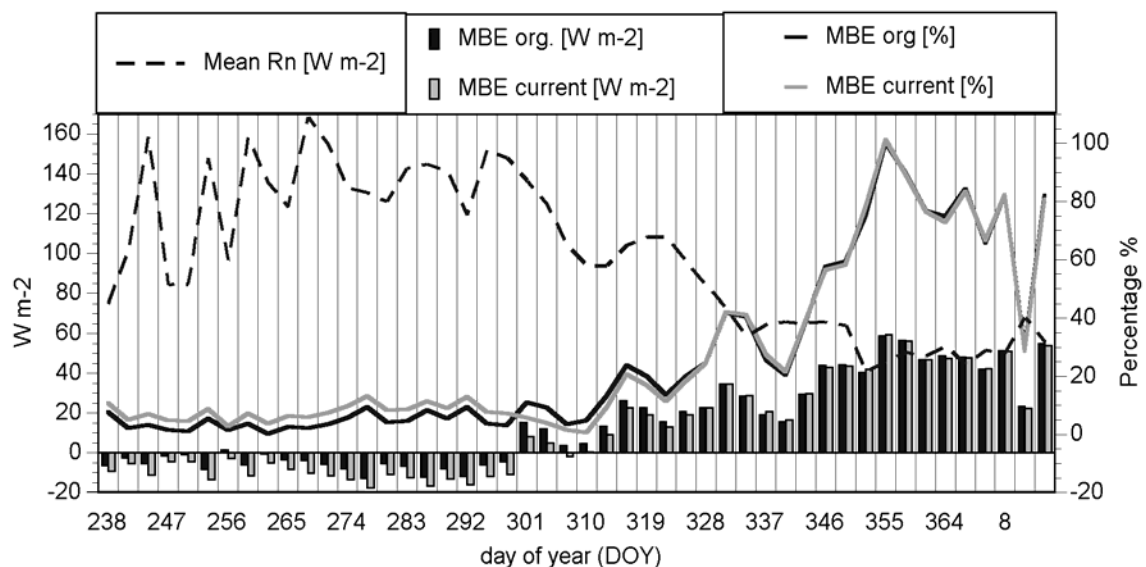


**Fig. 5.1b: Same as figure 1a for Tamale. Note the difference in time period.**

For the MBE of net radiation there is a clear trend for both parameterizations and sites (figure 4.1) from small negative values in the beginning (relative MBE smaller than 10% during the wet part of the season) to larger positive values towards the end. For Ejura there is a peak around the end of year 2002 and smaller values again as soon as the rains start (after DOY 23). For Tamale the MBE is growing until the end of the period, because the modeling stopped before the rain started again. The correlation coefficient of net radiation equals 0.99 for the three-day intervals for both parameterizations and sites throughout the studied season. The rmse is comparable for both, but changing during the season with higher values towards the end of the season. The direct comparison of the MBE illustrates that the current formulation gives similar results with slightly smaller values for the later part of the season at both test sites. For the wet part of the season the MBE is slightly higher for the current version. The evaluation at both sites shows that the decrease of net radiation is not reproduced by the LSM and that the errors are related to the process of drying up. This suggests that the role of albedo and parameters which influence skin temperature need to be explored.

Due to measurement problems there are no measurements for sensible and latent heat flux available for the test site in Tamale until DOY 287 and for the last three to four weeks of the studied time for both sites.

The seasonal dynamics of measured and modeled latent heat fluxes show a clear decrease at both sites (figure 4.2).

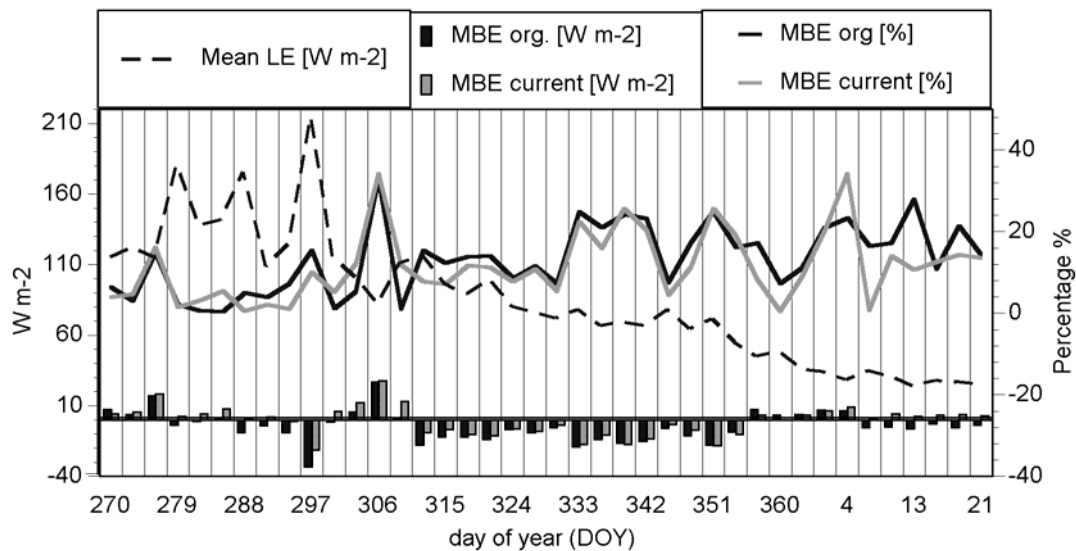


**Fig. 4.2a: Ejura: 3-day intervals of averaged measured latent heat flux (dashed line) and MBE for latent heat flux in  $W m^{-2}$  (black bars original parameterization, gray bars current version) and MBE as a percentage of total mean flux (lines) for the studied season.**

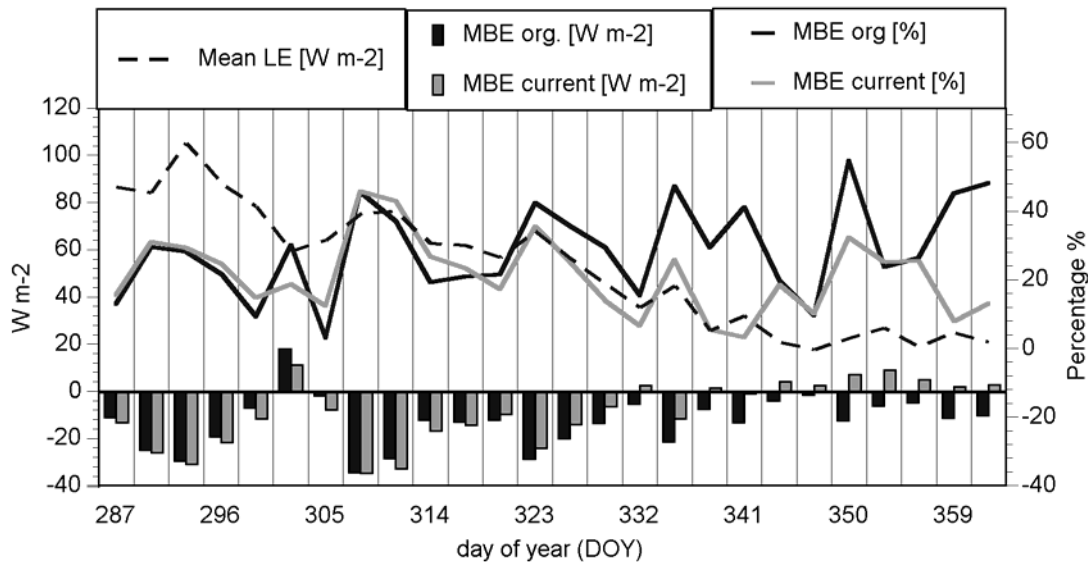


**Fig. 4.2b: Same as figure 4.2a for Tamale. Note the difference in time period.**

For Tamale the measured latent heat flux at the start of the measurements is lower compared to Ejura because of the earlier start of the drying up. The MBE is negative for both formulations during large parts of the season. The biggest errors appear during the part of the season, when the measured decrease starts, which suggests that the role of factors influencing transpiration like vegetation fraction, LAI, minimum resistance and soil moisture need to be explored in this context. For Ejura there are three peaks in the beginning, which correspond to rainfall events. During the last event (more than 50 mm precipitation during one day) both formulations show a different MBE than before and after. The different MBE should be related to an erroneous interception formulation and bare soil evaporation for extreme events. Measured sensible heat fluxes stay nearly constant throughout the season. Since the measured decrease in net radiation is not modeled correctly, the sensible heat flux must increase, because soil heat flux stays constant. As a consequence the MBE of sensible heat flux rises at both sites during the drying up. This suggests that a feedback exists between net radiation and sensible heat flux. A possible explanation for the MBE in sensible heat flux could be the exchange coefficient for heat. Chen et al. (1997) compared different atmospheric surface-layer parameterization schemes and concluded that the differences in the schemes and the resulting surface exchange coefficients did not, in general, lead to significant differences in model simulated surface fluxes and skin temperature. The models were more sensitive to changes of ratio of roughness length for momentum and heat. Therefore the impact of changed roughness length ratio or  $kB^{-1}$  with the Zilitinkevich constant (C) as a proxy has to be analyzed.

Concerning the direct comparison the differences in parameterizations (correlation, rmse and MBE) for sensible and latent flux are small for the wet part of the season at both test sites (figure 4.2 and 4.3). This is explained by regular rain events and soil moisture content close to saturation, which result in optimal evapotranspiration for both parameterizations. As soon as the rains stop and the surfaces are becoming dry the differences in model performance become visible. The MBE is lower for the current formulation in NOAH for large parts of the season. The correlation coefficients for sensible (latent) heat flux show a clear trend with decreasing (increasing) values towards the end of the season (figure 4.3) with higher values for the current parameterization. The rmse is lower for the current parameterization (on average  $6 \text{ W m}^{-2}$  for both sites). The higher correlation and lower rmse for both sites with the current parameterization are explained by a more physically realistic formulation, which is less dependent on the vegetation fraction and reacts more to changes in soil moisture.

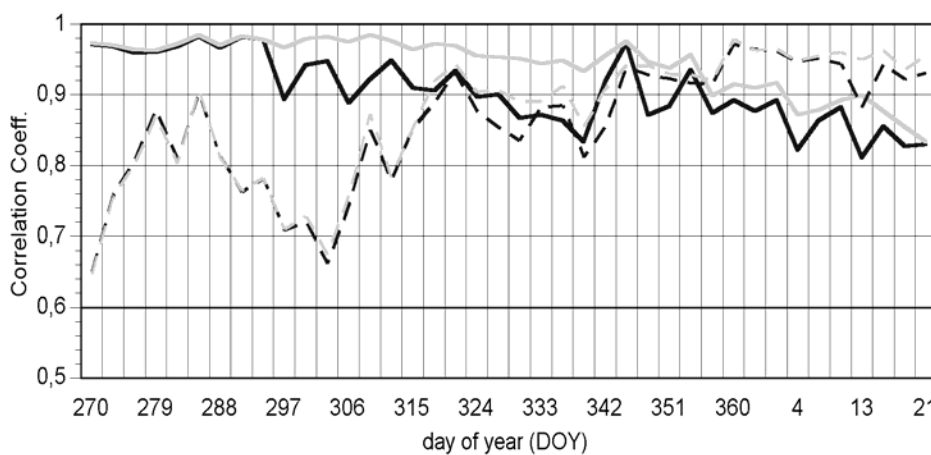


**Fig. 4.3a: Ejura: Seasonal development for 3-day intervals of correlation coefficient for sensible (dashed line) and latent heat flux (solid line) for both parameterizations (gray lines correspond to the current version) in NOAH.**

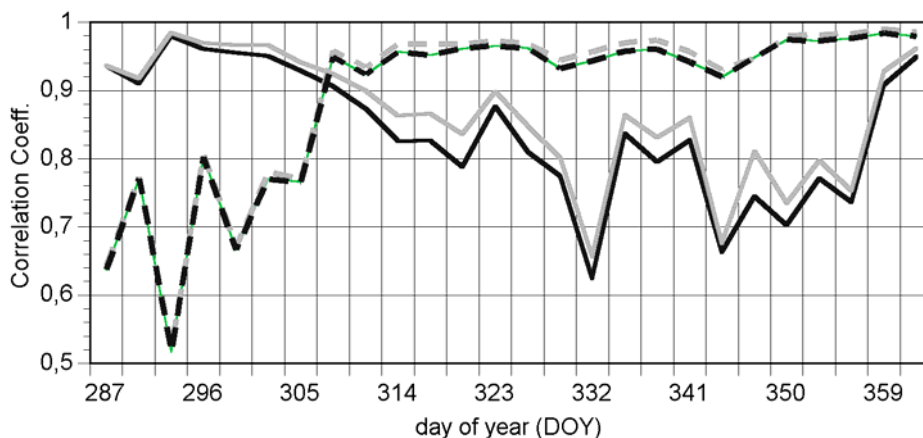


**Fig. 4.3b: Same as figure 4.3a for Tamale. Note the difference in time period.**



## 4.4 Response from factorial design

### 4.4.1 Theory of factorial design

The two-level factorial design quantifies the dependence of surface fluxes on input parameters for the current parameterization in NOAH. It resolves the effects ( $E_j$ ) into main effects and explicit interactions with maximum precision, with  $j$  being the number of changed parameters (factors) (Box et al. 1978). Two levels for each of a number of parameters (factors) are taken (low and high). The runs are done with all possible combinations with the assumption that the parameters change simultaneously with different combinations. For a one-at-time (OAT) method only an estimate of the effect of a single variable, with other variables fixed, is provided. The advantages of the two-level factorial design are that the effects of changed parameters, which act additively, are determined with higher precision and that interactions can be estimated. The number of runs required by a full design equals  $2^k$ , where  $k$  equals the number of factors. By applying Yates algorithm (Yates 1970) it is possible to carry out rapid calculation of all effects. Another advantage of the Yates algorithm is that after every step the calculations can be checked for possible errors.

It is generally not feasible to do such an analysis with a large number of factors. Therefore there is the need to find those variables, which have the biggest impact. Avissar (1995) stated that, among all land–surface characteristics considered in advanced SVAT schemes, only stomatal resistance, soil–surface wetness, leaf area index, surface roughness, and albedo play a major role in the redistribution of energy at the ground surface. From the evaluation of the two formulations within NOAH it is found that those factors should also have a major impact within NOAH. For the different functions in the Jarvis Stewart approach already optimized parameters for savanna conditions are applied, based on the work of Huntingford et al. (1995). Soil parameters were measured within the GLOWA-Volta project in a very detailed way (Agyare 2004). Since this is a first test with local data the measured parameters at each site are taken. Furthermore for those parameters, which might have an influence, but are not taken into account by now (e.g. soil or bottom temperature), a simple OAT sensitivity analysis was performed. It turned out that the influence of those parameters was small. For soil moisture it is apparent that it has a large impact especially on latent heat flux. Soil moisture, however, is a prognostic variable in NOAH, which means it cannot be varied.

Based on the mentioned facts the following parameters were chosen for the factorial design: albedo (ALB), vegetation fraction (VF), initial soil moisture (SM), minimum resistance (RS), leaf area index (LAI) and Zilitinkevich constant (C). The individual values (table 4.3) for each of the parameters are realistic, which means that no artificial effects should be expected.

**Table 4.3: Variables or factors used for the factorial design.**

Variables (factors)		low	original	high	Units
A albedo	Depending on org.	-0.04	See table 2b	+0.04	-
B vegetation cover	Fixed value	0.31	Max. of table 2b	0.91	-
C Initial soil moisture	Depending on org.	-0.1	Measured profile	+0.1	-
D min. resistance	Fixed value	40	120/150	300	s m <sup>-1</sup>
E LAI	Fixed value	1	2	4	-
F C	Fixed value	0.1	0.3	0.5	-

To determine which of the effects ( $E_j$ ) are statistically significant, the method of Lenth (1989) is used, where a significance level of 0.01 was chosen. It is based on the assumption, that all effects have the same variance and only some of the effects are active. It relies on a pseudo standard error (PSE) to estimate the standard deviation.

For analyzing the results from the factorial design Pareto plots are used. A Pareto plot is an ordered histogram going from highest to lowest importance data values.

#### 4.4.2 Results from two-level factorial design

The analyses for Ejura are done for three periods in 2002/2003 based on the distinction of the period where there were rain events (DOY 270 to DOY 344), the period when the rain events had stopped and the drying up started (DOY 344 to DOY 23), and the rains started again (DOY 23 to DOY 52).

For Tamale the periods are chosen based on the distinction between the first period when there were rain events (DOY 238 to DOY 288) and the second when the rain had stopped from DOY 288 to DOY 336. The distinction between the second and the third period is based on the decrease in net radiation (compare also figure 4.2), which is visible for the second period, whereas net radiation is nearly constant for the third period (DOY 336 to DOY 21).

##### a) Ejura

For all three periods the number of significant factors for net radiation is relatively stable (figure 4.4). Only for the second period the number of significant effects is larger (change from 14 to 17 significant effects) and therewith more interaction effects are found to be significant. For all periods the main effects dominate the outcome, where the Zilitinkevich constant (C), albedo and minimum resistance (RS) have the largest negative impact. Vegetation fraction (VF) and LAI have a positive impact on net radiation. There are

significant interaction effects but the values are smaller. Most significant main and interaction effects show the same sign for the three periods, only RS:LAI, VEG:RS:LAI and RS:LAI:C do change sign. The interaction effects between VF and RS and between RS, VF and C are the largest and show that interaction has to be taken into account, when optimizing model performance. Furthermore numerous interaction effects contain the factor C. The main effect of C is stable and the largest for all periods, which shows the importance of a proper estimation of this value. For albedo and vegetation fraction the absolute numbers are smaller for the second period, whereas the influence of minimum resistance and LAI rises for the second period. Furthermore most of the triple interactions are the largest for the second period.

According to Niyogi et al. (1999) the interaction effects modulate the surface energy balance by enhancing (synergistic interactions) or decreasing (antagonistic interactions) the net effect. The synergistic effect is observed for vegetation fraction and LAI. Both effects are positive and also the interactions between both show a positive effect. For C and albedo it can be observed that both parameters are negatively linked to net radiation but the interactions are positive and smaller. For the effects of minimum resistance and LAI the first one has a clear negative and the second one has a positive effect on net radiation, whereas the interaction effects do change sign during the different periods. For sensible heat flux the number of significant parameters is higher for the second period and lower again for the last period (figure 4.5). As already seen for net radiation the main effects show the largest impact for all three periods (figure 4.5). Minimum resistance shows the largest positive main effect. All the other main effects are negative. Initial soil moisture does not show a significant effect.

The positive effect of minimum resistance leads to higher sensible heat flux (H), which should be related to lower latent heat flux (LE) in first instance. Higher vegetation fraction leads to lower H due to a lower skin temperature and higher evapotranspiration. An increase of LAI leads to lower H, which should also be related to LE. A higher C decreases  $z_{0t}$  and leads to a higher term of  $kB^{-1}$  resulting in a reduction of the surface exchange coefficient. For a given magnitude of sensible heat flux, a lower  $z_{0t}$  leads to a higher temperature difference ( $\Delta T$ ) between the surface and the atmosphere. With a fixed 2 m temperature, a higher  $\Delta T$  leads to a higher surface temperature. A higher surface temperature also leads to a lower net radiation, which shows that a strong link exists between sensible heat flux and net radiation.

An increase in albedo leads to a lower H through a lower skin temperature. The effect of varying the minimum resistance is the largest of all effects for all three periods, but its absolute value is lower for the second period. The same is valid for vegetation fraction and LAI and various interaction effects. The total values for C and albedo rise for the second and

the third period. The rise of C cannot be explained by rising  $Re^*$ , since the friction velocity showed no significant increase.

The interaction effects of RS:LAI, VEG:RS:LAI do change sign as was also observed for net radiation before. Concerning the synergistic and antagonistic effects it can be concluded that similar effects exist, as observed for net radiation. For example both main effects of C and LAI have a negative effect on H but the interactions reveal a positive effect throughout the three periods. The obtained results show that a feedback exists between net radiation and sensible heat flux through changing skin temperature as already suggested in section 3.3.1.

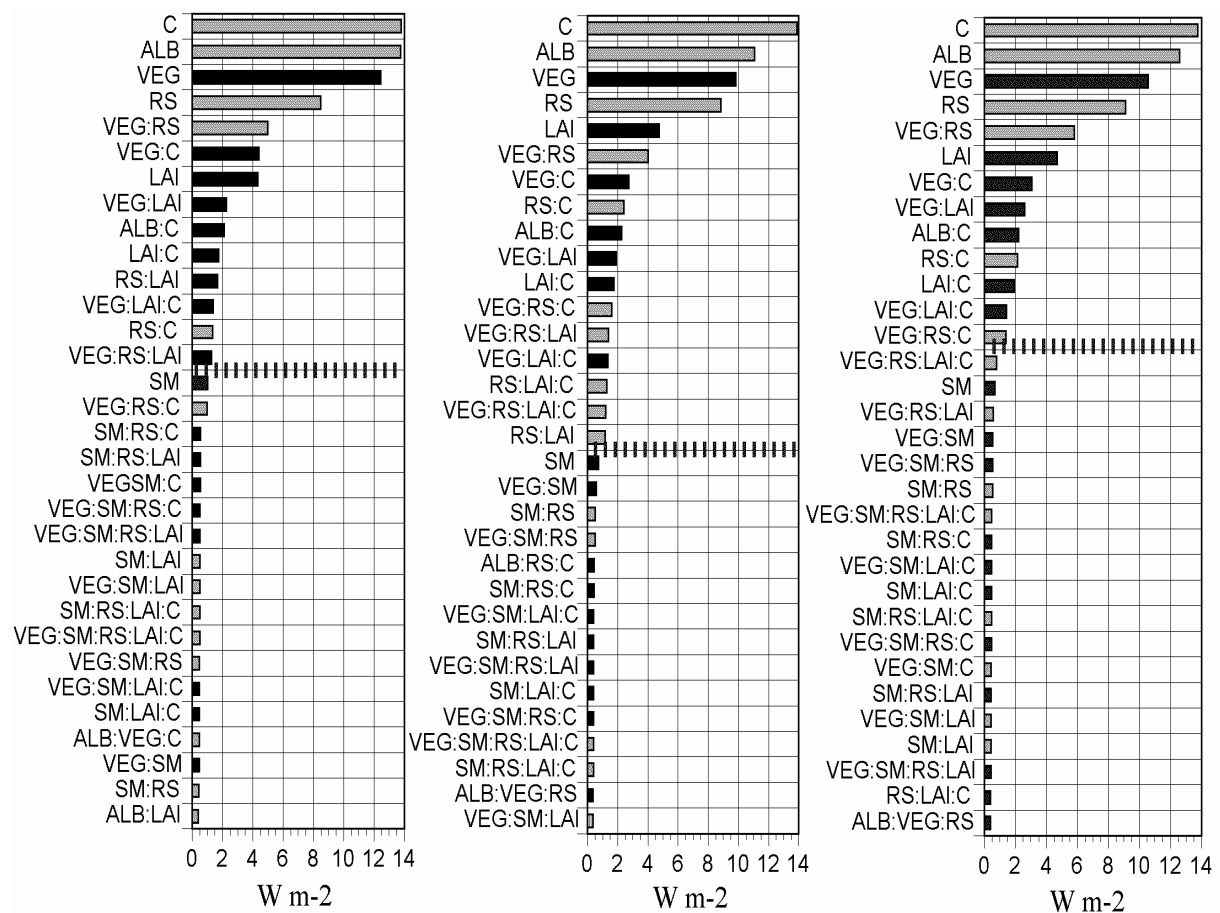


**Fig. 4.4: Ejura: Pareto plots of effects for net radiation in  $W m^{-2}$  for the three periods. Only the first 32 main and interaction effects are shown, since the other effects are negligible. The dashed lines divide significant effects from nonsignificant. Black bars correspond to positive effects, gray bars to negative effects.**

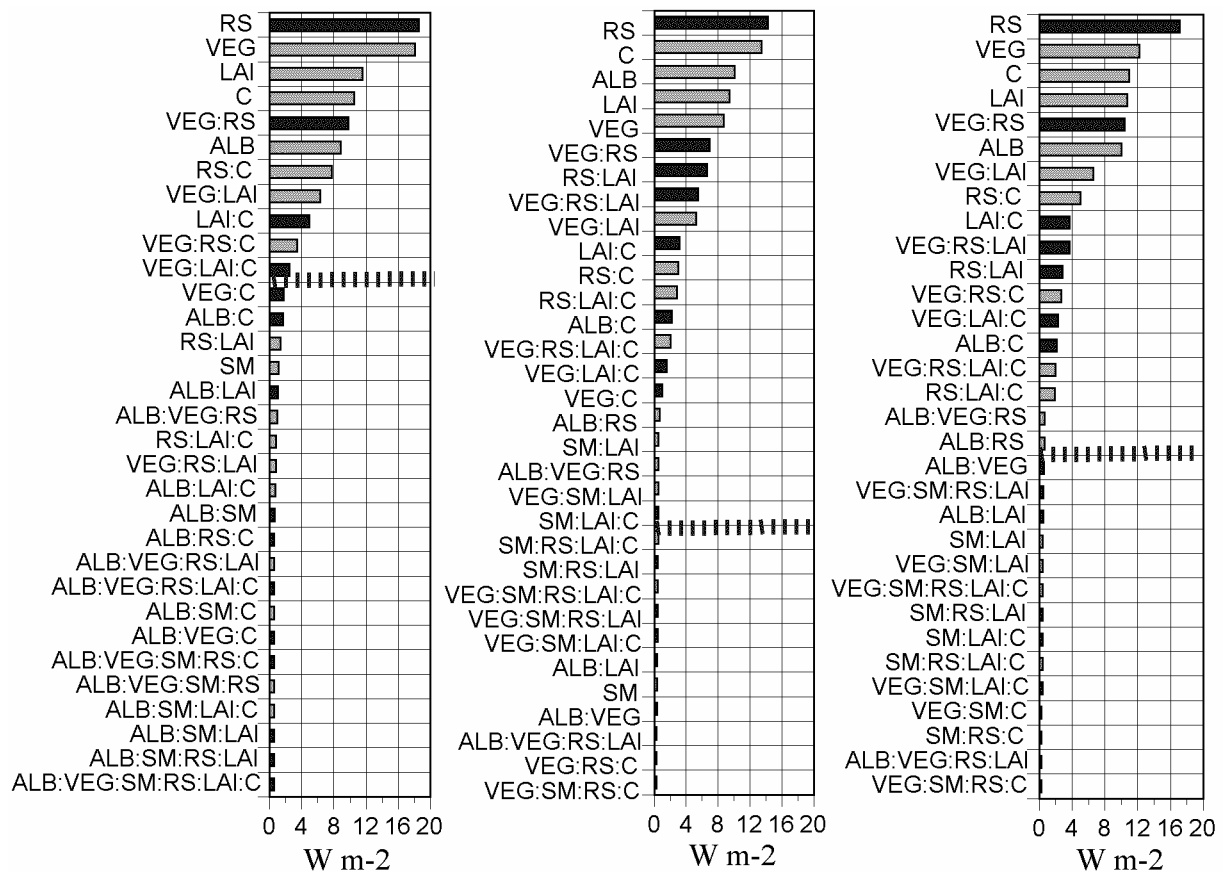


**Fig. 4.5: Ejura: Same as figure 4.4 for sensible heat flux. The number of significant effects is depending on the actual period.**

For latent heat flux figure 4.6 shows that fewer parameters influence the outcome significantly compared to net radiation and sensible heat flux. The number of significant parameters for latent heat flux increases for the second and third period, which means that more interaction effects become significant. The main effects are the most important for all periods, which was already observed by Niyogi et al. (2002) for a semi-arid region. The effect of changed initial soil moisture content is small but observable during all three periods, which means that initial conditions have an impact on larger time scales. The increase of minimum resistance, albedo and C results in a decrease of latent heat flux, which is documented in literature by Jacquemin and Noilhan (1990). The increase in LAI or vegetation fraction results in an increase of latent heat flux. This has been observed for similar surfaces (Hales et al. 2004) and different surfaces before (Bosveld and Bouten 2001). An increase in initial soil moisture content leads to higher latent heat flux, where the effect is rather small but observable (compare Harris et al. (2003) and Nagai (2002)). Furthermore the interaction effect of vegetation fraction and minimum resistance is large, which has to be taken into account, when parameters are optimized. The large interaction might be explained by the idea

that the effect between minimum resistance and vegetation fraction gives a stomatal control, which is proportional to the vegetation fraction. Therefore both are pivotal for calculating latent heat flux.

For Ejura modeled net radiation and sensible heat flux stay nearly constant throughout the season (changes smaller than 10%), whereas the averaged latent heat flux varies from 62.8 over 35.5 to 55.8  $W m^{-2}$ . Therefore the significant effects are divided by the mean flux during each period to investigate the change in effects (see figure 4.7). The second period is clearly different from the first and the third concerning most of the effects. The main effects show an increase from the first to the second period. Especially the effects of LAI and RS are changing, with the consequence that for example the interaction effect of VEG:RS, RS:LAI and VEG: RS:LAI become larger. Some of the interaction effects stay on a comparable level even when the rainy period started again.

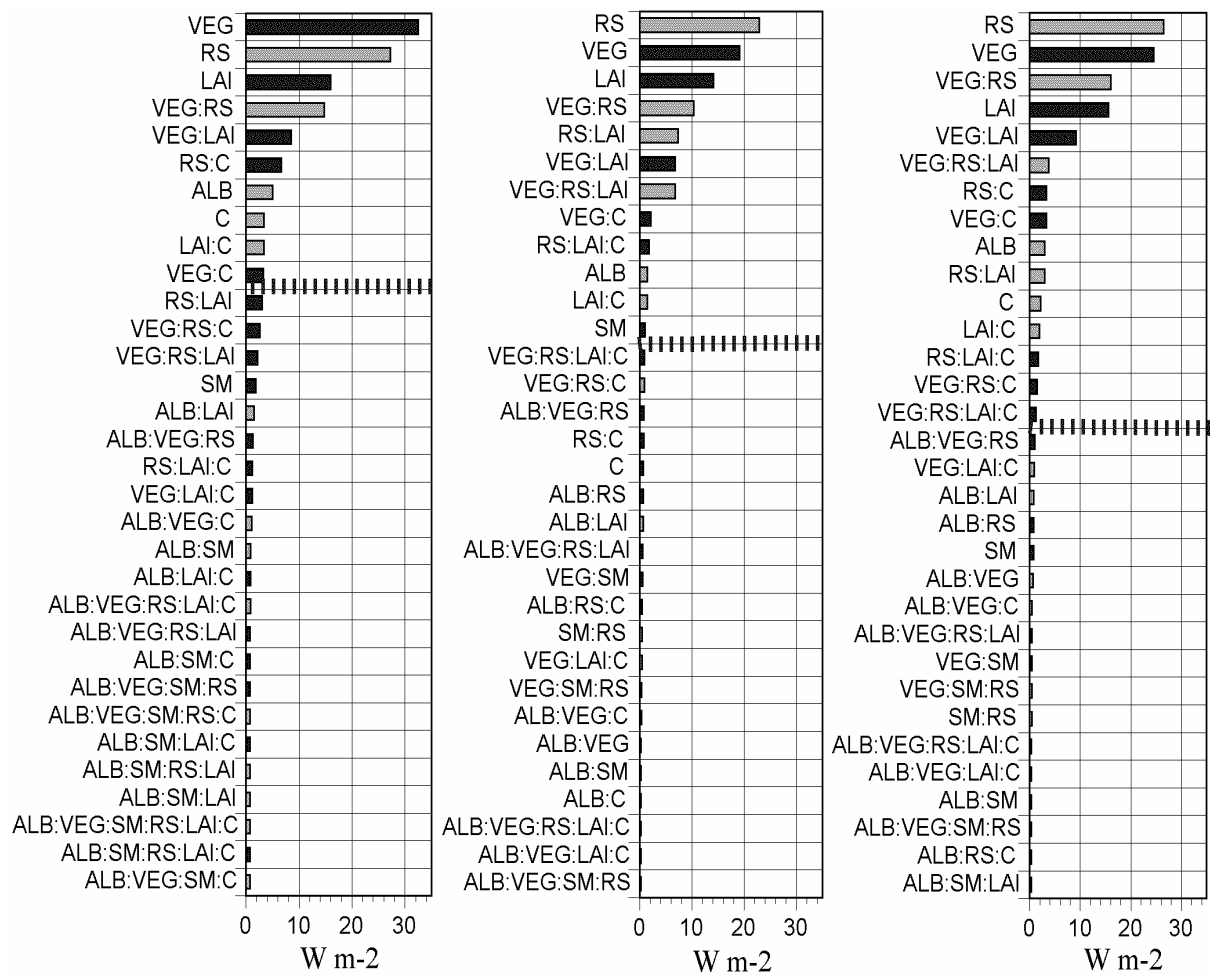


**Fig. 4.6: Ejura: Same as figure 4.4 for latent heat flux. The number of significant effects depends on the actual period.**

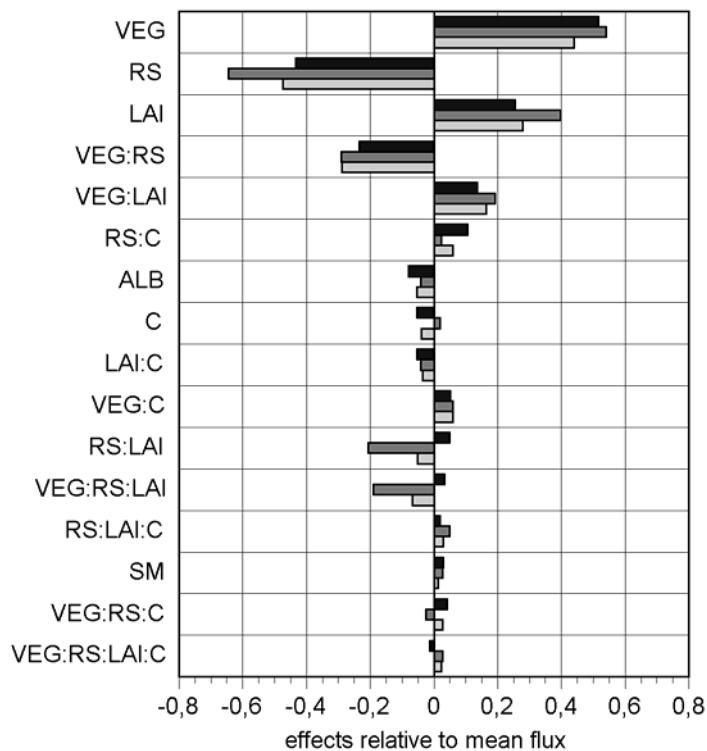


**Fig. 4.7: Ejura: relative ranking of significant effects for latent heat flux, with black bar for the first period, dark gray bar for the second period and gray bar for the last period.**

b) Tamale

The results for net radiation are comparable to those obtained for Ejura concerning the absolute size and the ranking of the effects. The number of significant factors is nearly the same. The differences to Ejura in net radiation are the larger effect of albedo for the first two periods and a smaller effect of C for the first period. For period 3 the effect of vegetation fraction is becoming smaller compared to the period before. For albedo and vegetation fraction the absolute numbers are smaller for the second period, whereas the influence of minimum resistance and LAI rises for the second period.

For sensible and latent heat flux the results are also comparable to those of Ejura, only the magnitude of some of the effects for sensible heat flux are larger compared to Ejura. Furthermore the number of significant parameters for sensible (latent) heat flux decreases for the second period from 12 (12) to 10 (6) and increases up to 25 (14) for the last period.

The magnitude of sensible (latent) heat fluxes increases (decreases) for the second and third period. This impacts on the relative ranking (figure 4.8). For sensible heat flux the effects of more evapotranspiration related factor decreases and the rest is constant for all three periods. For latent heat flux the opposite is observed.

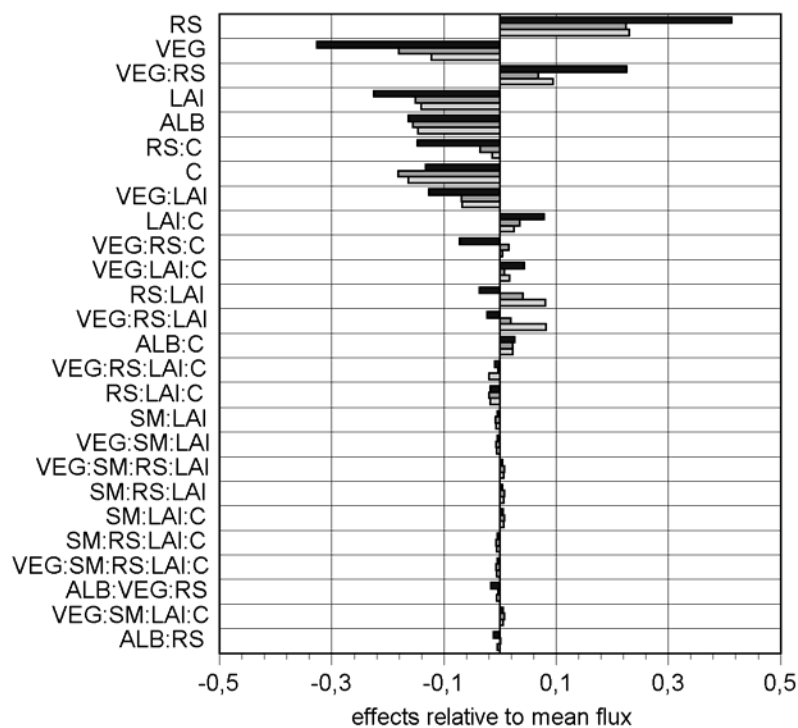


**Fig. 4.8a: Tamale: Relative ranking of significant effects for sensible heat flux, with black bar for the first period, dark gray bar for the second period and gray bar for the last period.**

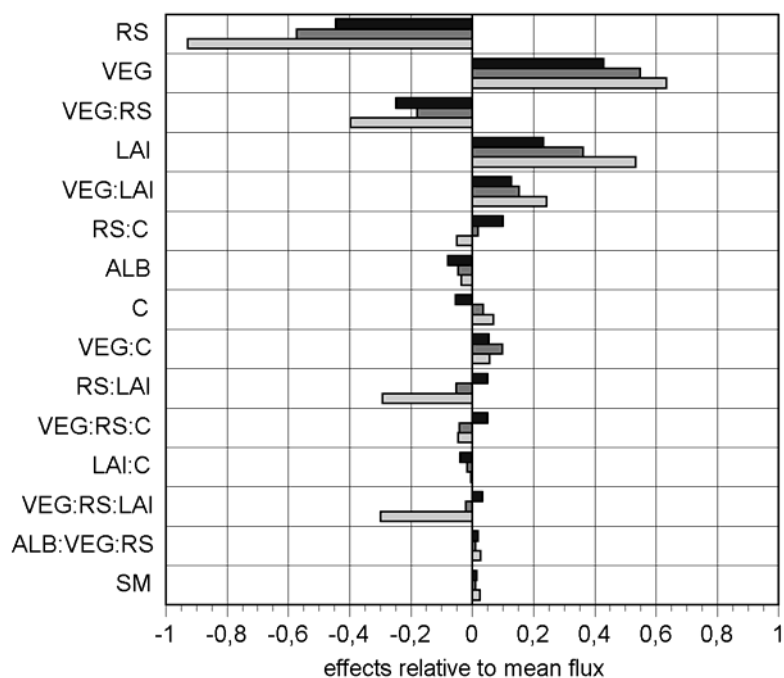


**Fig. 4.8b: Tamale: Same as figure 4.8a for latent heat flux.**



## 4.5 Discussion

The evaluation of modeled surface fluxes showed rising values for the MBE in net radiation and sensible heat flux, whereas the measured decrease in latent heat flux was reproduced by the LSM. The relationship between the model evaluation and the factorial design is discussed separately for each of the three components of the energy balance, followed by a subsection about the implications for further studies.

### 4.5.1 Net radiation

Both formulations within NOAH show small errors during the wet part of the season but fail to spot the dynamics of surface temperature and/or of the albedo due to the drying up. This is proven by the higher MBE during the drying up and is the result of several effects, which were explored by the two-level factorial design.

One effect can be related to albedo, which has a seasonal cycle but the seasonal dependence might be too small. This results in overestimation of the net shortwave flux at the surface. Since the model was run in offline mode there should be no uncertainties related to cloud schemes and clear-sky absorption. Modelers steadily address the seasonal dependence of albedo and it demonstrates that there is a need for real-time parameters under the changing conditions in West Africa. The rapid changes in surface cover lead to the question if monthly mean values are suitable or if higher resolution in time should be taken into account.

Another effect can be related to the use of the Zilitinkevich constant or more general the use of different roughness lengths for heat and momentum. Apparently the used ratios are reasonable for the wet part of the season but they are in need for seasonal adjustments. This might be explained by the changes in surface cover, which appear due to the process of drying up. For example in Tamale in the beginning the trees and the grass were green and towards the end the grass was brown and only the trees were green (coverage 15%) and able to transpire. This may lead to more homogenous conditions in the beginning. For those situations the use of one single surface temperature is justified. For more heterogeneous conditions towards the end the concept of one surface temperature can only be applied if the roughness length ratio is adjusted. Since net radiation is overestimated by the model and albedo and C show the largest net effect for net radiation it may be useful to start with those two parameters, when trying to optimize the performance of the LSM. On the other hand vegetation fraction and LAI also lower net radiation, when being lowered. At least for LAI the net effect on net radiation is smaller than the other parameters mentioned. The different

magnitude of effects in RS:LAI and VEG:RS:LAI should be related to sensible and latent fluxes (discussed below).

#### **4.5.2 Sensible Heat Flux**

It was concluded from the comparison of measured and modeled fluxes that during the wet part of the season the modeled results fitted the measurements but as soon as the drying up started, the model overestimated sensible heat flux with rising values towards the dryer part of the season for both sites. The net effects of minimum resistance and vegetation fraction are reduced for the later periods, whereas the effects of C and albedo are stable or even rise, when the surface becomes dryer. This should be taken into account when model results for sensible heat flux should be improved during a seasonal cycle. The stable magnitude of the main effects of C and albedo in combination with rising MBE demonstrates that there is a need for seasonally dependent parameters. Due to the concept of closing the surface energy balance, effects that are directly related to latent heat flux indirectly influence sensible heat flux and the other way around. Therefore one should at least analyze  $R_n$ , H and LE simultaneously. This is also demonstrated by the fact that a changed value of C has a small impact on LE but a compensating effect appears between H and  $R_n$ .

#### **4.5.3 Latent Heat Flux**

For latent heat flux it was concluded that the decrease in measured latent heat flux is reproduced by the LSM. The MBE is negative for most of the time with smaller values towards the end for both sites. Vegetation fraction might be in need for further adjustments, since the effect of changed vegetation fraction was the biggest (positive) for both sites. One suggestion could be that the actual vegetation fraction is different from the one used in the database. The analysis of MODIS data at both test sites in this context showed that the highest actual vegetation fraction (0.62) for Tamale is very close to the used one from the database (0.61). For Ejura the highest actual vegetation fraction from MODIS data was estimated to 0.76, which is as close to the one used (0.75). This shows that vegetation fraction is not in need for adjustments.

To a certain extent it could be the LAI that is in need for further adjustments, since it is the next largest effect. A higher LAI would give more transpiration for all periods. The comparison with measurements shows that the MBE was small when the surface was dryer. Therefore the consequence would be a seasonally dependent LAI. This is an option if a setup would be used, which employs as much real-time parameters as necessary. Interesting

phenomena in this context are the interaction effects of RS:LAI and VEG:RS:LAI. Those two effects show the biggest change during the seasonal cycle for both locations. During the first period they show a positive effect. After that they become negative. This shows that vegetation fraction, LAI and minimum resistance will control ongoing evapotranspiration to a larger extent than before.

Taking those facts into account one good option for improved model performance could be the minimum resistance. The evapotranspiration for the wet part of the season is coming from a mixture of grass, trees, bare soil and interception. When the drying up starts the evaporation from grass, bare soil and interception is not as large as before. The transpiration from trees continues, but with a different minimum resistance. Therefore minimum resistance could be linked to soil moisture content in the upper layer and switch to a larger value as soon as the layer is becoming dry.

The fact that the comparison to measured data shows that the largest errors appear when the drying up starts might be related to changes in minimum resistance.

#### **4.5.4 Implications for land surface modeling**

For the analyzed components of the energy balance at Ejura test site the number of significant effects rises when the surface is becoming dry. For Tamale the number of significant effects decreases during the second period before it increases for the last period. The changes during the drying up might make certain parameters more important when the surface becomes dry.

In first instance a better monitoring of certain input parameters and applying seasonal dependent parameters might help in obtaining improved modeling results. The crucial point in this context is that if seasonally dependent values from databases would be used there would be the implicit assumption that the seasonal cycle is constant. During the last 30 years this has not always been the case (Nicholson 1993), which shows that utilizing database values means that some problems would persist. We think that the obtained results show, that a fixed vegetation fraction could be one step in the right direction, but to proceed further studies are needed.

It was observed that surface conditions turned from relatively homogeneous (in terms of surface temperature) in the beginning to heterogeneous towards the end of the period considered. This change to heterogeneity makes the use of a single surface questionable. One solution could be the use of a 'tiled' approach as described by Koster and Suarez (1992), which might improve seasonal development of net radiation and sensible heat flux without tuning the roughness length ratio. This would make detailed data about fraction of high and low vegetation necessary and better knowledge about minimum resistance, root distribution

etc. Furthermore it implies the use of different roughness length ratios for high and low vegetation. In this context one upcoming issue is that separating only between grassland and forest is not a suitable solution for savanna conditions.

Since the decrease of net radiation and sensible heat flux are not correctly reproduced by the LSM, the relative ranking of effects should change when model performance is improved. Furthermore Margulis and Entekhabi (2001) found that the interactive boundary layer is warmed by surface temperature perturbations, such that the average sensible heat flux is decreased, which corresponds to a dampening in the sensible heat flux sensitivity to canopy and ground temperature in a coupled model. Therefore future studies should include the coupling to the boundary layer to investigate the feedback in relationship to net radiation and sensible heat flux.

The role of soil moisture is excluded in this study. One reason for this was the nonavailability of those measurements at the needed depths. This is another topic, which should be addressed in the future.

All analyses are done with the focus on the seasonal development of the components of the energy balance. This may have obscured the effects of parameters on the representation of the diurnal cycle.

## **4.6 Conclusions**

This study is meant as a first test bed for a land surface model in a remote region with a large contrast between wet and dry conditions. Those contrasts are prominent in the studied region compared to other midlatitudinal or tropical regions.

It was investigated how seasonal changes of the surface cover due to the drying up influence LSM performance and how this performance might be improved. The results with an alternative formulation for evapotranspiration show a good quality and consistency. Although it is not much superior to the original formulation in terms of mean bias error, it is physically more consistent. The two-level factorial design gave better insights to the question which effects of changed parameters are the most important also in comparison to measurements taken during the seasonal cycle. The two-level factorial design at both locations showed comparable results, which should make it less challenging to find robust parameters sets for the region even with the strong contrasts between wet and dry surfaces. The NOAH model utilizes physics, which are applied for numerous land surface models. The obtained results might be applied more generally from this perspective.

For further application a distinction of research questions might be necessary to optimize model performance. If the aim is analyzing the management of water resources for this region

the solution could be a better monitoring of important input parameters and employing as much real time parameter as possible, since model runs can be performed in hindcast mode. If the aim is climate change studies a tiled model with detailed information about vegetation and soil related parameters might be a more suitable solution. This option could allow addressing questions related to climate change: Is there a trend from turning savanna into grassland? What are the consequences for the surface energy balance if this occurs?



## **Chapter 5**

### **Satellite based actual evapotranspiration over drying semi-arid terrain in West Africa**

---

Material in this chapter is submitted to the Journal of Applied Meteorology with Ch. Schillings, A.F. Moene and H.A.R. De Bruin as co-authors.

## **Abstract**

A simple satellite based algorithm for estimating actual evaporation based on Makkink's equation is applied to a seasonal cycle in 2002 in the Volta Basin in Ghana, West Africa, notably at a location in the humid tropical southern region and two sites in the dryer northern region. The required algorithm input is incoming solar radiation, air temperature at standard level and the green vegetation fraction. Those data are obtained from METEOSAT and MODIS images. The observation period includes the rapid wet-to-dry transition after the wet season.

Incoming solar radiation and air temperature are validated with local measurements at the three sites. It is found that the incoming solar radiation obtained from METEOSAT corresponds well with the measurements. For air temperature from METEOSAT data the diurnal cycle is realistically reproduced, but it needs to be bias corrected.

The algorithm output is compared with the evapotranspiration data obtained from hourly large aperture scintillometer observations and simultaneous 'in situ' measurements of net radiation and soil heat flux. It is found that the actual evapotranspiration can be monitored with the modified Makkink method with a daily mean bias error (MBE) less than 1 mm/day and a seasonal MBE less than 0.5 mm/day. Furthermore, it appears that the algorithm realistically describes the daily cycle of evapotranspiration.



## 5.1 Introduction

A quantitative knowledge of the loss of water by actual evapotranspiration (latent heat flux) is crucial in hydrological studies and water resource management, because it serves as one link between the land surface and the atmosphere. Especially in the semi-arid tropical regions the knowledge of this loss of water by evapotranspiration is important, because of its large magnitude and the variability of rainfall amounts. During recent decades the skill of meteorological and hydrological models has improved to tackle that need. However there is still a lack of input and validation data for those models in the mentioned regions. The watershed of the Volta River, West Africa, is one example for such a region. The regional climate is characterized by a strong north-south gradient of mean annual rainfall and the occurrence of pronounced dry and wet seasons within one annual cycle. This causes a strong seasonal variation in the natural vegetation cover and therewith a large variability in actual evapotranspiration.

Due to the given lack of data there is a need to use remote sensing information for further validation and improvement of evapotranspiration models. Furthermore, available remote sensing information can be used to carry out water management with the background of land use change. During the last decade a growing number of satellite algorithms have been developed to estimate actual areal averaged evapotranspiration (SEBAL: Bastiaansen et al. 1998a, 1998b, SEBS: Jia et al. 2003 and the method proposed by Ma et al. 2004). Since those algorithms are based on the radiometric temperature they are limited to cloud-free situations, which makes it difficult to obtain evapotranspiration on a daily or weekly basis under the conditions in West Africa. Additionally a radiometer on board a satellite receives an instantaneous estimate of the radiometric temperature (Kustas et al. 2002), which may or may not be representative for a temporal average of the flux (Brunsell and Gillies 2003). This shows that there is a need for a robust algorithm that works under partly clouded situations.

In the interest of clarity one has to define some basic quantities in this context. Potential evaporation (PE) is the amount of water evaporated per unit area, per unit time from an idealized extensive free water surface under existing atmospheric conditions (Shuttleworth 1993). The optimal evapotranspiration (OE) corresponds to the ability of plants to transpire under ideal conditions (full vegetation cover, well watered) with a non-zero resistance to water vapor flux. Optimal evapotranspiration is always lower than PE. Finally one can estimate the actual evapotranspiration (AE), which should be dependent on actual vegetation cover and soil moisture status. The actual evapotranspiration should equal optimal evapotranspiration under ideal conditions.

One way to derive optimal evapotranspiration, which is not based on the radiometric temperature and is not necessarily a remote sensing technique, is the crop factor method (Doorenbos and Pruitt 1977; Allen et al. 1998). For this approach the optimal evapotranspiration is determined in the following way:

$$E_{opt} = k_c E_{ref} \quad (5.1)$$

where  $k_c$  is a crop factor and  $E_{ref}$  is the reference crop evaporation. For the estimation of  $E_{ref}$  some versions of the Penman-Monteith equation (e.g. Monteith and Unsworth 1990) are utilized, which require net radiation, air temperature, air humidity and wind speed. Especially the estimation of net radiation can cause large errors since it cannot be obtained directly from remotely sensed measurements and the surface conditions change noticeable during the year for the studied region.

An alternative and simpler way of deriving optimal evapotranspiration is the approach developed by Makkink (1957), who found that the equation of Penman (1956) could be simplified for well watered surface in the following way:

$$L_v E = 0.63 \frac{s}{s + \gamma} R_s + 14.0 \quad (5.2)$$

in which  $R_s$  is the incoming solar radiation,  $s$  is the slope of water vapor pressure at temperature and  $\gamma$  is the psychrometric constant.

De Bruin (1987) modified the Makkink formula and showed that it can also be ‘derived’ from the empirical formula of Priestley and Taylor (1972). For this modified Makkink formula the reference evapotranspiration can be defined as follows:

$$E_{ref} = 0.65 \frac{s}{s + \gamma} R_s \quad (5.3)$$

For calculating the optimal evapotranspiration the reference evapotranspiration has to be multiplied by the crop factor (equation 1). In the present study  $k_c$  is set to 1. Finally the actual evapotranspiration is defined as follows:

$$E_{act} = VF * E_{opt} \quad (5.4)$$

here VF is the actual green vegetation fraction. Since the method is fairly simple it can be regarded as a first order approach to estimate evapotranspiration. Justification of applying this modified Makkink approach is that in the semi-arid regions vegetation adjusts its cover to the available water: if there is less water to evaporate, this will be reflected in the vegetation cover. This is reasonable since recent research has revealed that the semi-arid areas are dominated by vegetative pathways (via stomatal conductance and vegetation cover), whereas the midlatitudes show a more soil wetness-related feedback (Niyogi et al. 2002). Furthermore this idea only holds for non-irrigated crops. The error in this calculation should increase when there is a considerable amount of bare soil evaporation. Garatuza-Payan and Watts (2003) showed that the modified Makkink approach worked with errors on the order of 1 mm per day for Northwest Mexico.

Choudhury and De Bruin (1995) examined various methods for using remotely sensed information to obtain optimal evapotranspiration and found the modified Makkink formula as a suitable approach, but stated that critical evaluation of the components is needed.

In the present study this approach is utilized and incoming solar radiation is obtained from Meteosat data. For calculating the slope of water vapor pressure  $s$  at temperature  $T$  the temperature obtained from Meteosat data is used. Small errors in temperature should not affect the results too much, since temperature is only used to calculate  $s$ . For the estimation of the green vegetation fraction the enhanced vegetation index (EVI) obtained from Moderate Resolution Imaging Spectroradiometer (MODIS) data is utilized.

When using remote sensing estimates for latent heat flux (or sensible heat flux), one critical issue is the validation of the estimates. No clear methodology exists for this purpose. Often methods suitable for homogenous surface (point observations) are used, which are not applicable for the heterogeneous surfaces in West Africa. The use of scintillometry proposed by e.g. De Bruin et al. (1995) for sparse vegetation in Spain should help in validating the remote sensing estimates. The advantage of the LAS technique is that areally averaged sensible heat flux can be obtained (up to scales of 5000m), which means that information is provided on satellites pixel scale. Therefore scintillometry is used in this study as a basis for validating evapotranspiration. This method has been applied for remote sensing validation before in other regions (Hemakumara et al. 2003; Jia et al. 2003).

The main objective of this study is to investigate if a long-term monitoring of actual evapotranspiration under partly clouded conditions in the tropics is feasible. Therefore firstly a validation of needed input parameters like incoming solar radiation and temperatures derived from Meteosat data is carried out. Secondly the evaluation of actual evapotranspiration estimates based on the derived products is done.

The focus is on discussing the accuracy and time variability of incoming solar radiation, air temperature and the estimated evapotranspiration. The algorithms to obtain solar radiation and temperature from Meteosat data and green vegetation fraction from MODIS are described in section 5.2. Section 5.3 describes the experimental setup and observations including a more detailed site description. In section 5.4 first the global radiation and temperature derived from METEOSAT data are validated with ground-based measurements. Then the actual evapotranspiration derived from the satellite data is compared to ground-based measurements. Section 5.5 provides a summary and conclusion.

## **5.2. Satellite data**

Satellite data are widely applied for the determination of atmospheric and surface properties. Depending on the satellite system, the spatial and temporal resolution can range from tens of meters to several kilometers and from half-hourly to half-daily images.

Data of geostationary satellites can be utilized for example to estimate incoming solar radiation or land surface temperature. With their so-called visible (VIS) and infrared (IR) sensors, information on the reflected shortwave and emitted longwave radiance of the earth-atmosphere system is gathered. For this study data of the geostationary satellite Meteosat (Meteorological Satellite) operated by EUMETSAT (European Organisation for the Exploitation of Meteorological Satellites) is used. This satellite revolves the earth sun-synchronously in an orbit of 36.000 km height at 0° latitude and 0° longitude. Meteosat scans the earth each 30 minutes from south to north with three radiometers, one at the visible wavelengths (VIS, 0.45 – 1.0  $\mu\text{m}$ ), one at infrared wavelengths (IR, 10.5 – 12.5  $\mu\text{m}$ ) and one at the wavelength of the water vapor absorption band (WV, 5.7 – 7.1  $\mu\text{m}$ ). Data of the WV-channel is not used in this study. One full-disk image consists of 2500 x 2500 pixels in the IR-channel and 5000 x 5000 pixels in the VIS-channel and therefore the spatial resolution is 5 x 5  $\text{km}^2$  and 2.5 x 2.5  $\text{km}^2$  respectively at the Sub-Satellite-Point perpendicular under the satellite at ground.

### **5.2.1 Determination of incoming solar radiation from Meteosat**

Many approaches exist to derive the incoming solar radiation at ground using geostationary satellite data. Newer methods are described for example in Stuhlmann et al. (1989), Hammer et al. (2003), Ineichen and Perez (1999) or Rigollier, Lefèvre and Wald (2001). All of these methods relate the reflected sunlight measured by the Meteosat VIS-channel covering the range 0.45  $\mu\text{m}$  - 1.0  $\mu\text{m}$ , to the incoming solar radiation at the surface. The method used in

this study is described in Perez et al. (2002), which is an evolution of the model of Cano et al. (1986). This method was developed for the determination of incoming solar radiation using data of the geostationary satellite GOES (Geostationary Operational Environmental Satellite). For this study, data of the VIS-channel of Meteosat-7 are adapted and included into the calculation scheme. The measured reflectance is usually low for earth surfaces and high for clouds. The information on the clouds is expressed in the cloud index CI:

$$CI = \frac{\rho - \rho_{\min}}{\rho_{\max} - \rho_{\min}} \quad (5.5)$$

where  $\rho$  is the actual satellite count,  $\rho_{\min}$  corresponds to the surface albedo, which is derived by an analysis of cloud-free satellite scenes.  $\rho_{\max}$  gives the maximum reflexivity for overcast clouds. The cloud index CI varies between 0 for cloud-free and 1 for overcast conditions. For the determination of the incoming solar radiation, also known as global horizontal irradiance (*GHI*) for cloudy conditions the cloud index *CI* is used according to Perez et al. (2002) with

$$GHI = (0.02 + 0.98 \cdot (1 - CI)) \cdot G_{hcl} \quad (5.6)$$

The global horizontal irradiance for clear-sky conditions is calculated according to Ineichen and Perez (2002) with

$$G_{hcl} = a_1 \cdot I_0 \cdot \sin(h) \cdot \exp(-a_2 \cdot am \cdot (f_{h1} + f_{h2} \cdot (T_L - 1))) \quad (5.7)$$

where  $I_0$  is the eccentricity corrected extraterrestrial irradiance,

$h$  is the solar elevation,

$am$  is the altitude corrected airmass,

$T_L$  is the Linke turbidity,

$$a_1 = 5.09 \cdot 10^{-5} \cdot \text{altitude} + 0.868,$$

$$a_2 = 3.92 \cdot 10^{-5} \cdot \text{altitude} + 0.0387,$$

$$f_{h1} = \exp^{(-\text{altitude}/8000)},$$

$$f_{h2} = \exp^{(-\text{altitude}/1250)},$$

with the altitude above mean sea level expressed in meters. The Linke turbidity  $T_L$  represents the number of clean and dry atmospheres that would be needed to produce the observed extinction. To take the cloud-free atmosphere into account, the Linke turbidity database

provided by the SODA-server (Solar Radiation Database) is used (Wald et al. 2002). For Ghana  $T_L$  varies between values of 4 and 6.

### 5.2.2 Determination of near surface temperature from Meteosat

The IR sensor measures the outgoing longwave irradiance of the system earth-atmosphere for a specific wavelength. The measured value can be used to assess a kind of land surface temperature (e.g. Schädlich et al. (2001) and Sun and Pinker (2003)). The approach used in this work was developed by Mannstein et al. (1999). The (near-)surface temperature is a by-product of the cloud-detection scheme. Clouds show up in the IR channel of Meteosat as cold pixels. For detection, a reference temperature is needed, which represents the cloud-free surface temperature (warmer than clouds). As measurements of surface temperature are not available in a sufficient temporal and spatial resolution especially in the rural areas of West Africa, the reference temperature is derived from the Meteosat data itself. To achieve this, we first calibrated the Meteosat count to obtain the equivalent black body temperature. We then sorted the available images as a 3-dimensional array for each day with the spatial coordinates X and Y and the temporal coordinates T (time, every half hour, from 1 to 48). The reference temperature of the land surface is described by the following parametric function for every pixel:

$$T = a_0 + a_1(\cos(x - a_3) + \sin(a_2) \cdot \sin(x - a_3)) + 0.1 \cdot \sin(x - a_3) \quad (5.8)$$

with  $x = t/24 * 2\pi$  and  $t =$  decimal hours of the satellite scan (UTC).  $a_0$  gives the daily mean temperature,  $a_1$  the temperature amplitude,  $a_2$  influences the width and steepness of the daily temperature wave and  $a_3$  gives the phase shift, which is dominated by the local solar time. These four parameters are fitted daily for each land-pixel using all cloud-free half-hourly values for each day for each pixel (max. 48 values per day and per pixel). The derived reference temperature is used in this work as an estimate for the 2m-air temperature.

### 5.2.3 Green vegetation fraction from MODIS

Since the launch of the first Advanced Very High Resolution Radiometer (AVHRR) information on the vegetation at the earth's surface is obtained from the normalized differential vegetation index (NDVI). Although related to vegetation properties as leaf area index (LAI) and green vegetation fraction (VF), NDVI is not a direct measure for those properties. For LAI values above two, NDVI saturates. The relationship between VF and

NDVI critically depends on the relative brightness of the soil and the vegetation, as well as on the NDVI of soil and vegetation separately (Hanan et al. 1991).

The enhanced vegetation index (EVI) was developed to take the influence of both the atmosphere and the soil on the vegetation index (Liu and Huete 1995) into account. The EVI appears to suffer less from saturation at high values of LAI and is more directly related to vegetation characteristics (Huete et al. 2002). If the maximum value of EVI ( $EVI_{max}$ ) is assumed to be the EVI of vegetation, and the minimum value ( $EVI_{min}$ ) is assumed to be the background value, the vegetation fraction can be determined as:

$$VF = \frac{EVI - EVI_{min}}{EVI_{max} - EVI_{min}} \quad (5.9)$$

Based on figure 17 in Huete et al. (2002), the extreme values of EVI,  $EVI_{max}$  and  $EVI_{min}$ , are estimated to be 0.65 and 0.08, respectively.

EVI data are routinely produced from the data of the Moderate Resolution Imaging Spectroradiometer (MODIS) on board of the Terra and Aqua satellites. In this study we use 16 day composites of EVI, gridded at a spatial resolution of 1 kilometer. Level 3 data (version 4) from the Aqua satellite were used. For the combination with the Meteosat data, a composite was made of the four pixels surrounding each of the field sites. The quality flag of the MODIS data was used to determine possible cloud contamination. Data with cloud contamination were discarded.

## 5.3 Experimental Setup and Observations

### 5.3.1 Site description and experimental setup

All analyzed measurements are part of long-term observations of the water- and energy balance in the Volta Basin within the GLOWA-Volta project (Global Change in the Hydrological cycle). GLOWA-Volta is a multidisciplinary effort to study the physical and socioeconomic determinants of the hydrological cycle (Van de Giesen et al. 2001). The climate system in the Volta basin is very much controlled by the meridional movement of the intertropical convergence zone (ITCZ), the African Easterly Jet (AEJ) and pressure disturbances, which traverse from east to west across Africa (Burpee 1972). They all act under the influence of the Hadley and Walker cell circulation. Those mechanisms lead to a pronounced wet and dry season during the year, of which the length depends on the actual latitude. During the time of the year when the wet period ends and the dry period starts (time

of transition), the contrast between dry and moist air is probably more pronounced in time and space than anywhere else (Hólm et al. 2002).

To account for the large variability during the year of the climate system in the Volta basin three meteorological test-sites (Navrongo, Tamale and Ejura) were established in June 2001.

The data used in this study are based on measurements from automatic weather stations (AWS) and large aperture scintillometer (LAS) measurements in Navrongo (10° 55' N; 1° 02' W), Tamale (9° 29' N, 0° 55' W) and Ejura (7° 20' N; 1° 16' W). The distance between the stations is about 100- 200 km. Tamale is the central station. The exact locations are given in Figure 5.1. The three sites show major differences concerning the vegetation, soils, land use, slopes and also climate.

The test site in Navrongo is located in northern Ghana. The area is characterized by some scattered trees, mainly baobabs, and extensive land use during the wet season. During the dry season it is mainly characterized by bare soil. The landscape is nearly flat. LAS transmitter and receiver are installed with a distance in between of 1040 m with a weighted effective height of 12.8 m.

The research site in Tamale is mainly characterized by grassland with scattered trees, which have a maximum height of five to eight meters. The landscape is slightly hilly. LAS transmitter and receiver are installed on two hills with a distance in between of about 2420 m. The weighted effective height of the LAS was estimated to 19.5 m. The automatic weather station is installed next to the receiver of the LAS.

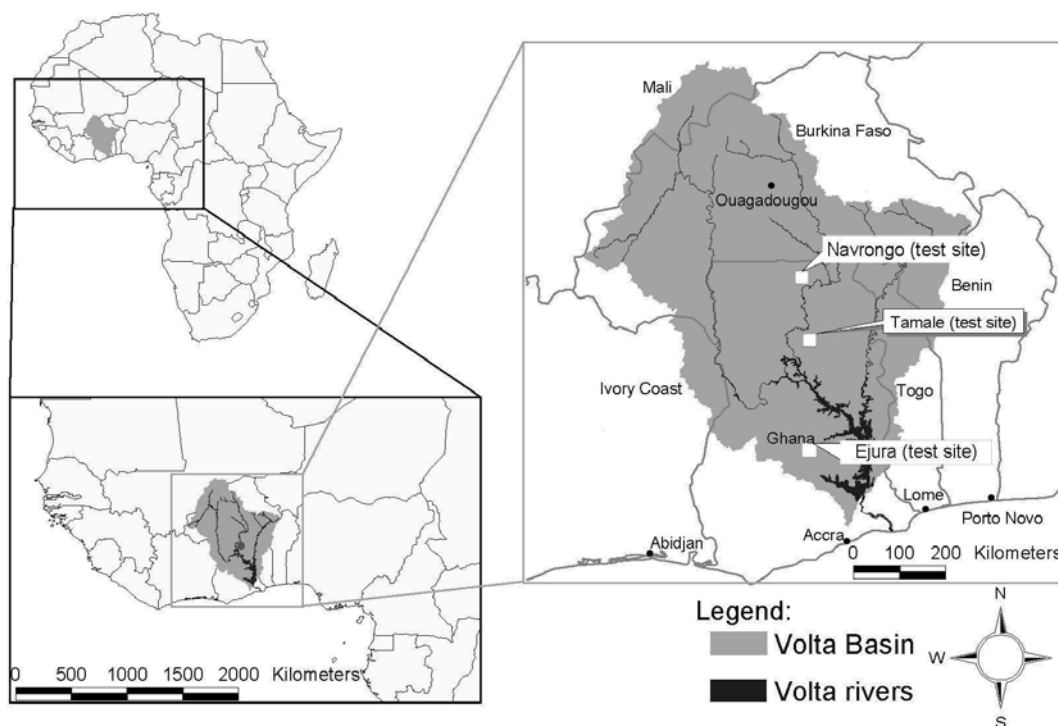


**Fig. 5.1: Location of experimental sites in Ghana within the GLOWA-Volta project.**



The site in Ejura is the tropical site. The landscape is hilly. Here the transmitter and the weather station are located in a cashew orchard. The receiver is located at the edge of a forest. The LAS path has a length of 2030 m. The weighted effective height of the LAS was estimated to 30.1 m. It is a heterogeneous terrain. The area between the transmitter and the receiver can roughly be divided into two parts. On the transmitter side the vegetation consists of cashew trees with a maximum height of four m and in between maize and grass. On the receiver side there are bushes and trees and small swamps, but nearly no agriculture. All sites are equipped with AWS, which measure temperature, humidity and incoming solar radiation at a reference level,  $z = 2$  m, according to a WMO standard meteorological weather stations. Wind speed and direction are measured at eight-meter height. Net radiation is measured directly at eight-meter height. Additionally, surface observation for soil heat flux, precipitation and runoff are recorded. Data availability exceeds more than 90% for most of the measurements for all three sites during the year 2002. The type and brand of the instruments used are described in table 5.1. All quantities are originally averaged for ten-minute intervals.

**Table 5.1: Instrument used within the GLOWA-Volta project.**

Variable	Location	Instrument
Air Temperature	2 m	50Y Temperature and RH probe (Vaisala)
Relative Humidity	2 m	50Y Temperature and RH probe (Vaisala)
Atmospheric pressure	Inbox	PTB101B Barometric Pressure Sensor (Vaisala)
Wind Speed	8 m	A100R Anemometer (Vector Instruments)
Wind Direction	8 m	Wind vane (Ecotech)
Net Radiation	8 m	NR-LITE (Kipp & Zonen)
Downward solar radiation	2 m	SP-LITE (Kipp & Zonen)
Precipitation	2 m	Tipping bucket (Stelzner)
Sensible Heat Flux	Site dependent	Large Aperture Scintillometer (LAS) (Manufactured by Wageningen Uni.)
Latent Heat Flux		Residual of the energy balance
Soil Heat Flux	0.035 m	HFP01 Heat Flux Plate (Hukseflux)
Soil Temperature	Different depth	PT <sub>100</sub> resistance thermometer (Manufactured by Wageningen Uni.)
Soil moisture	Different depth	TDR (Campbell) (Tamale), TDR (Delta-T) (Ejura)

For measuring incoming solar radiation Kipp & Zonen pyranometers CM3 are used. The CM3 pyranometer measures the solar irradiance from the whole hemisphere (180 degrees field of view). According to WMO standard it is a second-class instrument. The spectral range reaches from 305 to 2800 nm. The response time is about 18 s. The directional error is down

to  $\pm 25 \text{ W m}^{-2}$  at  $1000 \text{ W m}^{-2}$ . The expected accuracy for daily sums is about  $\pm 10\%$ . For all instruments it was regularly checked that the sensor is not tilted and for the studied period the sensors were cleaned on a one to two week basis, depending on the actual site.

For measuring air temperature the 50Y temperature and relative humidity probe from Vaisala is used. It uses a  $1000 \Omega$  PRT to measure temperature. The instrument is calibrated for a temperature range of  $-10$  to  $+60 \text{ }^\circ\text{C}$ . The accuracy is down to  $\pm 0.35 \text{ }^\circ\text{C}$  at  $-10 \text{ }^\circ\text{C}$  and  $\pm 0.6 \text{ }^\circ\text{C}$  at  $+60 \text{ }^\circ\text{C}$ . All measurements are recorded in UTC and there was no daylight saving time.

### 5.3.2 Flux measurements with Scintillometry

The LAS consists of a transmitter emitting electromagnetic radiation towards a receiver. The distance between both can be chosen up to 5000 m for a beam diameter of 0.15 m. In our case the distance varies between 1040 – 2420 m for the different sites. It is installed at a certain height above the surface. The emitted radiation is scattered by the turbulent medium in the path. The variance of intensity of received radiation is proportional to the structure parameter of the refractive index of air ( $C_n^2$ ). At the wavelength used (940 nm) the refractive index mainly depends on temperature, so  $C_n^2$  is mostly determined by temperature fluctuations ( $C_T^2$ ),

$$C_T^2 = C_n^2 \frac{T^2}{A_T^2} \left( 1 + \frac{A_q}{q} \frac{T}{A_T} \frac{c_p}{L_v} \beta^{-1} \right)^{-2} \quad (5.10)$$

$$\text{with } A_T = T \frac{\partial n}{\partial T} \text{ and } A_q = q \frac{\partial n}{\partial q}$$

which are both dependent on optical wavelength, pressure, temperature and humidity content. T is the mean air temperature, q is the mean specific humidity,  $c_p$  is the specific heat of air at constant pressure and  $L_v$  is the latent heat of vaporation. The last factor at the right-hand-side of equation 5.10 reflects an estimate of the influence of humidity on the refractive index (Wesely 1976; Moene 2003). Here  $\beta$  is estimated as follows:

$$\beta = \frac{H_{LAS}}{R_n - G - H_{LAS}} \quad (5.11)$$

Sensible heat flux is calculated from  $C_T^2$  by using the following expression:  $H_{LAS} = \rho c_p u^* \Theta^*$  with  $u^*$  being the friction velocity and  $\Theta^*$  being the temperature scale from Monin-Obukhov

similarity theory (MOST). In this study a standard Businger–Dyer flux-profile relation is utilized for estimating  $u_*$  from wind speed and roughness length and  $H_{LAS}$  is calculated iteratively. Stability functions proposed by Wyngaard (1973) were used for daytime values. For nighttime values we follow the formulation of De Bruin et al. (1993). Several tests are made for the use of different stability functions for day and nighttime situations. In general the results are steady and differ at most 10%, but especially during nighttime the formulation of de Bruin gave the most reliable results. For a more detailed description of the LAS theory and its applications see for example De Bruin et al. (1995) and Meijninger et al. (2002).

The LAS at each site is installed on top of two opposite hills using towers with a minimum height of 5 m. The setup with small differences in installation height of transmitter and receiver and changes in terrain height along the path implies that the beam above the terrain varies along the path. Therefore the effective height was calculated using the method of Hartogensis et al. (2003) using the fact that the LAS signal is weighted towards the middle of the path.

Latent heat flux is calculated as a residual from the energy balance, which showed good correspondence with eddy covariance data obtained during an intensive observation period (IOP) during the drying up in 2002. One has to remember that this approach forces the measured energy balance to close. The error in measured energy balance closure was smaller than 10% for the IOP in 2002 in Tamale and for large parts of the season in Ejura (Schüttemeyer et al., submitted to *Boundary-Layer Meteorology*).

### **5.3.3 Algorithm evaluation**

The evaluation is performed for the period from 26 August 2002 until 31 December 2002. The period covers the transition time from the wet to the dry season in the studied region. 40 years of rainfall for different stations in the Volta basin were analyzed for the on- and offset of the rainy period using the method of Kasei (1988). It was found that the start and the end of the rainy season for 2002 are within the range of one standard deviation when compared to the climatology.

Satellite based estimates are compared to measured quantities namely incoming solar radiation, 2m air temperature and latent heat flux. Days containing rainfall are excluded from the statistical analyses (see discussion below). To explore the limits of the satellite based AE, the AE is calculated with locally observed incoming solar radiation and measured 2m temperature as well.

As a first check for the different components of the energy balance the correlation coefficient, the mean bias error (MBE) and rmse are calculated. The term MBE refers to the difference

between the modeled value and the measured value. Positive (negative) MBE occurs when the modeled value is higher (lower) than the measured value. Furthermore the relative MBE is calculated by dividing the absolute MBE by the mean flux. To account for the seasonal dynamics this procedure is done for daily values over the entire period. As a second check for the quality of estimated AE a comparison of daily values is done. The first criterion in this context is that the daily MBE should not exceed 1mm per day. This criterion works as long as latent heat flux is high enough during the day. A second criterion is that the daily MBE should not exceed 20% of the daily sums.

## **5.4 Results and Discussion**

In this section the key variables for estimating AE are validated with a focus on discussing the accuracy and time variability. Satellite based AE is validated with taken measurements. Besides, the remote sensing algorithm is also tested with ground-based input parameters (incoming solar radiation and temperature).

### **5.4.1 Validation of satellite derived incoming solar radiation**

The overall results based on hourly observations show a reliable estimation of incoming solar radiation by the satellite retrieval when compared to the local measurements for all three sites (figure 5.2). The correlation coefficient is high for Navrongo (0.97) and Tamale (0.96) and lower for Ejura (0.94). A linear regression gives a slope close to 1 and intercept, which is smaller than  $1 \text{ W m}^{-2}$  for all three sites. The MBE has a negative value for Navrongo and is positive for Tamale and Ejura. The rmse gives similar values for Navrongo and Tamale and a higher value for Ejura (figure 5.2). This could be due to the fact that the rainy period stopped later in Ejura and more clouds can be seen during the studied period. In total the rmse is high for all three sites. This is confirmed by the amount of scatter seen in figure 5.2. One explanation for the amount of scatter seen is the comparison of a point measurement to an areal average from the satellite. The Meteosat algorithm cannot resolve every single detail from the point measurements. Figure 5.3 shows that the diurnal cycle of incoming solar radiation is realistically reproduced for most of the shown days, but not every detail can be resolved by Meteosat data. The only solution for this problem would be the use of a network of radiometers to obtain areal averaged incoming solar radiation. During days with rain the daily differences get larger. This could be related to changing albedo after rain events and also because the sensors were not cleaned immediately after rain events.

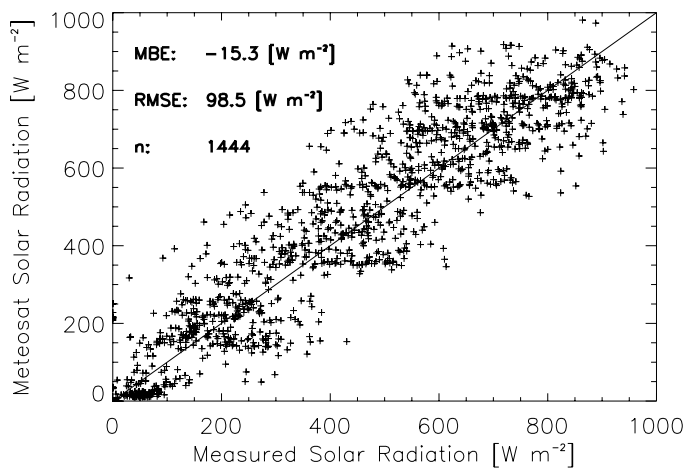
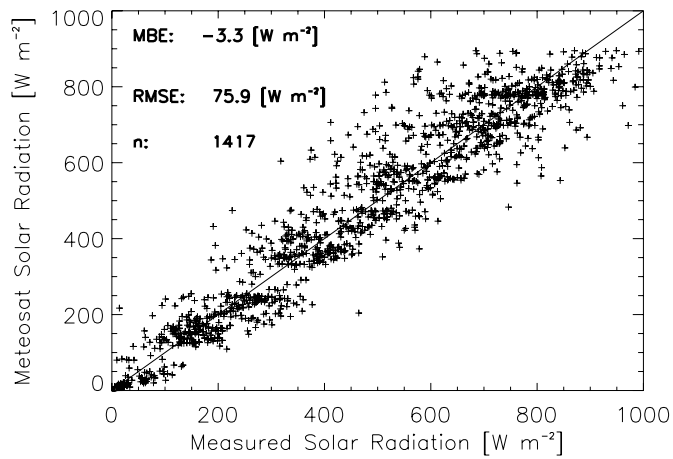
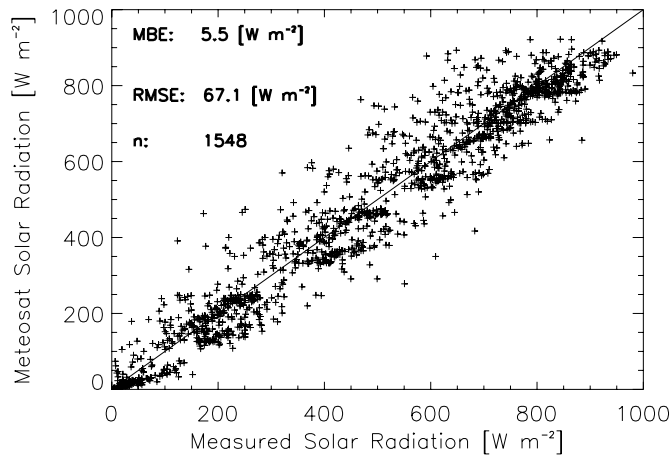


**Fig. 5.2: Meteosat derived radiation vs. measured radiation scatterplot for the analyzed period from the end of August 2002 until the end of the year 2002 for Navrongo (upper), Tamale (middle) and Ejura (lower).**

The seasonal dynamics based on the daily daytime differences of satellite based and measured incoming solar radiation (Figure 5.4) show similar results for the three sites. The Meteosat algorithm works well throughout the season with fluctuating values around zero. Only during days with rain the daily difference gets larger. The period after 30 September 2002 shows higher daily differences and also higher values for the rmse compared to the rest of the season with a time shift between the three sites. The errors might be explained by large-scale features, which traverse from east to west across Africa. This is confirmed by the daily cloud cover derived from Meteosat data and the local precipitation measurements. For the period when the rain stopped the rmse decreases for all three sites to values smaller than  $20 \text{ W m}^{-2}$ .

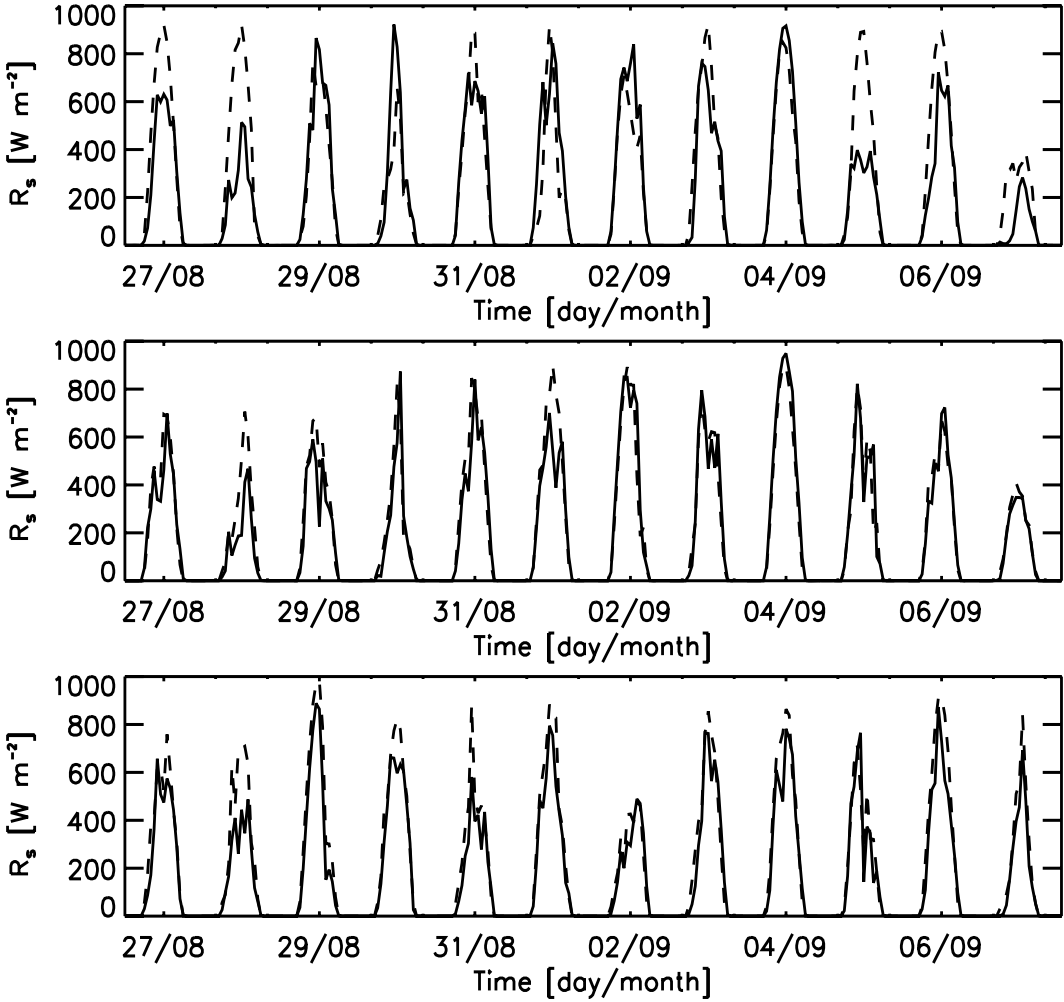


**Fig. 5.3: Daily evolution of incoming solar radiation for all three sites (Navrongo, Tamale, Ejura) for a 12 day period starting from 26 August 2002 (DOY 238). Solid lines correspond to measured radiation and dashed line to Meteosat derived radiation.**

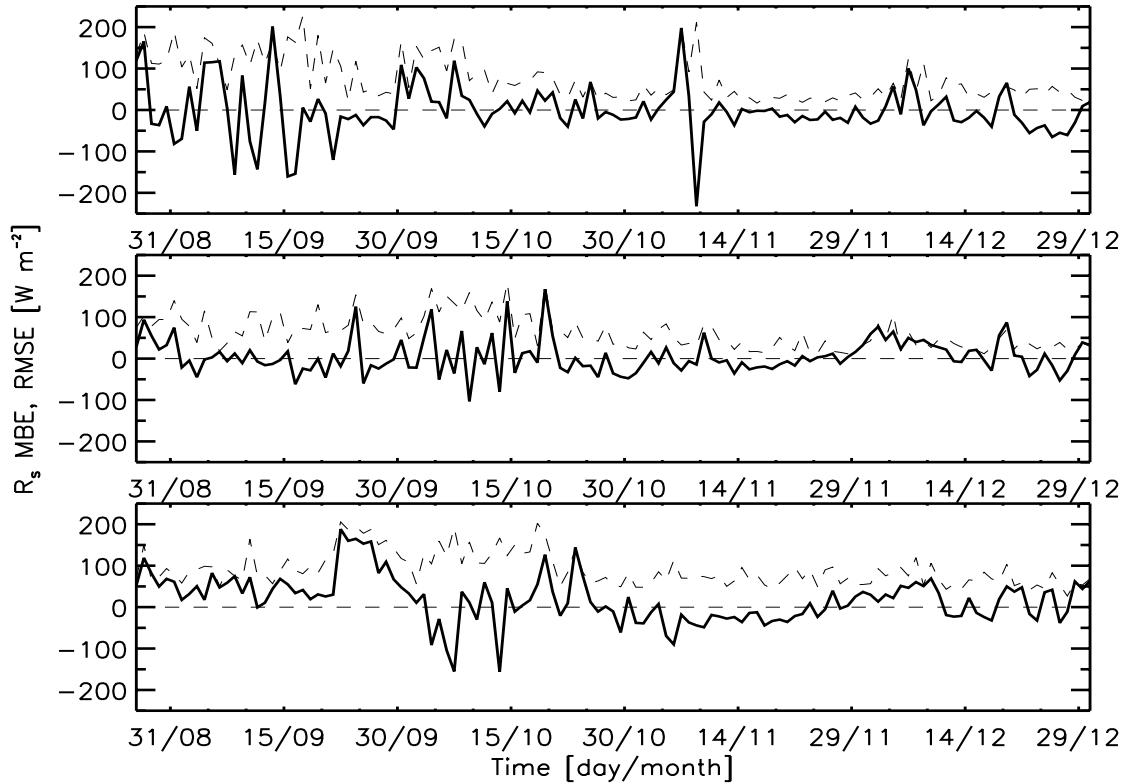


**Fig. 5.4: Daily values of MBE and rmse for incoming solar radiation for all three sites (Navrongo, Tamale, Ejura) for the analyzed period from August 2002 until December 2002. Solid lines correspond to MBE and dashed line to rmse.**

#### 5.4.2 Validation of satellite derived reference temperature

The overall results for temperature estimation show a similar MBE for the three sites (table 5.2). The similar MBE implies that the reference temperature can be used as a proxy for the 2-m temperature, with a simple adjustment that is constant over a considerable region. The correlation coefficient is lower compared to incoming solar radiation. For Navrongo and Tamale the correlation and rmse is similar. For Ejura the rmse is higher and correlation is lower.

**Table 5.2: Evaluation of reference temperature obtained from Meteosat for the three test sites.**

Temperature	Correlation	MBE [K]	rmse [K]
Navrongo	0.77	-5.4	3.8
Tamale	0.79	-5.1	3.6
Ejura	0.20	-6.1	7.6

The more heterogeneous terrain might explain the lower correlation and higher rmse for Ejura. The AWS is located in a cashew orchard, between the trees, which might influence the taken measurements. Furthermore the landscape is hilly, which poses the question of how representative the point measurements are.

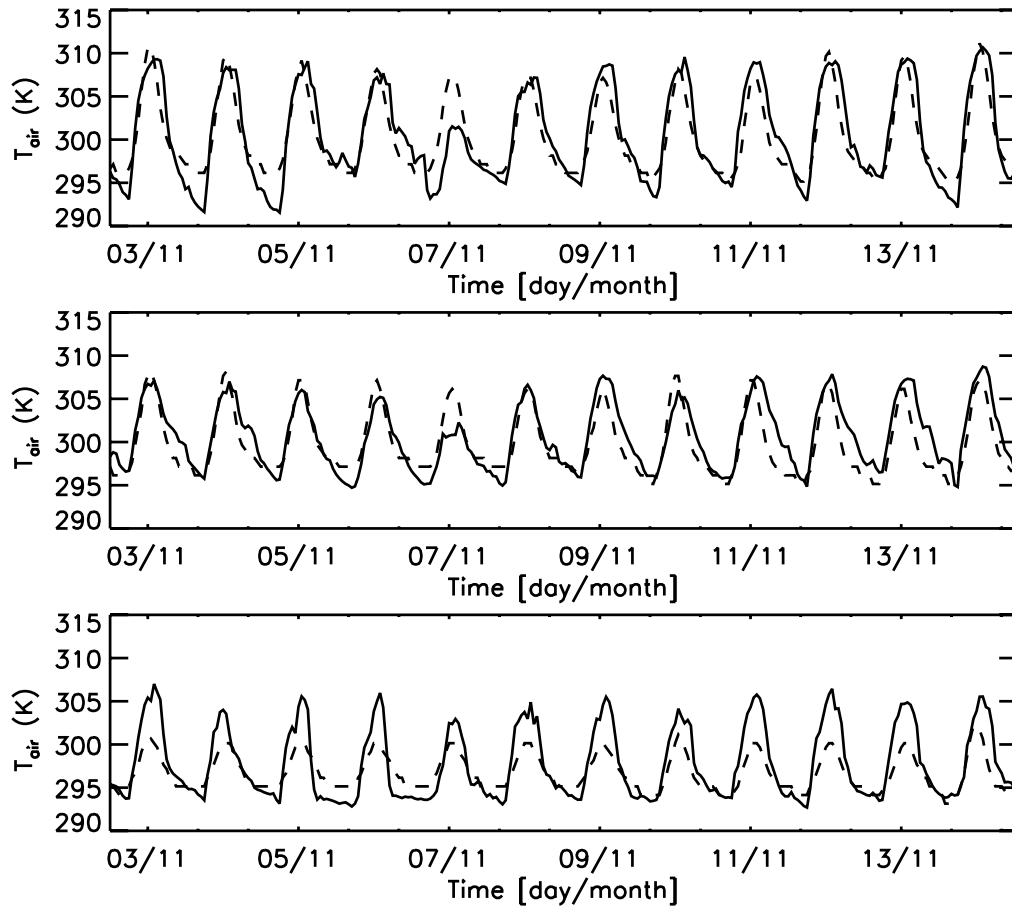


**Fig. 5.5: Daily evolution of 2m air temperature for all three sites (Navrongo, Tamale, Ejura) for a 12-day period starting from 03 November 2002. Solid lines correspond to measured temperature and dashed line to reference temperature obtained from Meteosat.**

Figure 5.5 shows the diurnal cycles for temperature for a 10-day period at the three different sites. It was adjusted using the mean of the MBE of all three sites. The diurnal cycle is realistically reproduced by Meteosat data. During some days the differences get larger. This should not affect the results for the estimation of AE too much, since temperature is only used to calculate the slope of water vapor pressure  $s$  at temperature  $T$ . For a couple of days the reference temperature drops too early in the afternoon, which might be due to the fact that equation 5.8 gives a limited degree of freedom in the shape of the diurnal cycle.



The seasonal dynamics based on the daily differences of satellite based and measured temperature show a trend to smaller differences towards the end of the season for the Meteosat algorithm. This is explained by a decrease in the amount of water vapor in the air towards the dry season.

### 5.4.3 Validation of actual evapotranspiration

The comparison of incoming solar radiation and temperature started at 26 August 2002, but due to measurement problems of the LAS the comparison of latent heat flux is limited in Navrongo. For Tamale it starts at 14 October 2002 and continues until the end of the year and for Ejura it starts at 27 September 2002 and also continues until the end of the year. Since rain introduced an error already in the estimation of incoming solar radiation, those days are excluded from further analysis. Furthermore the evapotranspiration of intercepted rainfall should definitely give erroneous results for evapotranspiration under rainy conditions. Due to the limitation in measurements the data from the site in Navrongo is excluded from the statistical analysis and only discussed qualitatively. During nighttime the satellite based AE cannot be used to calculate evapotranspiration. This introduces an error in daily sums of evapotranspiration, which should be small (discussed below).

Figure 5.6 shows the daily averages of measured available energy ( $R_n - G$ ) and estimated actual evapotranspiration for the analyzed period at Navrongo test site. The results indicate that evapotranspiration is modeled realistically, since daily values of evapotranspiration follow the seasonal course of available energy. Only small variations are not detected in the daily values of evapotranspiration. Furthermore from the fraction of evapotranspiration from available energy it is seen that it is large during the wet part of the season and decreases during the drying up. During and after rain events (e.g. beginning of November) the daily AE is not estimated correctly, which is a weakness of the approach. From the limited amount of LAS measurements it is concluded, that the daily cycle of evapotranspiration is also modeled realistically.

The overall results for satellite and ground based AE estimation at the two test sites in Tamale and Ejura are given in table 5.3. The correlation coefficient is lower compared to incoming solar radiation, but higher than for 2 m temperature. The MBE for both sites is small. The rmse is on a high level for both sites given a maximum flux of about  $300 \text{ W m}^{-2}$ . The seasonal dynamics for Tamale based on daily MBE show values lower than 1 mm per day for all days. For 70% of all days the MBE is smaller than 20%. The seasonal dynamics for Ejura based on daily MBE show in 89% of the days values lower than 1 mm per day. For 70% of all days the MBE is smaller than 20%. From the daily values it is concluded that for both sites the biggest

errors appear after the rain has stopped. The assumption behind the use of vegetation cover was that if there is less water to evaporate, this would be reflected in the vegetation cover. This might not be valid for the period immediately after the rain stops, since first a reduction in soil moisture might happen before the vegetation cover adjusts. Figure 5.7 show the scatter plots for satellite based AE at Tamale and Ejura including only daytime values for rain free situations.

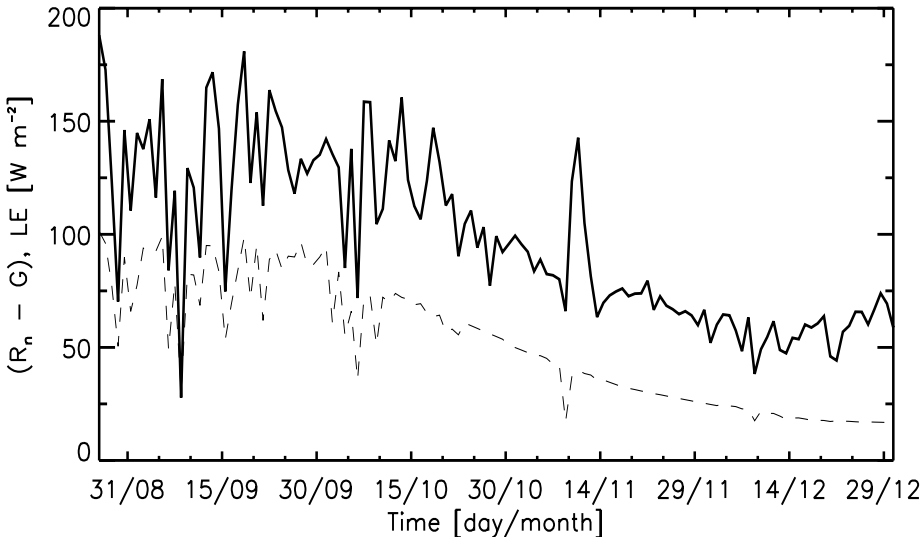


**Fig. 5.6: Navrongo: Daily averages of measured available energy ( $R_n - G$ ) and satellite based actual evapotranspiration for the analyzed period in Navrongo. The solid line corresponds to measured ( $R_n - G$ ) and dashed line to the satellite based evaporation.**

**Table 5.3: Evaluation of satellite and ground based AE for Tamale and Ejura test site.**

Actual evaporation (Latent Heat Flux)	Correlation	MBE [ $W m^{-2}$ ]	rmse [ $W m^{-2}$ ]	Percentage of MBE %
Tamale (Meteosat)	0.90	10.5	49.1	10.5
Tamale (ground based)	0.93	7.3	46.4	8.1
Ejura (Meteosat)	0.84	7.7	59.3	6.2
Ejura (ground based)	0.93	-1.1	47.2	1.0

For both sites it is seen that especially for high evapotranspiration the satellite based AE is underestimated. For Tamale it is seen that AE is lower compared to Ejura and there is more scatter for higher values. The lower AE shows that the criteria of accepting an error of 1mm per day might not always be suitable and relative criteria are needed.

To explore the limits of the satellite based AE, AE is also calculated with locally observed incoming solar radiation and measured 2m temperature. All scatter between AE estimated with local variables and the LAS-derived AE is due to errors in the method used. All

additional scatter when using remote sensing incoming solar radiation and temperature is due to differences between remotely sensed and measured values.

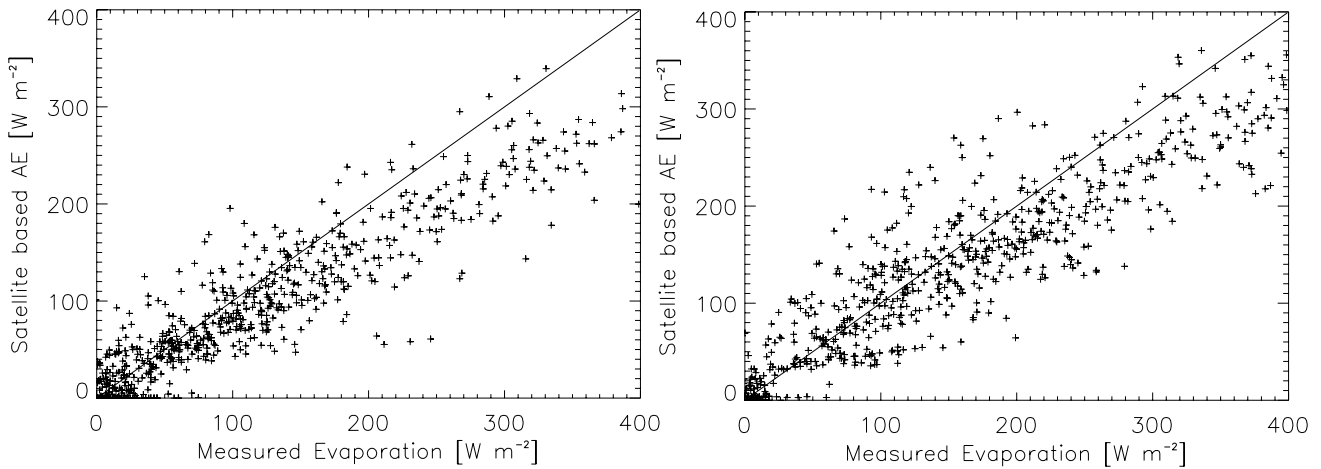


**Fig. 5.7: Satellite based AE vs. measured scatterplot for the analyzed periods at the two test sites (Tamale (left) and Ejura (right)). Only data from rain free days is included.**

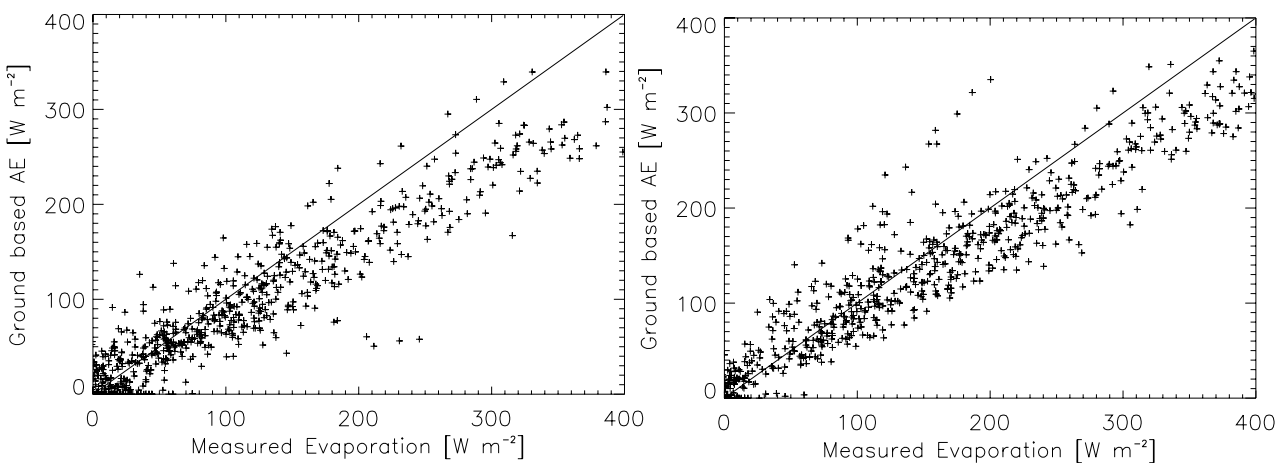


**Fig. 5.8: Ground based AE vs. measured scatterplot for the analyzed periods at the two sites (Tamale (left) and Ejura (right)). Only data from rain free days is included.**

The ground based AE shows less scatter (figure 5.8) and from a direct comparison (figure 5.9) it is concluded that the satellite based estimates introduce some extra scatter, which should be related to errors in estimated incoming solar radiation and/or temperature. However, it should be kept in mind that when two different methods for measuring evapotranspiration, or more generally surface fluxes, are compared, there will always be a certain amount of scatter. This scatter may be due to statistical errors, deficiencies in the measurement method and to a

failure of the measured energy balance to close. Schüttemeyer et al. (submitted to Boundary Layer Meteor.) compared LAS to eddy-covariance data from an intensive observation period at Tamale and Ejura test site and found similar scatter as observed in the present study for daytime evapotranspiration between the direct method (eddy-covariance) and LAS derived evapotranspiration.

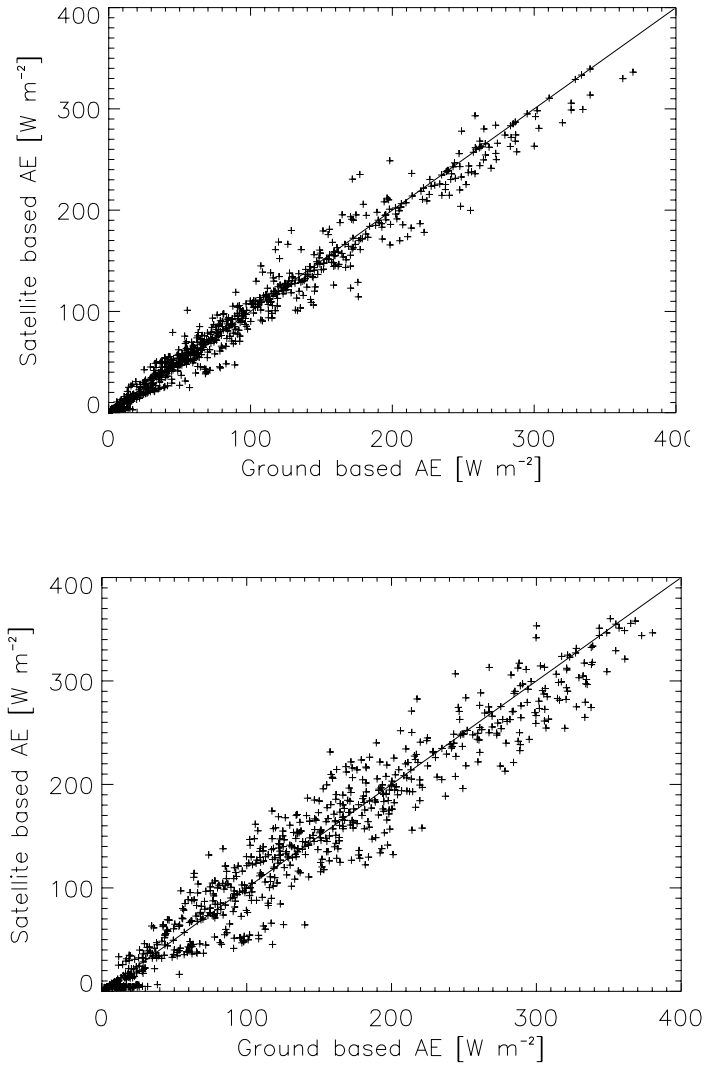


**Fig. 5.9: Direct comparison of ground based vs. satellite based AE at the two sites (Tamale (upper) and Ejura (lower)).**

Figure 5.10 shows the mean diurnal cycle for measured and satellite based evapotranspiration for two 10-day periods at the two sites. Those periods are situated at the end of the wet season and in the dry period. The diurnal cycle is reproduced by the algorithm for both periods. The measured evapotranspiration during the night is close to zero, which shows that indeed the error of the satellite algorithm should be small.

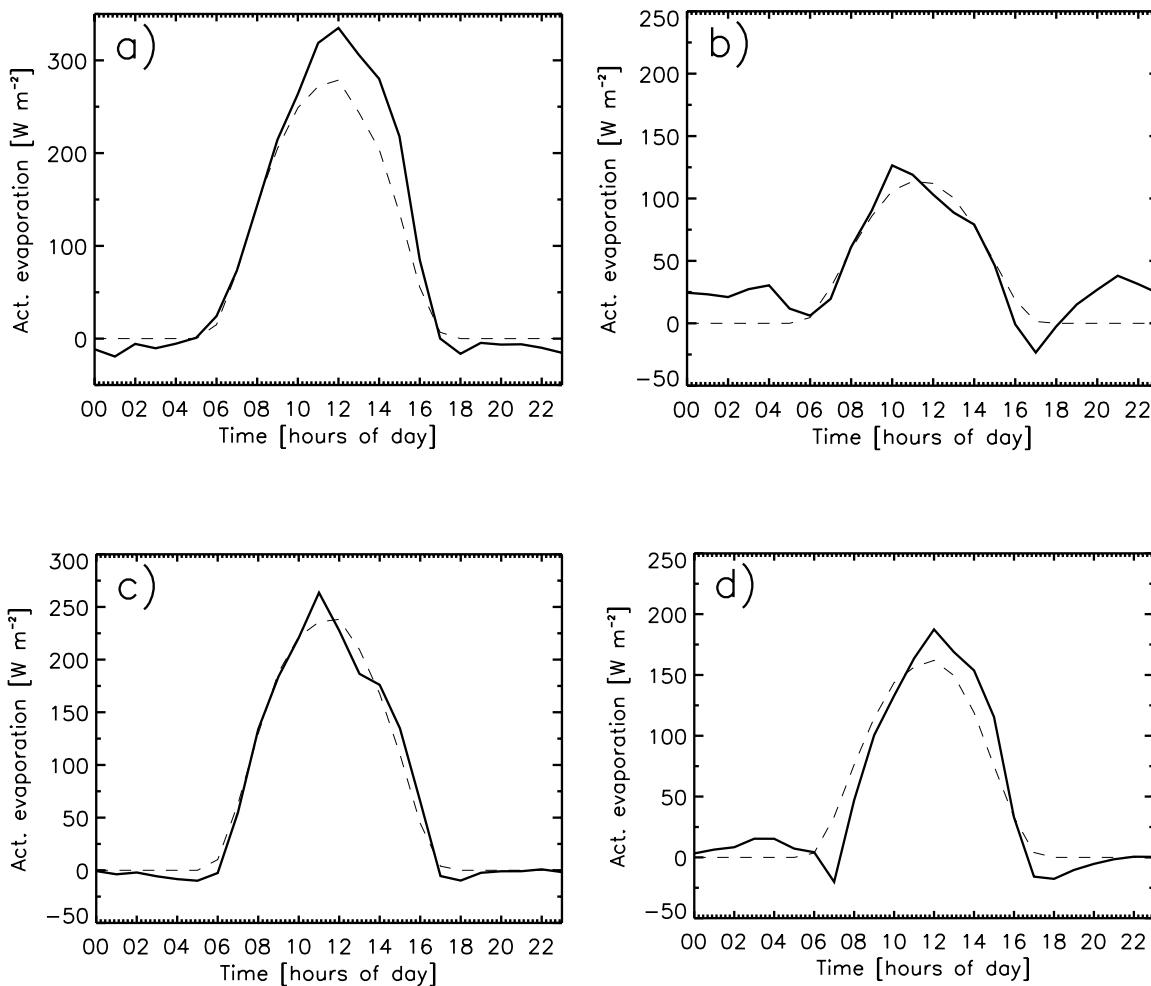


**Fig. 5.10: Diurnal cycle of measured (solid line) and satellite based AE (dashed line) for two 10 day periods at the end of the rainy season and in the dry season for Tamale (a, b) and Ejura (c, d).**

## 5.5 Summary and Conclusions

The accuracy and variability in time of satellite based estimates of incoming solar radiation, 2m air temperature and actual evapotranspiration according to Choudhury and De Bruin (1995) was presented. The evaluation was carried out using ground observations from three different sites in Ghana during the time of transition from the wet to the dry period. The evapotranspiration was calculated from the residual of the energy balance, by using area averaged sensible heat flux from a large aperture scintillometer.

It was shown that the satellite retrieval for incoming solar radiation is in good agreement with the local measurements. Only small differences cannot be resolved, which cannot be expected when only one point measurement is used for comparison. It has been shown that the

reference temperature used in the Meteosat retrieval correlates with local measurements but needs to be bias corrected when used for evapotranspiration calculation. The bias correction for temperature is nearly constant for the test sites.

The approach for estimating AE, which was developed for evapotranspiration estimation under ideal conditions for grass, works well for seasonal and diurnal time scales under the conditions in the Volta basin.

The errors become larger if there is considerable amount of evaporation from interception. A limit is the use of the vegetation fraction with direct vegetation adjustments to the available water. Here seasonally dependent values for the crop factor could help in reducing the errors.

We think it is possible to monitor area averaged actual evapotranspiration on a seasonal scale with daily MBE lower than 1mm/day and a long term MBE lower than 0.5mm/day. The method is meant as a first order approach to estimate evapotranspiration for an entire season, without needing to exclude cloudy situations. The results suggest that the simple satellite-based method is also suitable to verify meteorological models in regions under consideration where ground-truth weather data are scarce. A small network of scintillometers might be added to validate the satellite-based algorithm at a limited number of sites.

For the future a combined approach of the shown method and skin temperature estimation from Meteosat as shown by Sun and Pinker (2003) might help to improve quality for evapotranspiration estimation.

With the new satellite Meteosat-8, also known as Meteosat Second Generation (MSG), more accurate information on the incoming solar radiation can be achieved due to increased spatial (15 minutes) and temporal resolution (1 km x 1 km) and due to a higher amount of scanning sensors. Meteosat-8 will officially replace the actual Meteosat-7 by the end of 2005.

## **Chapter 6**

### **Summary and Perspective**

## 6.1 Summary

This thesis deals with the surface energy balance over drying semi-arid terrain in West Africa in the context of the hydrological cycle. The central objective is to measure the components of the land-atmosphere interface and to model them correctly. Therefore different methods for measuring and modeling the different components of the surface energy balance have been utilized. It has been investigated, which are the most suitable methods with a focus on diurnal and seasonal cycles including the involved changes of the land surface during a season in the Volta basin, West Africa. There are several main topics involved:

- To test the performance of LAS over heterogeneous terrain during a seasonal cycle with a large amplitude;
- To investigate, which type of land surface scheme to employ;
- To assess the sensitivity of a land surface scheme for soil and vegetation related parameters and their change of sensitivity during the season;
- To apply the gained knowledge for a satellite based retrieval, which allows evapotranspiration estimation for the entire Volta basin.

In chapter 2 one of the key measurement techniques of the GLOWA-Volta project is introduced. It is compared to eddy-covariance measurements during an intensive observation period in 2002. The use of large aperture scintillometers is novel for the region and the results show that it is a suitable technique for the kind of environment, given the fact that area averaged sensible heat flux can be obtained on an operational basis. The operational application would be very difficult or even impossible with eddy-covariance measurements under the conditions in the Volta basin since a network of eddy-covariance stations would be needed and additional supervision is required for maintenance.

The results in chapter 2 demonstrate that testing the quality of turbulent energy flux data for energy balance closure with independent measurements is required to gain further confidence in the gathered data. In this context footprint estimation is crucial to evaluate the influence of surface heterogeneity in order to allow a correct interpretation of measurement results. Additionally energy balance closure is an important tool for evaluating strengths and weaknesses of applied parameterizations for canopy conductance. For numerous regions the critical evaluation of parameterizations for canopy conductance has been done before, but it is shown that the obtained results are sometimes in contrast to those.



In chapter 3 two different types of surface schemes are evaluated with measurements of the surface energy balance. The main research question is to find the most suitable one. The obtained results indicate that both types of land surface schemes are not able to simulate the seasonal cycle of the surface energy balance correctly, when driven with standard parameters. The land surface scheme, which uses the “tiled” approach physically performs more realistically. The erroneous results during the dry season for both schemes indicate the need for further development of land surface schemes especially for regions with large extremes during a seasonal cycle. The performance of both models can be improved by applying more seasonally dependent parameters, which is the obvious solution and the need has been stressed before (e.g. Van den Hurk et al. 2000). The difficulty of applying seasonally dependent parameters is the natural climate variability in the region, as already mentioned in the introduction. Therefore seasonally dependent values from databases should lead to inferior model performance during times, when the seasonal cycle is not constant.

In chapter 4 the ideas of chapter 2 and 3 are utilized to explore the performance of a land surface scheme on a seasonal basis in more detail. A different approach for estimating evapotranspiration is applied, which is less dependent on the vegetation fraction and reacts more to changes in soil moisture. The results indicate that the different formulation leads to a more realistic flux estimation. Additionally it is shown that when modeling land surface processes there are not only feedback mechanisms between sensible and latent heat flux, but also between net radiation and sensible heat flux.

The sensitivity of the most important input parameters is also explored in chapter 4 by utilizing a two-level factorial design. It is demonstrated that the ratio of roughness length for momentum and heat, canopy resistance, albedo and vegetation fraction are central parameters for controlling the processes at the land surface and therewith are crucial for improved model performance. The sensitivity of the parameters used, changes during the seasonal cycle. A first attempt is made to explain the seasonal changes for the mentioned parameters, by taking interaction between the parameters into account.

In chapter 3 and 4 it is detected that the vegetation fraction appears to be a big control mechanism for estimating evapotranspiration for the analyzed periods and test sites. Chapter 5 makes use of the gained knowledge to estimate evapotranspiration with a satellite based first order approach developed by Choudhury and De Bruin (1995). This approach depends on the correct estimation of incoming solar radiation, vegetation fraction and air temperature. Here again the seasonal evolution of evapotranspiration is the main topic. It is shown that it is possible to monitor evapotranspiration on a seasonal scale in the Volta basin within some limits.

## 6.2 Perspective

The construction of a land surface scheme in chapter 4, combining the best parts of each of the two evaluated land surface schemes in chapter 3, leads to enhanced model performance concerning the RMSE and correlation coefficient. Concerning the mean bias error it is not much superior to the original formulation. Some of the persisting problems in model performance, especially during the dry season, are related to the use of a single skin temperature representing the heterogeneous surfaces at the test sites. For a deeper understanding of the underlying mechanisms that control the processes at the land surface interface and to improve model performance in relationship to the involved changes of surface cover, a more suitable solution for land surface parameterization could be the use of the tiled approach as analyzed in chapter 3. Furthermore the application of a tiled approach could be justified by the fact that during the seasonal cycle the transpiration is coming from all the plants as long as the soil is wet enough. This may lead to more homogenous conditions in terms of surface temperature in the beginning. As soon as the drying up starts only the plants with deep rooting systems are able to transpire and the differences between the skin temperature of green vegetation fraction and the other fraction rises. In this context one upcoming issue is that separating only between grassland and forest is not a suitable solution for savanna conditions as already mentioned in chapter 4. To employ and to evaluate a tiled scheme, extended measurements for plant related parameters like vegetation type, minimum resistance for different vegetation types, root distribution etc. are needed to optimize the model performance. In addition more detailed measurements of the components of the energy balance together with the area averaged fluxes from the LAS would help in evaluating a tiled scheme in more detail.

The sensitivity analyses for the new formulation of evapotranspiration within the land surface scheme give first suggestions about how to optimize the land surface scheme. The main results of the sensitivity analyses should also be valid for a tiled land surface scheme. Further optimization for a tiled approach could focus on the details related to the different tiles like canopy resistance and root distribution for different vegetation types. Additionally chapter 3 and 4 show the importance of the role of the roughness length ratio for momentum and heat and its seasonal dependence. The tiled land surface scheme together with different roughness lengths for different vegetation types could help in explaining the seasonal change of roughness length ratios.

The focus of measuring and modeling the components of the land surface interface until now was on the evaluation of its main components. For the future the role of soil moisture and runoff generation in the context of the surface energy balance should be explored to eliminate

eventual model deficiencies for those variables. Due to the large seasonal cycle in the region it would also be desirable to analyze the continuous measurements within the GLOWA-Volta project for a full seasonal cycle. This would guarantee that a closed soil water budget is analyzed following Horton's ideas of the hydrological cycle. The related question would be if soil moisture lacks memory from one year to the next due to the large seasonal cycle. If it does lack memory the question is whether this holds for the entire Volta basin, or only for certain parts.

All performed studies in this thesis utilize the "offline" mode in which the different land surface schemes are driven by prescribed atmospheric forcings. One possible route for future research could be the extension of the land surface model to a coupled model including the atmospheric boundary layer (ABL) physics. The "offline" model runs could be compared to the coupled runs to investigate eventual differences between the two and explore important feed back mechanisms between the land surface and the ABL. Furthermore the role of soil moisture in the development of clouds could be explored in a deeper manner (compare Ek and Holtslag 2004; Betts 2004). One critical topic in this context is the nonexistence of upper air soundings in the region to examine the boundary layer structure.

To analyze the impact of climate change on hydrology and water resources in detail (compare section 1.1) the next step would be the use of the optimized land surface scheme in a large scale model, including the results of the coupled study. For the GLOWA-Volta project the first choice would be the PSU/NCAR mesoscale model (known as MM5), since the core of the land surface scheme is already implemented and only small changes need to be applied. Large scale features need to be taken into account, when 3-d model runs are performed for the Volta basin. Therefore it is highly desirable to have deeper knowledge about the involved processes on the large scale. The African Monsoon Multidisciplinary Analyses (AMMA) project (<http://medias.obs-mip.fr/amma>) tries to tackle that need.

The satellite based approach for estimating evapotranspiration of chapter 5 could be used to compare the 3-d output from the meteorological model to the satellite algorithm in the Volta basin. Detailed maps of vegetation types and related adjustments for the crop factor during the season would allow an enhanced satellite based evapotranspiration estimation.

Another possible route for future research is based on the fact that relatively little attention has been given to the spatial heterogeneity issue concerning soil moisture and resulting runoff production until now to improve runoff in land surface schemes. New ideas dealing with this topic are presented for example by Ronda et al. (2002) and Warrach et al. (2002). Two approaches are widely used:

- 1) A variable infiltration capacity model approach, or VIC indirectly accounts for the impact that topography and soil distribution have on surface infiltration (Wood et al. 1992; Liang et al. 1994).
- 2) TOPMODEL approach (Beven and Kirkby 1979) uses topographic information to determine the statistical distribution of the catchment's water table depth and the impact this heterogeneity has on runoff generation.

Both VIC-model and TOPMODEL approaches can be applied at regional scales (Famiglietti and Wood 1994; Liang et al. 1994). In this context a needed step is the division into sub watersheds as the principal hydrological units, since the area of the Volta basin is too large to assume that the base flow is the same throughout the watershed. Koster et al. (2000) divided the North-American continent into those catchment areas. Following this idea landforms could be classified by catchment response e.g. flat or sloping areas or dry and humid regions. An impact assessment could be applied for estimating all relevant parameters for the actual application by still being sufficiently realistic and reasonably simple. For an overview of related techniques see Spaling and Smit (1993). One suitable way for impact assessment could be the grouping of land-surface processes in categories based on the distinction if water movement is mainly vertical or mainly horizontal. The vertical processes are dominant in the more northern region in the Volta basin due to flat lands and a more arid climate. Navrongo and Tamale test sites act as examples for those areas. The horizontal processes are more dominant in the southern region (including Ejura) with a more humid climate and sloping land especially towards the coast line. For parameterizing the vertical land surface interactions the important processes are for example interception by vegetation, infiltration and soil water redistribution. For the horizontal interaction the important processes are for example surface runoff and surface flow routing. With the help of this distinction a ranking system could be applied to see which processes are the most important in order to obtain deeper knowledge about which processes have to be modeled in which detail.

## Bibliography:

- Agyare, W., 2004: Soil characterization and modeling of spatial distribution of saturated hydraulic conductivity at two sites in the Volta Basin of Ghana. *Ecology and Development series*, **17**, 194 pp.
- Allen, R.G., L.S. Pereira, D. Raes, and M. Smith, 1998: Crop Evapotranspiration: Guidelines for Computing Crop Water Requirements. *FAO Irrigation and Drainage Paper*, 56, Rome.
- Asnani, G.C., 1993: *Tropical Meteorology*, volumes 1 and 2, published by G.C.Asnani, C/0 Indian Institute of Tropical Meteorology, Pune 411 008, India, 1202 pp.
- Avissar, R., 1995: Which type of soil-vegetation-transfer scheme is needed for general circulation models: Proposal for a higher-order scheme. *J. Hydrol.*, **212/213**, 136-154.
- Baldocchi, D., E. Falge, L. Gu, R. Olson, D. Hollinger, S. Running, P. Anthoni, Ch. Bernhofer, K. Davis, R. Evans, J. Fuentes, A. Goldstein, G. Katul, B. Law, X. Lee, Y. Malhi, T. Meyers, W. Munger, W. Oechel, K.T. Paw, K. Pilegaard, H.P. Schmid, R. Valentini, S. Verma, T. Vesala, K. Wilson, and S. Wofsy, 2001: FLUXNET: A New Tool to Study the Temporal and Spatial Variability of Ecosystem-Scale Carbon Dioxide, Water Vapor, and Energy Flux Densities. *Bull. Amer. Meteor. Soc.*, **82**, 2415–2434.
- Baldocchi, D., L. Xu, and N. Kiang, 2004: How plant functional-type, weather, seasonal drought, and soil physical properties alter water and energy fluxes of an oak-grass savanna and an annual grassland. *Agric. For. Meteorol.*, **65**, 21-45.
- Bastiaanssen, W.G.M., M. Menenti, R.A. Feddes, and A.A.M. Holtslag, 1998a: A remote sensing energy balance algorithm for land, SEBAL: 1. Formulation. *J. Hydrol.*, **212-213**, 198-212.
- Bastiaanssen, W.G.M., H. Pelgrum, J. Wang, Y. Ma, J.F. Moreno, G.J. Roerink, and T. van der Wal, 1998b: A remote sensing surface energy balance algorithm for land (SEBAL): 2. Validation. *J. Hydrol.*, **212-213**, 213-229.
- Beljaars, A.C.M., and A.A.M. Holtslag, 1991: On flux parameterization over land surfaces for atmospheric models. *J. Appl. Meteor.*, **30**, 327-341.
- Beljaars, A.C.M., P. Viterbo, M. Miller, and A.K. Betts, 1996: The Anomalous Rainfall over the United States during July 1993: Sensitivity to Land Surface Parameterization and Soil Moisture Anomalies. *Mon. Wea. Rev.*, **124**, 362-383.
- Betts, A. K., F. Chen, K. E. Mitchell, and Z. I. Janjic, 1997: Assessment of the Land Surface and Boundary Layer Models in Two Operational Versions of the NCEP Eta Model Using FIFE Data. *Mon. Wea. Rev.*, **125**, 2896-2916.

- Betts, A. K., 2004: Understanding Hydrometeorology Using Global Models. *Bull. Amer. Meteor. Soc.*, **85**, 1673-1688.
- Beven, K.J., and M. J. Kirkby, 1979: A physically-based variable contributing area model of basin hydrology. *Hydrol. Sci. J.*, **24**, 43–69.
- Birkes, D., and Dodge, Y. 1993: *Alternative methods of regression*. John Wiley and Sons, Inc., New York, 228 pp.
- Bolle, H.-J., J.C. Andre, and J.L. Arrue, 1993: EFEDA: European field experiment in a desertification-threatened area. *Ann. Geophysicae*, **11**, 173-189.
- Boone, A., F. Habets, J. Noilhan, D. Clark, P. Dirmeyer, S. Fox, Y. Gusev, I. Haddeland, R. Koster, D. Lohmann, S. Mahanama, K. Mitchell, O. Nasonova, G.-Y. Niu, A. Pitman, J. Polcher, A. B. Shmakin, K. Tanaka, B. van den Hurk, S. V erant, D. Verseghy, P. Viterbo and Z.-L. Yang, 2004: The Rh one-Aggregation Land Surface Scheme Intercomparison Project: An Overview. *J. Climate*, **17**, 187-208.
- Bosveld F. C. and W. Bouten, 2001: Evaluation of transpiration models with observations over a Douglas fir forest. *Agric. For. Meteorol.*, **108**, 4, 247-264.
- Box, G., W. Hunter and J. Hunter, 1978: *Statistics for Experimenters: An Introduction to Design, Data Analysis, and Model Building*. John Wiley and Sons, 672 pp.
- Brunsell N.A., and R.R. Gillies, 2003: Length Scale Analysis of Surface Energy Fluxes Derived from Remote Sensing. *J. Hydrometeor.*, **4**, 1212-1219.
- Burpee, R. W., 1972: The origin and structure of easterly waves in the lower troposphere of North Africa. *J. Atmos. Sci.* **29**, 77-90.
- Cano D., J.M. Monget , M. Albuissou, H. Guillard, N. Regas, and L. Wald, 1986: A method for the determination of the global solar radiation from meteorological satellite data. *Sol. Energy*, **37**, 31-39.
- Chang, S., D. Hahn, C.-H. Yang, D. Norquist, and M. Ek, 1999: Validation Study of the CAPS Model Land Surface Scheme Using the 1987 Cabauw/PILPS Dataset. *J. Appl. Meteor.*, **38**, 405-422.
- Chen, F., Z. Janjic and K. Mitchell, 1997: Impact of atmospheric surface-layer parameterizations in the new land surface scheme of the NCEP mesoscale Eta model. *Bound.-Layer Meteor.*, **85**, 391-421.
- Chen, F., and J. Dudhia, 2001: Coupling an Advanced Land Surface–Hydrology Model with the Penn State–NCAR MM5 Modeling System. Part I: Model Implementation and Sensitivity. *Mon. Wea. Rev.*, **129**, 569-585.
- Choudhury, B.J., and H.A.R. De Bruin, 1995: First order approach for estimating unstressed transpiration from meteorological satellite data. *Adv. Space Res.*, **16**, pp. 167.

- Cobos, D.R., and J.M. Baker, 2003: Evaluation and modification of a domeless net radiometer. *Agron. J.*, **95**, 177-183.
- Crossley, J. F., J. Polcher, P. M. Cox, N. Gedney, and S. Planton, 2000: Uncertainties linked to land-surface processes in climate change simulations, *Clim. Dyn.*, **16**, 949–961.
- De Bruin, H.A.R., 1987: From Penman to Makkink, in J.C. Hopghart (Ed.), *Evaporation and Weather, (technical Meeting of the Committee for Hydrological Research, February, 1981)*, Comm. Hydrol. Res. TNO, Den Haag, Proc. And Inform.,39, 5-30.
- De Bruin, H. A. R., W. Kohsiek, and B. J. M. van den Hurk, 1993: A Verification of Some Methods to Determine the Fluxes of Momentum, Sensible Heat, and Water Vapor Using Standard Deviation and Structure Parameter of Scalar Meteorological Quantities. *Bound. Layer Meteor.*, **63**, 231-257.
- De Bruin, H. A. R., W. Kohsiek, and B. J. M. van den Hurk, 1995: The scintillation method tested over a dry vineyard area. *Bound.-Layer Meteor.*, **93**, 453-468.
- Deardorff, J.W., 1978: Efficient prediction of ground surface temperature and moisture, with inclusion of a layer of vegetation. *J. Geophys. Res.*, **83**, 1889-1903.
- Dijk, A. Van, Kohsiek, W., and H.A.R. De Bruin, 2003: Oxygen sensitivity of krypton and Lyman-alpha hygrometers. *J. Atmos. Oceanic Technol.* **20**, 143–151.
- Dolmann, A.J., 1993: A multiple-source land surface energy balance model for use in general circulation models. *Agric. For. Meteorol.*, **65**, 21-45.
- Dolman, A. J., J. H. C. Gash, J. -P. Goutorbe, Y. Kerr, T. Lebel, S.D. Prince, and J. N. M. Stricker, 1997: The role of the land surface in Sahelian climate: HAPEX-Sahel results and future research needs. *J. Hydrol.*, **188-189**, 1067-1079.
- Dooge, J., 1992: Sensitivity of runoff to climate change: A Hortonian approach. *Bull. Amer. Meteor. Soc.*, **73**, 2013-2024.
- Doorenbos, J., and W. O. Pruitt, 1977: Guidelines for predicting crop water requirements. *FAO Irrigation and Drainage Paper*, **24**, 35-41.
- Dorman, J.L., and P.J. Sellers, 1989: A Global Climatology of Albedo, Roughness Length and Stomatal Resistance for Atmospheric General Circulation Models as Represented by the Simple Biosphere Model (SiB). *J. Appl. Meteor.*, **28**, 833-855.
- Ek, M. B., and A.A.M. Holtslag, 2004: Influence of Soil Moisture on Boundary Layer Cloud Development. *J. Hydrometeorol.*, **5**, 86-99.
- Ek, M. and L. Mahrt, 1991: A formulation for boundary-layer cloud cover. *Ann. Geophysicae*, **9**, 716-724.
- Ellis J.E., and D.M. Swift, 1988: Stability of African pastoral systems: alternate paradigms and implications for development. *J. Range Managem.*, **41** (6), 450-459.

- Eltahir, E.A.B., and C. Gong, 1996: Dynamics of Wet and Dry Years in West Africa. *J. Climate*, **9**, 1030-1042.
- Famiglietti, J. S., and E. F. Wood, 1994: Multiscale modeling of spatially variable water and energy balance processes. *Water Resour. Res.*, **30**, 3061–3078.
- FAO Report, 1984: Agroclimatological data for Africa. No 22, Vol.1: Countries north of the equator. Food and Agriculture Organization (FAO) of the United Nations, Rome.
- Foken, Th., and B. Wichura, 1996: Tools for quality assessment of surface-based flux measurements. *Agric. For. Meteorol.*, **78**, 83-105.
- Friesen, J., 2002: Spatio-temporal Patterns of Rainfall in Northern Ghana. Diploma thesis, University of Bonn.
- Garatuza-Payan, J. and C.J. Watts, 2003: The use of remote sensing for estimating ET in NW Mexico. *International workshop on use of remote sensing of crop evapotranspiration for large regions*, Montpellier, September 17, 2003.
- Gleick, P.H., 1989. Climate Change, hydrology, and water resources. *Rev. geophys.*, **27**, 3, 32-344.
- GLOWA VOLTA PROJECT PROPOSAL 1999: Sustainable Water Use under Changing Land Use, Rainfall, and Water Demands in the Volta Basin. ZEF. Bonn.
- GLOWA VOLTA ANNUAL REPORT 2001 2002: Sustainable Water Use under Changing Land Use, Rainfall Reliability and Water Demands in the Volta Basin. ZEF. Bonn.
- GLOWA VOLTA Project Proposal 2002: GLOWA Volta Phase II: From Concepts to Application. ZEF. Bonn.
- Goutorbe, J. -P., T. Lebel, A. Tinga, 1994: HAPEX-Sahel: a large-scale study of land atmosphere interactions in the semiarid tropics. *Ann. Geophysicae*, **12**, 53-64.
- Goutorbe, J.P., J. Noilhan, P. Lacarrere, and I. Braud, 1997: Modeling of the atmospheric column over the Central sites during HAPEX-Sahel. *J. Hydrol.*, **188-189**, 1017-1039.
- Gu, J., E.A. Smith, and J.D. Merritt, 1999: Testing energy balance closure with GOES retrieved net radiation and in situ measured eddy correlation fluxes in BOREAS. *J. Geophys. Res.*, **104**, 27-81.
- Gustafsson, D., E. Lewan, B.J.J.M. van den Hurk, P. Viterbo, A. Grelle, A. Lindroth, E. Cienciala, M. Mölder, S. Halldin, L.-C. Lundin, 2003: Boreal Forest Surface Parameterization in the ECMWF Model—1D Test with NOPEX Long-Term Data. *J. Appl. Meteor.*, **42**, 95-112.
- Gutman G., and A. Ignatov, 1998: The derivation of the green vegetation fraction from NOAA/AVHRR data for use in numerical weather prediction models. *Int. J. Remote Sens.*, **19**, 533-543.



- Hales, K., J.D. Neelin, and N. Zeng, 2004: Sensitivity of Tropical Land Climate to Leaf Area Index: Role of Surface Conductance versus Albedo. *J. Climate*, **17**, 1459-1473.
- Halldin, S. and A. Lindroth, 1992: Errors in net radiometry: Comparison and evaluation of six radiometer designs. *J. Atmos. Oceanic Technol.*, **9**, 762-783.
- Halldin, S., S.E. Gryning, L. Gottschalk, A. Jochum, L.C. Lundin, and A.A. Van de Griend, 1999: Energy, water and carbon exchange in a boreal forest – NOPEX experiences. *Agric. For. Meteorol.*, **98-99**, 5-29.
- Hammer A., D. Heinemann, C. Hoyer, R. Kuhlemann, E. Lorenz, R. Mueller and H.G. Beyer, 2003: Solar energy assessment using remote sensing technologies. *Remote Sens. Environ.*, **86** (3), 423-432.
- Hanan, N.P., S.D. Prince and P.H.Y. Hiernaux, 1991: Spectral modelling of multicomponent landscapes in the Sahel. *Int. J. Remote Sens.*, **12** (6), 1243-1258.
- Harris, P.P., C. Huntingford, P.M. Cox, J.C.H. Gash, and Y. Malhi, 2003: Effect of soil moisture on canopy conductance of Amazonian rainforest. *Agric. For. Meteorol.*, **122**, 215-227.
- Hartogensis, O. K., Watts, C. J., Rodriguez, J.-C., and H.A.R. De Bruin, 2003: Derivation of a Effective Height for Scintillometers: La Poza Experiment in Northwest Mexico. *J. Hydrometeor.*, **4**, 915-928.
- Hatfield, J.L., and J.H. Prueger, 2000: Spatial and temporal variations of soil heat flux in a corn field. In: *Proceedings of the 24<sup>th</sup> Conference on Agricultural and Forest Meteorology, American Meteorological Society*, pp. 8-9.
- Hemakumara, H.M., L. Chandrapala, and A.F. Moene, 2003: Evapotranspiration fluxes over mixed vegetation areas measured from large aperture scintillometer. *Agric. Water Management*, **58**, 109-122.
- Henderson-Sellers, A., 1993: A Factorial Assessment of the Sensitivity of the BATS Land-Surface Parameterization Scheme. *J. Climate*, **6**, 227-247.
- Heusinkveld, B., A.F.G. Jacobs, A.A.M. Holtslag, and S.M. Berkowicz, 2004: Surface energy balance closure in an arid region: role of soil heat flux, *Agric. For. Meteorol.*, **122**, 21-37.
- Hólml, E., E Andersson, A Beljaars, P Lopez, J-F Mahfouf, A Simmons and J-N Thépaut, 2002: Assimilation and modeling of the hydrological cycle: ECMWF's status and plans.
- Holtslag, A.A.M., and M. Ek, 1996: Simulation of Surface Fluxes and Boundary Layer Development over the Pine Forest in HAPEX-MOBILHY. *J. Appl. Meteor.*, **35**, 202-213.

- Horton R.E. (1931) The field scope and status of the science of hydrology, *Trans. Am. Geo. Union*, pp 189-202.
- Hsieh, C.I., G.G. Katul, and T.W. Chi: 2002, 'An approximate analytical model for footprint estimation of scalar fluxes in thermally stratified atmospheric flows', *Adv. Water Res.*, **23**, 765-772.
- Huete A, K. Didan, T. Miura, E.P. Rodriguez, X. Gao, and L.G. Ferreira, 2002: Overview of the radiometric and biophysical performance of the MODIS vegetation indices. *Remote Sens. Environ.*, **83**, 195-213.
- Hulme, M., 1996: Climate Change and Southern Africa: an Exploration of Some Potential Impacts and Implications in the SADC Region. Report commissioned by WWF International and coordinated by the Climate Research Unit, UEA, Norwich, United Kingdom, 104 pp.
- Huntingford C., S.J. Allen, and R.J. Harding, 1995: An inter-comparison of single and dual-source vegetation-atmosphere transfer models applied to transpiration from Sahelian Savannah. *Bound.-Layer Meteor.*, **74**, 397-418.
- Idso, S. B. and R.B. Jackson, 1969: Thermal radiation from the atmosphere. *J. Geophys. Res.*, **74**, 5397-5403.
- Ineichen P. and R. Perez 1999: Derivation of cloud index from geostationary satellites and application to the production of solar irradiance and daylight illuminance data. *Theoret. Appl. Climatology*, **64**, 119-130.
- Ineichen P. and R. Perez 2002: A new air mass independent formulation for the Linke turbidity coefficient. *Sol. Energy*, **73** (3), 151-157.
- Intergovernmental Panel on Climate Change, Climate Change 1995: *The Science of Climate Change. Contribution of Working Group I to the Second Assessment Report of the Intergovernmental Panel on Climate Change.* edited by J. T. Houghton et al., Cambridge Univ. Press, New York 572 pp.
- IPCC, 1998. *The Regional Impacts of Climate Change: An Assessment of Vulnerability.* (Eds RT Watson, MC Zinyowera, RH Moss), Cambridge University Press, Cambridge, UK.
- IPCC, 1999: *Special Report on Aviation and the Global Atmosphere.* Penner, J.E., D.H. Lister, D.J. Griggs, D.J.
- IPCC, 2001: *Climate Change: Impacts, Adaptation and Vulnerability.* Contribution of Working Group II to the Third Assessment Report of the Intergovernmental Panel on Climate Change.
- Jacobs, C.M.J., 1994: Direct Impact of Atmospheric CO<sub>2</sub> Enrichment on Regional Transpiration. Thesis. Wageningen Agricultural University. 179 pp.

- Jacquemin, B., and J. Noilhan, 1990 : Sensitivity study and validation of al land-surface parameterization using the HAPEX-MOBHILY data set. *Bound.-Lay. Meteor.*, **52**, 93-134.
- Janicot, S., 1992: Spatiotemporal Variability of West African Rainfall. Part I: Regionalizations and Typings. *J. Climate*, **5**, 489-497.
- Jarvis, P., 1976: The interpretation of the variations in leafwater potentials and stomatal conductances found in canopies in the field. *Philos. Trans. R. Soc. London*, Ser. B 273, 593-610.
- Jia, L., Z. Su, B.J.J.M. Van den Hurk, M. Menenti, A.F. Moene, H.A.R. De Bruin, J.J. Basalga Yrisarry, M. Ibanez and A. Cuesta, 2003: Estimation of sensible heat flux using the Surface Energy Balance System (SEBS) and ATSR measurements. *Phys. Chem. Earth*, **28**, 75–88.
- Kasei, C. N., 1988: *The Physical Environment of Semiarid Ghana*. In: Unger, P.W., et al. (eds) *Challenges in Dryland Agriculture – A Global Perspective*. Texas Agricultural Experiment Station, Amarillo/Bushland, 350-354.
- Klemes, V. 1985: Sensitivity of Water Resource Systems to Climate Variations. World Clim. Appl. Programme WCP – 98, World Meteorol. Organ., Geneva, 17 pp.
- Koster, R.D., and M.J. Suarez, 1992: A Comparative Analysis of Two Land Surface Heterogeneity Representations. *J. Climate*, **5**, 1379-1390.
- Koster, R.D., M.J. Suarez, A. Ducharne, K. Praveen, and M. Stieglitz, 2000: A catchment-based approach to modeling land surface processes in a GCM - Part 1: Model structure. *J. Geophys. Res.*, **105** (D20), 24809-24822.
- Kubota, A. and M. Sugita, 1994: Radiometrically determined skin temperature and scalar roughness to estimate surface heat flux. Part I: Parameterization of radiometric scalar roughness. *Bound.-Layer Meteor.*, **69**, 397-416.
- Kustas W. P., Prueger, J.H., and L.E. Hipps, 2002: Impact of Using Different Time-averaged Inputs for Estimating Sensible Heat Flux of Riparian Vegetation Using Radiometric Surface Temperature. *J. Appl. Meteor.*, **41**, 319-332.
- Lamaud, E., J. Ogée, Y. Brunet, and P. Berbigier, 2001: Validation of eddy flux measurements above the understorey of a pine forest. *Agric. For. Meteorol.*, **106**, 173-186.
- Lare, A.R., and S.E. Nicholson, 1994: Contrasting Conditions of Surface Water Balance in Wet Years and Dry Years as a Possible Land Surface-Atmosphere Feedback Mechanism in the West African Sahel. *J. Climate*, **7**, 653-668 .

- Lee X., and X. Hu, 2002: Forest-Air Fluxes Of Carbon, Water And Energy Over Non-Flat Terrain. *Bound.-Layer Meteor.*, **103**, 277-301.
- Lemonsu, A., C. S. B. Grimmond, and V. Masson, 2004: Modeling the Surface Energy Balance of the Core of an Old Mediterranean City: Marseille. *J. Appl. Meteor.*, **43**, 312-327.
- Lenth, R., 1989: Quick and easy analysis of unreplicated fractional factorial. *Technometrics*, **31**, 469-473.
- Liang, X., D. P. Lettenmaier, E. F. Wood, and S. J. Burges, 1994: A simple hydrologically based model of land surface water and energy fluxes for general circulation models. *J. Geophys. Res.*, **99**, 14, 415–14 428.
- Liu, H.Q. and A.R. Huete, 1995: A feedback based modification of the NDVI to minimize canopy background and atmospheric noise. *IEEE. Trans. Geosci. Remote Sensing*, **33**, 457-465.
- Ma, Y., M. Menenti, O. Tsukamoto, H. Ishikawa, J. Wang, and Q. Gao, 2004: Remote sensing parameterization of regional land surface heat fluxes over arid area in northwestern China, *J. Arid Environ.*, **57** (2), 257-273.
- Mahrt, L., 1998: Flux sampling errors for aircrafts and towers. *J. Atmos. Oceanic Technol.*, **15**, 416-429.
- Mahrt, L. and M. Ek, 1984: The influence of atmospheric stability on potential evaporation. *J. Clim. Appl. Meteorol.*, **23**, 222-234.
- Makkink G.F., 1957: Testing the Penman formula by means of lysimeters. *Int. J. Water Eng*, **11**, 277-288.
- Manabe, S., 1969: Climate and the ocean circulation 1. the atmospheric circulation and the hydrology of the earth's surface. *Mon. Weather. Rev.*, **97**(11), 739-774.
- Mannstein H., C. Schillings, H. Broesamle and F. Trieb 1999: *Using a Meteosat Cloud Index to Model the Performance of Solar Thermal Power Stations*. Presentation at EUMETSAT Conference, Copenhagen.
- Margulis, S.A., and D. Entekhabi, 2001: Feedback between the Land Surface Energy Balance and Atmospheric Boundary Layer Diagnosed through a Model and Its Adjoint. *J. Hydrometeor.*, **2**, 599-620.
- Martano, P., 2000: Estimation of Surface Roughness Length and Displacement Height from Single-Level Sonic Anemometer Data. *J. Appl. Meteor.*, **39**, 708-715.
- Meijninger W. M. L., A. E. Green, O. K. Hartogensis, W. Kohsiek, J. C. B. Hoedjes, R. M. Zuurbier, and H. A. R. De Bruin, 2002: Determination of Area-Averaged Water Vapor Fluxes with Large Aperture and Radio Wave Scintillometers over a Heterogeneous Surface Flevoland-Field-Experiment. *Bound.-Layer Meteor.*, **105**, 63-83.

- Meyers, T.P. and S.E. Hollinger, 2004: An assessment of storage terms in the surface energy balance of maize and soybean. *Agric. For. Meteor.*, **125**, 105-115.
- Mimikou, M.A., 1995: *Climatic change in Environmental Hydrology*. Singh V.P. (ed.). Kluwer Academic Publishers, Dordrecht, The Netherlands, pp. 69-106.
- Mölders, N., 1999: Einfache und akkumulierte Landnutzungsänderungen und ihre Auswirkungen auf Evapotranspiration, Wolken- und Niederschlagsbildung. *Wiss. Mitteil. Inst. f. Meteor. Univ. Leipzig / Inst. f. Troposphärenforsch. Leipzig* 15.
- Moene A. F., 2003: Effects of water vapor on the structure parameter of the refractive index for near-infrared radiation. *Bound.-Layer Meteor.*, **107**, 635-653.
- Moncrieff, J.B., 1996: The propagation of errors in long-term measurements of land atmosphere fluxes of carbon and water. *Global Change Biol.*, **2**, 231-240.
- Monteith, J. L., 1965: The state and movement of water in living organisms, in *Evaporation and Environment*, edited by G. E. Fogg, Academic Press, New York.
- Monteith, J., 1981: Evaporation and surface temperature. *Quart. J. R. Meteorol. Soc.*, **107**, 1-27.
- Monteith, J., and M.H. Unsworth, 1990: *Principal of environmental physics*. (2<sup>nd</sup> edition, Arnold, London, 291 pp.
- Moore, C., 1986: Frequency response corrections for eddy correlation systems. *Bound.-Layer Meteor.*, **37**, 17-35.
- Nagai, H., 2002: Validation and Sensitivity Analysis of a New Atmosphere–Soil–Vegetation Model. *J. Appl. Meteor.*, **41**, 160-176.
- Nicholson, S. E., 1986: The Spatial Coherence of African Rainfall Anomalies: Interhemispheric Teleconnections. *J. Appl. Meteor.*, **25**, 1365-1381.
- Nicholson, S. E., 1993: An Overview of African Rainfall Fluctuations of the Last Decade. *J. Climate*, **6**, 1463-1466.
- Niyogi, D. S., S. Raman and K. Alapaty, 1999: Uncertainty in the Specification of Surface Characteristics, Part ii: Hierarchy of Interaction-Explicit Statistical Analysis. *Bound.-Layer Meteor.*, **91**, 341-366.
- Niyogi, D. S., Y. Xue, and S. Raman, 2002: Hydrological Land Surface Response in a Tropical Regime and a Midlatitudinal Regime. *J. Hydrometeor.*, **3**, 39-56.
- Noilhan, J. and S. Planton, 1989: A simple parameterization of land surface processes for meteorological models. *Mon. Wea. Rev.*, **117**, 536-549.
- Obukhov, A.M., 1960: Structure of Temperature and Velocity Fields under Conditions of Free Convection. *Works Inst. Theor. Geophys. Acad. Sci. USSR*, **1**, 95-115.

- Oort, A. H. and J. P. Peixoto, 1983: Global angular momentum and energy balance requirements from observations. *Theory of Climate*, Saltzman, B., Ed., Academic Press, 355-490.
- Paulson, C., 1970: The mathematical representation of wind speed and temperature profiles in the unstable atmospheric surface layer. *J. Appl. Meteor.*, **9**, 857-861.
- Penman, H.L., 1948: Natural evaporation from open water, bare soil and grass. *Proc. Roy Soc. London*, **A193**, 120-145.
- Penman, H.L., 1956: *Estimating evaporation*. Trans. Amer. Geophys. Union, **37**, 43-46.
- Perez R., P. Ineichen, K. Moore, M. Kmiecik, C. Chain, R. George and F. Vignola, 2002: A new operational satellite-to-irradiance model - description and validation. *Sol. Energy*, **73** (5), 307-317.
- Priestley, C.H.B., and R.J. Taylor, 1972: On the assessment of surface heat flux and evaporation using large-scale parameters. *Mon. Wea. Rev.*, **100**, 81-82.
- Riebsame, W.E., K.M. Strzepek, L.L. Wescoat, Jr., R. Perritt, G.L. Gaile, J. Jacobs, R. Lieichenko, C. Magadza, H. Phien, B.J. Urbiztondo, P. Restrepo, W.R. Rose, M. Saleh, L.H. Ti, C. Tucci, and D. Yates, 1995: Complex river basins. In: *As Climate Changes: International Impacts and Implications* [Strzepek, K.M. and J.L. Smith (eds.)] Cambridge University Press, Melbourne, Australia, pp. 57-91.
- Rigollier C., M. Lefèvre and L. Wald, 2001: Heliosat version 2. EU-project SODA: Integration and exploitation of networked solar irradiation Databases for environment monitoring. Deliverable No. D3.2. IST-1999-12245.
- Ronda, R. J., HAR. De Bruin, and A.A.M. Holtslag, 2001: Representation of the Canopy Conductance in Modeling the Surface Energy Budget for Low Vegetation. *J. Appl. Meteor.*, **40**, 1431-1444.
- Ronda, R. J., B.J.J.M. van den Hurk, and A.A.M. Holtslag, 2002: Spatial Heterogeneity of the Soil Moisture Content and Its Impact on Surface Flux Densities and Near-Surface Meteorology. *J. Hydrometeor.*, **3**, 556-570.
- Sakai, R.K., D.R. Fitzjarrald, and K.E. Moore, 1997: Detecting leaf area and surface resistance during transition seasons. *Agric. For. Meteorol.*, **84**, 273-284.
- Schaap, M.G., F.J. Leijf, and M.Th. van Genuchten, 1998: Neural network analysis for hierarchical prediction of soil water retention and saturated hydraulic conductivity. *Soil Sci. Soc. Am.*, **62**, 847-855.
- Schädlich S., F.M. Göttsche and F.-S. Olesen, 2001: Influence of land surface parameters and atmosphere on Meteosat brightness temperatures and generation of land surface temperature maps by temporally and spatially interpolating atmospheric correction. *Remote Sens. Environ.*, **75**, 39-46

- Schlosser, C. A., A. G. Slater, A. Robock, A. J. Pitman, K. Y. Vinnikov, A. Henderson-Sellers, N. A. Speranskaya, K. Mitchell, and the PILPS 2(d) contributors, 2000: Simulations of a boreal grassland hydrology at Valdai, Russia: PILPS Phase 2(d). *Mon. Weather Rev.*, **128**, 301-321.
- Schotanus, P., F. Nieuwstadt, and H.A.R. De Bruin, 1983: Temperature measurement with a sonic anemometer and its application to heat and moisture fluxes. *Bound.-Layer Meteor.*, **26**, 81-93.
- Sellers, P. J., B. W. Meeson, J. Closs, J. Collatz, F. Corprew, D. Dazlich, F. G. Hall, Y. Kerr, R. Koster, S. Los, K. Mitchell, J. McManus, D. Myers, K.-J. Sun, and P. Try, 1996: The ISLSCP Initiative I global datasets: Surface boundary conditions and atmospheric forcings for land-atmosphere studies. *Bull. Amer. Meteor. Soc.*, **77**, 1987-2005
- Seth, A., F. Giorgi, and R. E. Dickinson, 1994: Simulating fluxes from heterogeneous land surfaces: Introducing a vectorized version of Biosphere-Atmosphere Transfer Scheme (VBATS). *J. Geophys. Res.*, **99**, 18,651.
- Shuttleworth, W.J., 1993: *Evaporation. Handbook of Hydrology*, D.R. Maidment, Ed., McGraw-Hill, 4.1-4.53.
- Solbrig, O. T., E. Medina, and J.F. Silva, 1996: Biodiversity and tropical savanna properties: A global view. *Functional Roles of Biodiversity*. H. A. Mooney et al., Eds., Springer, pp185-211.
- Spaling, H., and B. Smit, 1993: Cumulative environmental change: Conceptual frameworks, evaluation approaches, and institutional perspectives. *Environ. Manage.* **17**, 587-600.
- Stannard, D.I., J.H. Branford, W.P. Kustas, W.D. Nichols, S.A. Amer, T.J. Schmugge, and M.A. Weltz, 1994: Interpretation of surface flux measurements in heterogeneous terrain during the Monsoon'90 experiment. *Water Resour. Res.*, **30**, 1227-1239.
- Stewart, J. B., 1988: Modelling surface conductance of pine forest. *Agric. For. Meteorol.*, **43**, 19-35.
- Stuhlmann R., M. Rieland and E. Raschke, 1989: An improvement of the IGMK model to derive total and diffuse solar radiation at the surface from satellite data. *J. Appl. Meteor.*, **29**, 586-603.
- Stull, R. B., 1988: *An introduction to boundary layer meteorology*. Kluwer Acad., Norwell, Mass. 666 pp.
- Sun D. and R. T. Pinker, 2003: Estimation of land surface temperature from Geostationary Operational Environmental Satellite (GOES-8). *J. Geophys. Res.*, **108** (D11), 10.1029/2002JD002422.

- Twine, T.E., W. P. Kustas, J. M. Norman, D.R. Cook, P. R. Houser, T. P. Meyers, J. H. Prueger, P. J. Starks and M.L. Wesely, 2000: Correcting eddy-covariance flux underestimates over a grassland. *Agric. For. Meteorol.*, **103**, 279-300.
- Van de Giesen, N., H. Kunstmann, G. Jung, J. Liebe, M. Andreini, and P.L.G. Vlek, 2001: The GLOWA Volta project: Integrated assessment of feedback mechanisms between climate, landuse, and hydrology. *Adv. Glob. Change Res.*, **10**, 151-170.
- Van den Hurk, B.J.J.M. 1995: Sparse canopy parameterizations for meteorological models. Ph.D, Dissertation, University of Wageningen, 271 pp.
- Van den Hurk, B.J.J.M., and A.C.M. Beljaars, 1996: Impact of Some Simplifying Assumptions in the New ECMWF Surface Scheme. *J. Appl. Meteor.*, **35**, 1333-1343.
- Van den Hurk, B.J.J.M., P. Viterbo, A.C.M. Beljaars and A.K. Betts, 2000: Offline validation of the ERA40 surface scheme. ECMWF Tech Memo 295, 42 pp.
- Verhoef, A., 1995: Surface energy balance of shrub vegetation in the Sahel. Ph.D, Dissertation, University of Wageningen, 247 pp.
- Verhoef, A., S.J. Allen, H.A.R. De Bruin, C.M.J. Jacobs, and B.G. Heusinkveld, 1996a: Fluxes of carbon dioxide and water vapour from a Sahelian savanna. *Agric. For. Meteorol.*, **80**, 231-248.
- Verhoef, A., B.J.J.M. van den Hurk, A.F.G. Jacobs, and B.G. Heusinkveld, 1996b: Thermal soil properties for vineyard (EFEDA-I) and savanna (HAPEX-Sahel) sites. *Agric. For. Meteorol.*, **78**, 1-18.
- Verhoef, A., S.J. Allen, and C.R. Lloyd, 1999: Seasonal Variation Of Surface Energy Balance Over Two Sahelian Surfaces. *J. Climate*, **19**, 1267-1277.
- Verma, S., 1989: Aerodynamic resistances to transfers of heat, mass and momentum in estimation of areal evaporation. IAHS Publ., p.177.
- Viterbo, P. and C. Beljaars, 1995: An improved land surface parameterization scheme in the ECMWF model and its validation. *J. Climate.*, **8**, 2716-2748.
- Viterbo, P., 2002: A review of parameterization schemes for land surface processes. Meteorological Training Course Lecture Series, ECMWF, 49pp.
- Wald L., Albuissou M., Best C., Delamare C., Dumortier D., Gaboardi E., Hammer A., Heinemann D., Kift R., Kunz S., Lefèvre M., Leroy S., Martinoli M., Ménard L., Page J., Prager T., Ratto C., Reise C., Remund J., Rimoczi-Paal A., Van der Goot E., Vanroy F., and A. Webb, 2002: *SoDa: a project for the integration and exploitation of networked solar radiation databases*. In: Environmental Communication in the Information Society, W. Pillmann, K. Tochtermann Eds, Part 2, pp. 713-720.



- Wallace, J.S., S.J. Allen, A.D. Culf, A.J. Dolman, J.H.C. Gash, C.J. Holwill, C.R. Lloyd, J.B. Stewart, I.R. Wright, M.V.K. Sivakumar, and C. Renard, 1992: SEBEX: the Sahelian Energy Balance Experiment. ODA Report no. 92/9. IH, Wallingford, UK. pp. 51.
- Warrach, K., M. Stieglitz, H.-T. Mengelkamp and E. Raschke, 2002: Advantages of a topographically controlled runoff simulation as in a soil-vegetation-atmosphere transfer model. *J. Hydrometeor.*, **3** (2), 131-148.
- Webb, E., Pearman, G., and R. Leuning, 1980: Correction of flux measurements for density effects due to heat and water vapour transfer. *Q.J.R.Meteorol.Soc.*, **106**, 85-100.
- Wesely, M. L., 1976: The Combined Effect of Temperature and Humidity Fluctuations on Refractive Index. *J. Appl. Meteor.*, **15**, 43-49.
- Wesely, M.L., 1989: Parameterization of surface resistances to gaseous dry deposition in regional-scale numerical models. *Atmos Environ.*, **23**, 1293-1304.
- Wilczak, J., Oncley, S., and S.A. Stage, 2001: Sonic anemometer tilt correction algorithms. *Bound.-Layer Meteor.*, **99**, 127-150.
- Wilson, K., A. Goldstein, E. Falge, M. Aubinet, D. Baldocchi, P. Berbigier, C. Bernhofer, R. Ceulemans, H. Dolman, C. Field, 2002: Energy balance closure at FLUXNET sites. *Agric. For. Meteorol.*, **113**, 223-243.
- Wood, E. F., D. P. Lettenmaier, and V. G. Zartarian, 1992: A land surface hydrology parameterization with subgrid variability for general circulation models. *J. Geophys. Res.*, **97**, 2717-2728.
- Wyngaard, J.C., 1973: On Surface-layer turbulence. In: Haugen D.A. (ed), Workshop on Micrometeorology, Boston, Mass. American Meteorological Society, pp. 101-149.
- Xue, Y., P.J. Sellers, J.L. Kinter, and J.A. Shukla, 1991: Simplified Biosphere Model for Global Climate Studies. *J. Climate*, **4**, 345-364.
- Yates, F. ,1970: *Selected Papers*, Hafner Macmillan.
- Zeng, X., Y-J. Dai, R.E. Dickinson, and M. Shaikh, 1998: The role of root distribution for land climate simulation. *Geophys. Res. Letters*, **25**, 4533-4536.
- Zeng, N., J. D. Neelin, 2000: The role of vegetation-climate interaction and interannual variability in shaping the African Savanna. *J. Climate*, **13**, 2665-2670.
- Zilitinkevich, S.S., 1995: Non-local turbulent transport: pollution dispersion aspects of coherent structure of convective flows. In: Air Pollution III - Volume I. Air Pollution Theory and Simulation (Eds. H. Power, N. Moussiopoulos and C.A. Brebbia). Computational Mechanics Publications, Southampton Boston, 53-60.



## Samenvatting

Een van de fundamentele aspecten van het huidige onderzoek in aardsysteemwetenschappen is een goede beschrijving van aardatmosfeer interacties. De rol van het landoppervlak is cruciaal in het klimaatstelsel aangezien een groot deel inkomende zonnestraling aan het aardoppervlak wordt omgezet in turbulente fluxen. In veel gebieden, inclusief semi-aride gebieden, is maar weinig bekend over de dagelijkse en seizoenscyclus van landoppervlak interacties. Vooral semi-aride gebieden zijn een grote uitdaging, waar de variatie tussen droge en natte omstandigheden in een seizoen groot is. Dit geldt met name voor semi-aride gebieden in West-Afrika, een van de meest klimaatgevoelige en ecologisch onstabiele gebieden van de wereld. De variabiliteit van het weer en klimaat wordt sterk beïnvloed door complexe interacties en terugkoppelingen tussen het aardoppervlak en de atmosfeer. Om deze uitwisseling en terugkoppelmechanismen te kunnen analyseren en voorspellen is het van belang om de relevante processen te meten en modelleren.

Om deze relevante processen te kunnen meten waren grote openingshoek scintillometers (Large Aperture Scintillometer, LAS) geplaatst in 3 experimentele stroomgebieden voor het direct meten van de voelbare warmtestroom ( $H$ ) over padlengtes van meer dan 2 kilometer. Voordelen van de LAS methode zijn het verkrijgen van de gebiedsgemiddelde voelbare warmtestroom (tot een schaal van 5000 m), en de robuustheid van het instrument waardoor deze techniek geschikt is voor lange termijn metingen onder de omstandigheden in West Afrika. De latente warmtestroom (ook wel verdamping,  $L_v E$ ) kan vervolgens worden afgeleid als sluitingsterm uit de energiebalans met behulp van de gemeten bodemwarmtestroom ( $G$ ) en netto straling ( $Q^*$ ).

De LAS metingen, samen met de andere gemeten componenten van de energiebalans worden gebruikt voor validatie van landparameterisaties, welk onderdeel zijn van een operationeel meteorologisch en hydrologisch hindcasting systeem. Effectieve parameters voor de bodem- en vegetatieindex van het landgebruiktype op de drie meetlocaties zijn bepaald, waarbij rekening is gehouden met veranderingen van deze parameters gedurende het seizoen. In deze context wordt de vraag beantwoord of de effectieve parameters representatief genoeg zijn voor het gehele stroomgebied. Daarnaast is het van belang rekening te houden met de subgrid-schaal heterogeniteit, hetgeen resulteert in een betere weergave van de waargenomen omstandigheden. Naast evaluatie en kalibratie op lokaal niveau, zijn ook nieuwe ideeën

vereist voor een evaluatie van belangrijke componenten van de oppervlakteenergiebalans op stroomgebied schaal in het hindcasting systeem.

De centrale doelstellingen van dit proefschrift zijn:

- Het analyseren van metingen door het onderzoeken van de sterke en zwakke punten van de gebruikte methode en door vergelijking met de andere meettechnieken;
- Het testen van de respons van huidige parameterisaties van de oppervlaktegeleiding op veranderingen met tijdschalen van een dag en een seizoen;
- Het vinden van de optimale landoppervlakte parameterisatie voor de evaluatie van 2 verschillende benaderingen;
- Het optimaliseren van een parameterisatie met behulp van een factorial design, welke rekening houdt met hoofd en interactie effecten;
- Het toepassen van een factorial design op twee contrasterende locaties voor het testen van de robuustheid van belangrijke parameters;
- Het gebruiken van de opgedane kennis uit voorafgaande doelstellingen en het ontwikkelen van een simpel en robuust satelliet algoritme voor het verkrijgen van gebiedsgemiddelde verdamping op grotere schaal.

Dit proefschrift omvat 6 hoofdstukken. De bovengenoemde doelstellingen zullen worden onderzocht in hoofdstuk 2 tot en met 5. In hoofdstuk 6 worden alle resultaten samengevat en wordt gewezen op perspectieven voor toekomstig onderzoek.

In hoofdstuk 2 wordt één van hoofdmeettechnieken van het GLOWA-Volta project geïntroduceerd, de LAS. Deze wordt vergeleken met eddy-covariantie (EC) metingen verzameld tijdens een intensieve meetperiode in 2002. Het toepassen van de LAS in deze regionen is nieuw en de resultaten laten zien dat het een geschikt instrument is voor dit type klimaat, gegeven het feit dat de gebiedsgemiddelde voelbare warmtestroom kan worden verkregen op een operationele basis. Gezien de omstandigheden in het Volta stroomgebied, zijn het doen van EC metingen erg moeilijk of zelfs onmogelijk, aangezien een netwerk van EC systemen is vereist en de daarbij benodigde supervisie en onderhoud. De resultaten in hoofdstuk 2 laten zien dat controle van de energiebalanssluiting van de turbulente fluxen met behulp van onafhankelijk metingen nodig is om meer vertrouwen te krijgen in de verzamelde data. In deze context zijn footprint schattingen, ter bestudering van de invloed van landschapheterogeniteit, cruciaal voor een goede interpretatie van de gemeten resultaten. Bovendien is de energiebalanssluiting een belangrijke techniek voor het evalueren van de

sterke en zwakke punten van de toegepaste parameterisaties voor het geleidingsvermogen van gewassen. In veel regionen zijn al eens kritische evaluatiestudies van parameterisaties van het geleidingsvermogen van gewassen gedaan, er wordt echter aangetoond dat de in deze studie verkregen resultaten soms contrasteren met deze eerdere studies.

In hoofdstuk 3 worden twee verschillende oppervlakteschema's geëvalueerd met metingen van de oppervlakteenergiebalans. De hoofdonderzoeksvraag is het vinden van de meest geschikte. De gevonden resultaten geven aan dat beide type landoppervlakte schema's niet in staat zijn om de seizoenscyclus van de oppervlakteenergiebalans correct te beschrijven met behulp van standaard parameters. Het landoppervlakte schema dat gebruik maakt van een "tiled" (tegel) benadering presteert fysisch meer realistisch. De foute resultaten van beide schema's gedurende het droge seizoen geven de noodzaak aan voor verder onderzoek van landoppervlakte schema's voor gebieden met grote extremen in de seizoenscyclus. Een voor de hand liggende oplossing waardoor de prestatie van beide modellen kan worden verbeterd, is het toepassen van seizoensafhankelijke parameters, een noodzaak die al vaker is geopperd. Zoals al eerder is genoemd in de inleiding, is een probleem van het toepassen van seizoensafhankelijke parameters, de natuurlijke variabiliteit van het klimaat in het gebied. Het gebruik van seizoensafhankelijke waarden uit databestanden zou kunnen leiden tot verminderde modelprestaties tijdens situaties waarbij de seizoenscyclus niet constant is.

In hoofdstuk 4 zijn de ideeën van hoofdstuk 2 en 3 gebruikt om de prestatie van een landoppervlakte schema op seizoensbasis te onderzoeken. Er wordt gebruik gemaakt van een andere benadering voor het bepalen van de evapotranspiratie, welke minder afhankelijk is van de vegetatiefractie en sneller reageert op veranderingen in bodemvocht. De resultaten geven aan dat deze andere benadering leidt tot een beter fluxschatting. Daarnaast wordt aangetoond dat bij het modelleren van landoppervlakte processen er niet alleen terugkoppelmechanismen zijn tussen de voelbare en latente warmtestroom, maar ook tussen de netto straling en de voelbare warmtestroom.

In hoofdstuk 4 worden ook de gevoeligheden van de belangrijkste parameters onderzocht met behulp van een twee-laags factorial design. Aangetoond wordt dat de verhouding tussen de ruwheidlengte voor impuls en warmte, gewasweerstand, albedo en vegetatiefractie centrale parameters zijn in landoppervlakte processen en daarmee cruciaal voor verbeterde modelprestaties. De gevoeligheid van de gebruikte parameters verandert gedurende de seizoenscyclus. Een eerste poging wordt gedaan om deze seizoensverandering van de genoemde parameters te verklaren door rekening te houden met interacties tussen de parameters.

In hoofdstuk 3 en 4 wordt aangetoond dat de vegetatiefractie een belangrijke rol speelt in het schatten van de evapotranspiratie voor de geanalyseerde periodes en voor de meetlocaties. Deze opgedane kennis wordt toegepast in hoofdstuk 5 voor het schatten van evapotranspiratie met behulp van een op satellietwaarnemingen gebaseerde eerste orde aanpak, ontwikkeld door Choudburry en De Bruin (1995). Deze aanpak hangt af van een correcte schatting van de inkomende kortgolvlige straling, vegetatiefractie en luchttemperatuur. Opnieuw speelt de seizoensevolutie van de evapotranspiratie een hoofdrol. Er wordt aangetoond dat het mogelijk is om de verdamping, binnen een bepaalde marge, te monitoren op seizoensschaal in het Volta stroomgebied.

In hoofdstuk 6 worden alle resultaten besproken en suggesties gedaan voor toekomstig onderzoek.

## Curriculum vitae

Dirk Schüttemeyer, birth name Burose

Date and place of birth: 29 December 1970 in Wipperfürth, Germany

### Education:

---

February 2005 - Present

Postdoctoral Fellow, Meteorology and Air Quality Group, Wageningen University

November 2000 – January 2005

Doctorate, Meteorology and Air Quality Group, Wageningen University

October 1995 - June 2000

Studies of Meteorology, Physical Chemistry and Hydrology, University of Bonn, Germany

Thesis: Rain detection over land surfaces using passive microwave satellite data (in German)

April 1992 - October 1995

Studies of Geography, University of Bonn, Germany

June 1990

Abitur (High-school Graduate), Wipperfürth, Germany

### Employment History

---

November 2000 - October 2004

Research assistant at Center of Development Research (ZEF), Bonn, Germany

June 2000 - October 2000

Research assistant at DLR (German Aerospace Center), Cologne, Germany

September 1998 - June 2000

Student assistant at DLR (German Aerospace Center), Cologne, Germany

December 1994 – August 1998

Student worker at Creditreform, Bonn, Germany

October 1994 – June 2000

Visitor guide at the Public Relations Office at DLR Cologne, Germany

January 1992 – April 1992

Worker at a construction company

August 1990 – December 1991

Civil service at a school for disabled children, Wipperfürth, Germany

This study was carried out at the Meteorology and Air Quality Group, Wageningen University, the Netherlands. Financial support was provided by the Federal Ministry of Education and Research, Germany.

Thesis printing: Difo Druck GmbH, Bamberg, Germany

Front Cover: Trygve Bolstad, Cristoph & Friends Media + Trade Agents & Das Fotoarchiv